UMR 7647 CNRS

Introduction to Molecular Dynamics

Holger Vach

LPICM, Ecole Polytechnique
Palaiseau

réunion plénière du GDR Pulse 2017

5 octobre 2017

Department of Energy
National Laboratory

Real education for the real world

seit 1558

Plan

- Méthodes de la simulation numérique de type dynamique moléculaire
  - **Introduction**
  - **Algorithmes**
  - **Conditions aux limites périodiques**
  - **Fonctions de corrélation**
- Dynamique non réactive

  - Diffusion d'agrégats Ar_n purs sur une surface de graphite
  - Diffusion d'agrégats mixtes Ar_nR_m sur une surface de graphite
- Dynamique réactive

  - Diffusion réactive d'agrégats Si_nH_m par un substrat de silicium
  - Croissance d'agrégats Si_nH_m dans un réacteur plasma

Introduction

Newton : $F_i = m_i a_i(t)$

$a_i(t) = d^2 r_i(t) / dt^2$

- $F_i = 0$

$r_i(t) = v_{0,i} t + r_{0,i}$

$v_i(t) = v_{0,i}$

- F_i = constant

$r_i(t) = 1/2\ a_{0,i}\ t^2 + v_{0,i} t + r_{0,i}$

$v_i(t) = v_{0,i} + a_{0,i}\ t$

- $F_i = - du (r_i , \ldots , r_n) / dr_i(t)$

Par suite d'un défaut de solution analytique, les trajectoires ne sont pas directement déterminées par la résolution analytique de l'équation de Newton précédente, mais numériquement.

Algorithme de Verlet

Considérons l'équation du mouvement simple :

$$md^2r/dt^2 = F(t)$$

développement de Taylor

$$r(t + \Delta t) = r(t) + v(t)\,\Delta t + F(t) / 2m\,(\Delta t)^2 + d^3r / dt^3\,(\Delta t)^3 + \vartheta((\Delta t)^4)$$

et de manière similaire,

$$r(t - \Delta t) = r(t) - v(t)\,\Delta t + F(t) / 2m\,(\Delta t)^2 - d^3r / dt^3\,(\Delta t)^3 + \vartheta((\Delta t)^4)$$

en faisant la somme de ces deux équations:

$$r(t + \Delta t) + r(t - \Delta t) = 2r(t) + F(t)/m\,(\Delta t)^2 + \vartheta((\Delta t)^4)$$

$$v(t) = r(t + \Delta t) - r(t - \Delta t) / 2\,\Delta t + \vartheta((\Delta t)^2)$$

Précision de calcul

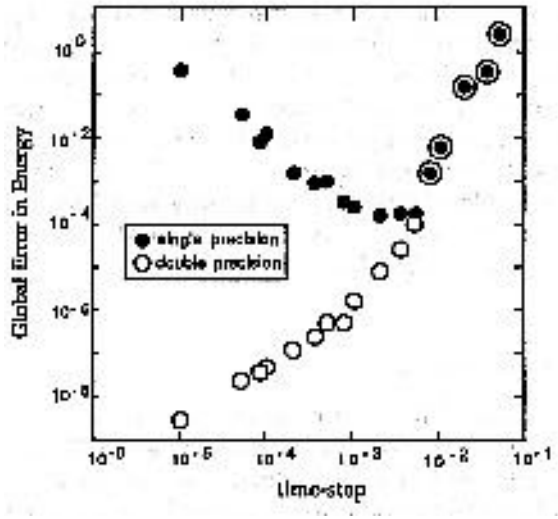

Variation de l'erreur globale de l'énergie en fonction du pas temporel Δt et de la précision de calcul

(SP: 32 octets – DP: 64 octets).

Algorithme de Gear : Predicteur-correcteur

La méthode du prédicteur-correcteur est basée sur trois étapes :

1.) Prédire les positions $r(t+\Delta t)$ et les vitesses $v(t+\Delta t)$ à partir de $r(t)$ et $v(t)$ en utilisant par exemple le développement de Taylor du cinquième ordre.

- $r_i(t+\Delta t) = r_i(t) + r'_i(t)\,\Delta t + r''_i(t)\,(\Delta t)^2/2! + r'''_i(t)\,(\Delta t)^3/3! + r^{(iv)}_i(t)\,(\Delta t)^4/4! + r^{(v)}_i(t)\,(\Delta t)^5/5!$
- $r'_i(t+\Delta t) = r'_i(t) + r''_i(t)\,\Delta t + r'''_i(t)\,(\Delta t)^2/2! + r^{(iv)}\,(\Delta t)^3/3! + r^{(v)}_i(t)\,(\Delta t)^4/4!$
- $r''_i(t+\Delta t) = r''_i(t) + r'''_i(t)\,\Delta t + r^{(iv)}_i(t)\,(\Delta t)^2/2! + r^{(v)}_i(t)\,(\Delta t)^3/3!$
- $r'''_i(t+\Delta t) = r'''_i(t) + r^{(iv)}_i(t)\,\Delta t + r^{(v)}_i(t)\,(\Delta t)^2/2!$
- $r^{(iv)}_i(t+\Delta t) = r^{(iv)}_i(t) + r^{(v)}_i(t)\,\Delta t$
- $r^{(v)}_i(t+\Delta t) = r^{(v)}_i(t)$

2.) Evaluer la force F_i d'interaction à l'instant $(t+\Delta t)$ à partir des positions et des vitesses prédites.

3.) Corriger les positions et leurs dérivées précédemment prédites en utilisant l'écart $\Delta r''$ entre les accélérations prédites et celles évaluées à partir des forces F_i calculées précédemment

- $\Delta r'' = [r''_i(t+\Delta t) - r''^{P}_i(t+\Delta t)]$

Algorithme de Gear : Predicteur-correcteur

- SUBROUTINE PREDICT

```
C
C     use fifth-order Taylor series to predict positions and
C     their derivatives at the next time step
C
      DO 200 I = 1, NATALL
        X(I) = X(I) + X1(I)+X2(I)+X3(I)+X4(I)+X5(I)
        Y(I) = Y(I) + Y1(I)+Y2(I)+Y3(I)+Y4(I)+Y5(I)
        Z(I) = Z(I) + Z1(I)+Z2(I)+Z3(I)+Z4(I)+Z5(I)
C
        X1(I) = X1(I)+2.E0*X2(I)+3.E0*X3(I)+4.E0*X4(I)+5.E0*X5(I)
        Y1(I) = Y1(I)+2.E0*Y2(I)+3.E0*Y3(I)+4.E0*Y4(I)+5.E0*Y5(I)
        Z1(I) = Z1(I)+2.E0*Z2(I)+3.E0*Z3(I)+4.E0*Z4(I)+5.E0*Z5(I)
C
        X2(I) = X2(I)+3.E0*X3(I)+6.E0*X4(I)+10.E0*X5(I)
        Y2(I) = Y2(I)+3.E0*Y3(I)+6.E0*Y4(I)+10.E0*Y5(I)
        Z2(I) = Z2(I)+3.E0*Z3(I)+6.E0*Z4(I)+10.E0*Z5(I)
C
        X3(I) = X3(I)+4.E0*X4(I)+10.E0*X5(I)
        Y3(I) = Y3(I)+4.E0*Y4(I)+10.E0*Y5(I)
        Z3(I) = Z3(I)+4.E0*Z4(I)+10.E0*Z5(I)
C
        X4(I) = X4(I) + 5.E0*X5(I)
        Y4(I) = Y4(I) + 5.E0*Y5(I)
        Z4(I) = Z4(I) + 5.E0*Z5(I)
C
  200  CONTINUE
C
      RETURN
      END
```

Algorithme de Gear : Predicteur-correcteur

- SUBROUTINE CORRECTOR

```
C
C       correct predicted positions and their derivatives
C
 DO 500 I = 1, NATOM
-          XERROR = STPSQH * FX(I) - X2(I)
           YERROR = STPSQH * FY(I) - Y2(I)
           ZERROR = STPSQH * FZ(I) - Z2(I)
C
           X (I) = X (I) + XERROR*ALFA0
           X1(I) = X1(I) + XERROR*ALFA1
           X2(I) = X2(I) + XERROR
           X3(I) = X3(I) + XERROR*ALFA3
           X4(I) = X4(I) + XERROR*ALFA4
           X5(I) = X5(I) + XERROR*ALFA5
C
           Y (I) = Y (I) + YERROR*ALFA0
           Y1(I) = Y1(I) + YERROR*ALFA1
           Y2(I) = Y2(I) + YERROR
           Y3(I) = Y3(I) + YERROR*ALFA3
           Y4(I) = Y4(I) + YERROR*ALFA4
           Y5(I) = Y5(I) + YERROR*ALFA5
C
           Z (I) = Z (I) + ZERROR*ALFA0
           Z1(I) = Z1(I) + ZERROR*ALFA1
           Z2(I) = Z2(I) + ZERROR
           Z3(I) = Z3(I) + ZERROR*ALFA3
           Z4(I) = Z4(I) + ZERROR*ALFA4
           Z5(I) = Z5(I) + ZERROR*ALFA5
  500  CONTINUE
C
       RETURN
       END
```

Verlet versus Gear

L'erreur globale par étape calculée à partir de l'algorithme Gear est nettement inférieure à celle issue de l'algorithme de Verlet

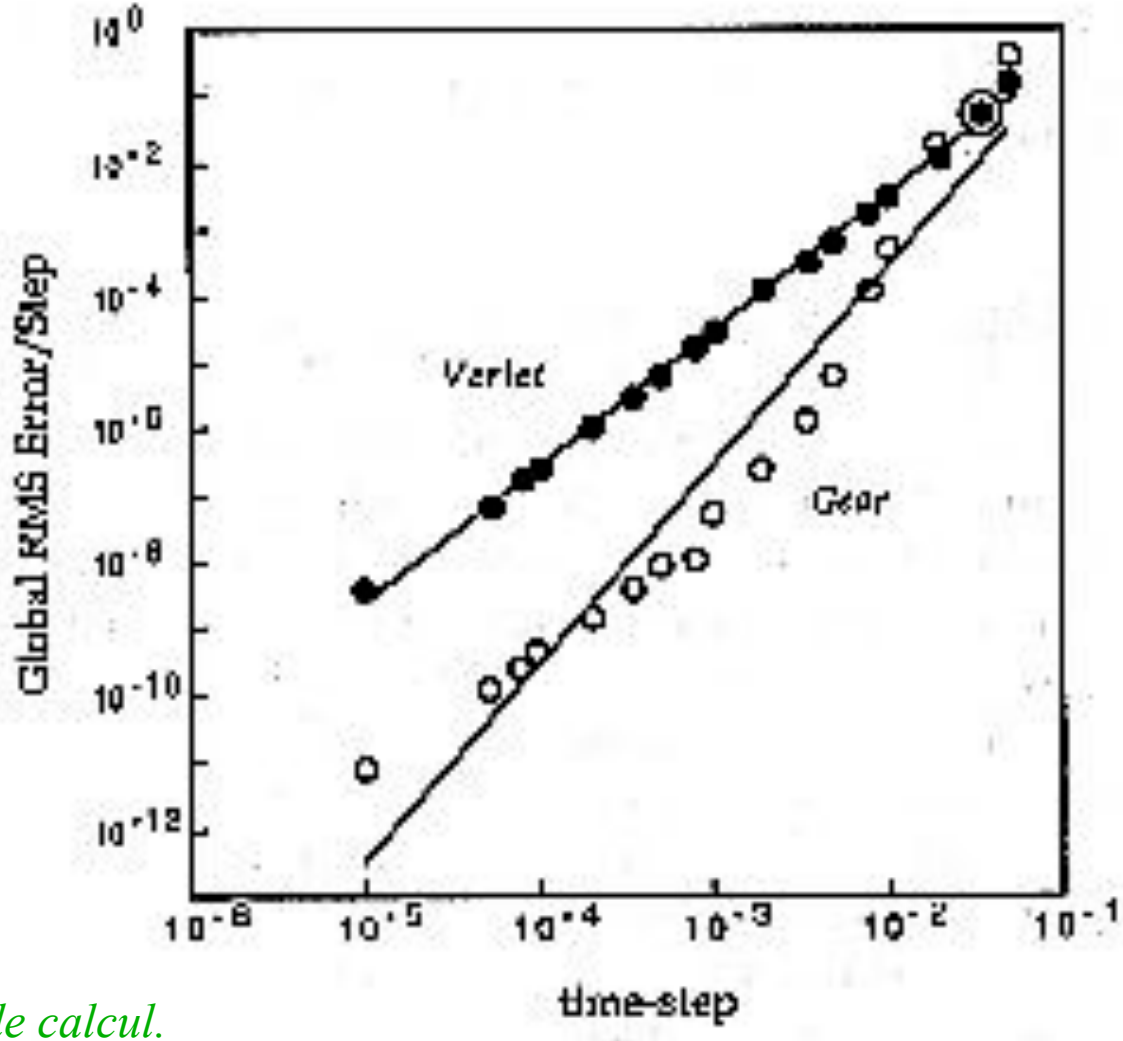

Evolution de l'erreur globale de l'énergie par étape en fonction du pas temporel et de l'algorithme de calcul.

Basic of Molecular Dynamics (MD) simulations

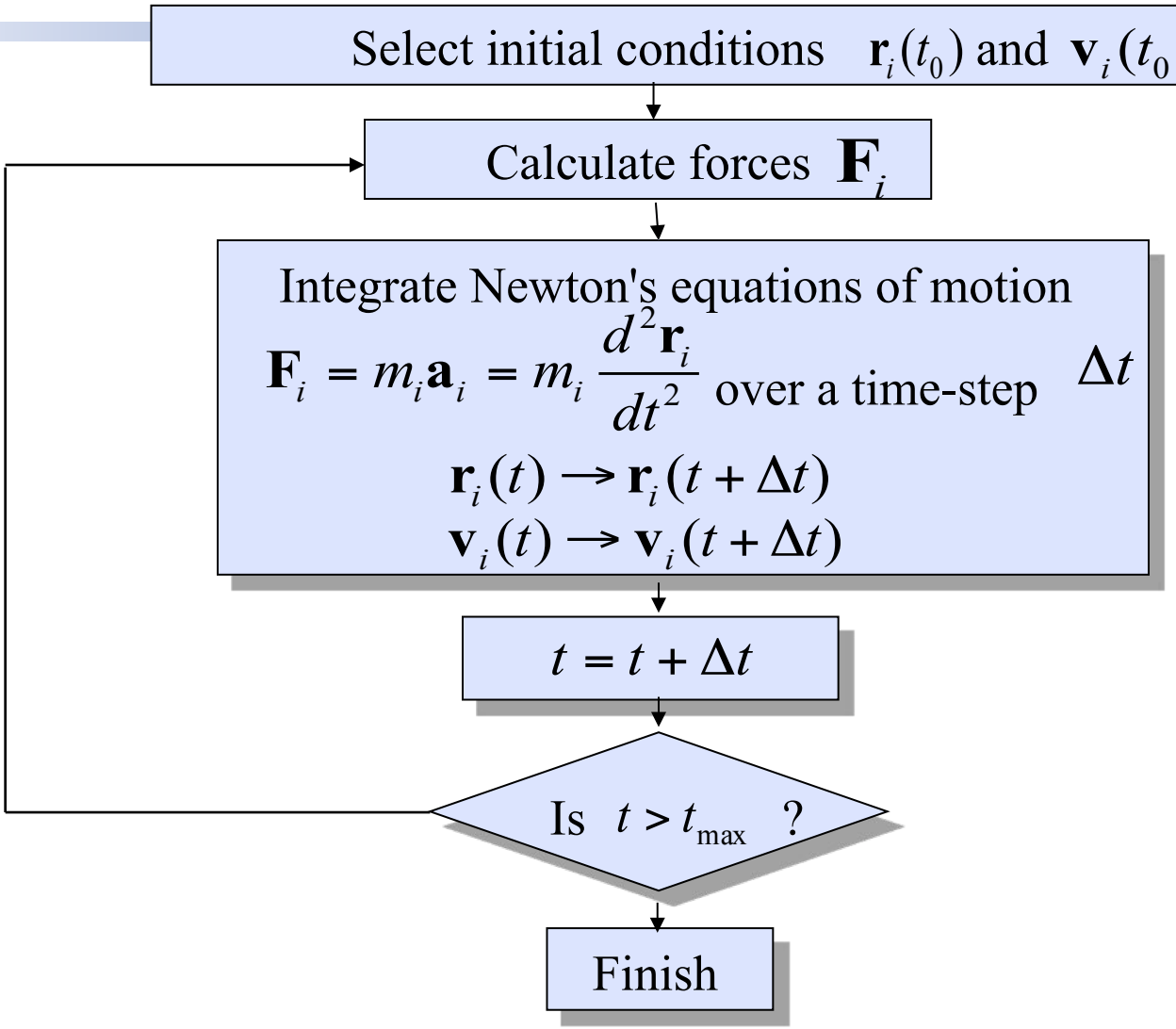

La Force F_i

The forces $\mathbf{F}_i$ can be determined as the negative gradient of the total potential energy of the system:

$$\mathbf{F}_i = -\frac{\partial}{\partial \mathbf{r}_i} V(\mathbf{r}_1, \mathbf{r}_2, ..., \mathbf{r}_N)$$

$$V(\mathbf{r}_1, \mathbf{r}_2, ..., \mathbf{r}_N)$$

Model potentials

- Do not explicitly take into account the electrons
- Parameterized from either experimental data or the results of *ab-initio* calculations of small model systems

The solution of electronic Schrödinger equation

Potentiels modèles

N-N : Potentiel de Morse

$$u(r) = D_e\,[1 - exp - \beta(r - r_e)]$$

D_e: Energie de dissociation

r_e : Longueur de liaison à l'équilibre

Ar-Ar; N_2-N_2 : Potentiel de Lennard-Jones

$$u(r) = 4\varepsilon\,[(\sigma/r)^{12} - (\varepsilon/r)^{6}]$$

ε et σ : paramètres de Lennard-Jones

Caractère "aléatoire" d'une trajectoire

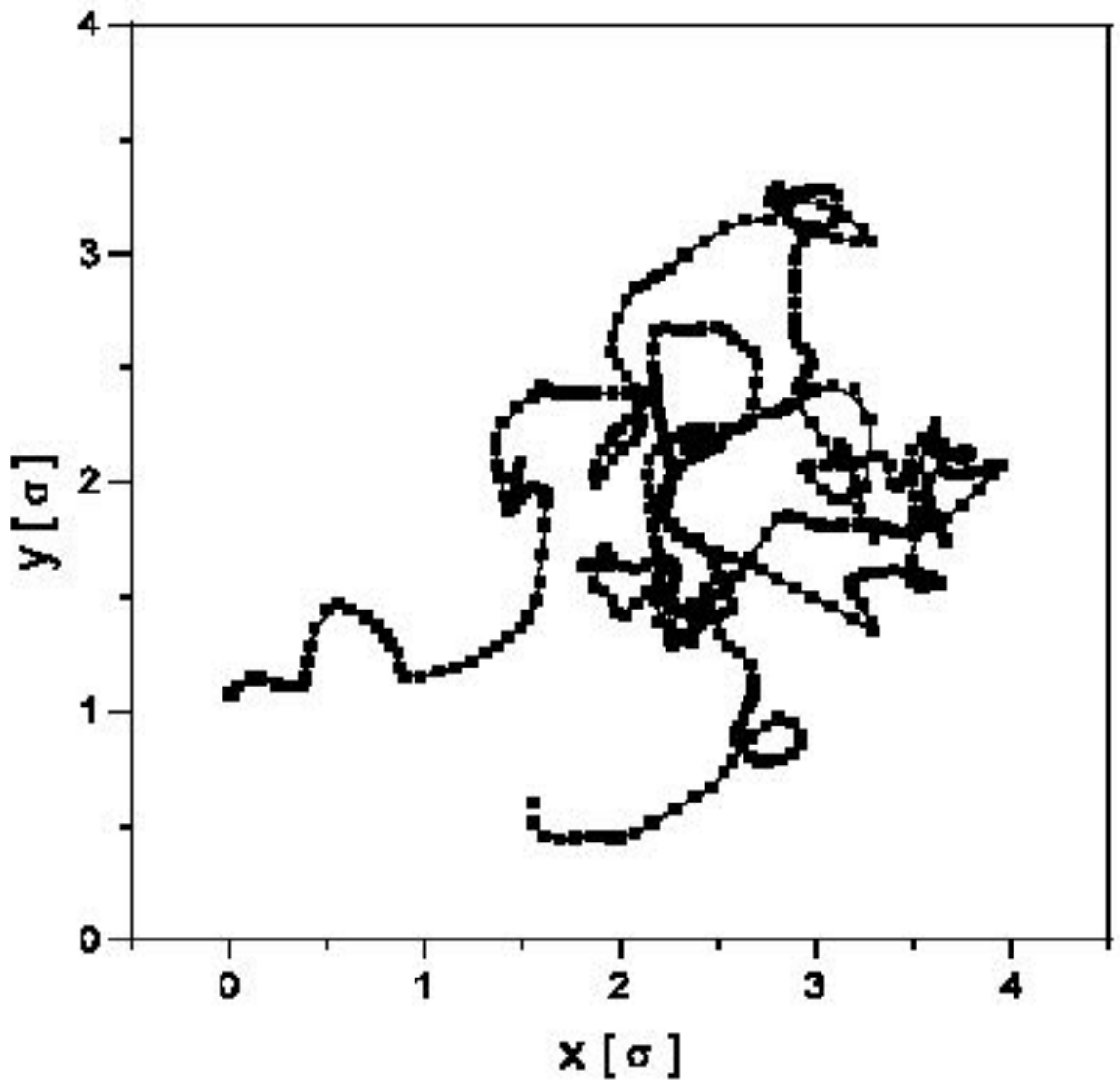

Trajectoire d'une particule *Ar* sous l'influence des 108 autres atomes d'argon.

Conditions aux limites périodiques

- N atomes => 6*N équations différentielles
  => limitation dans le nombre d'atomes

- e.g. simulation d'azote liquide avec 500 molécules
- => L(cube de calcul) ~ 8.5 σ (pour assurer une densité liquide)
- MAIS L(interaction paroi-molécule) ~ 4…10 σ

⇒ information sur l'interaction de molécules N_2 avec la paroi et non sur l'azote liquide

Solution: conditions aux limites périodiques

Conditions aux limites périodiques

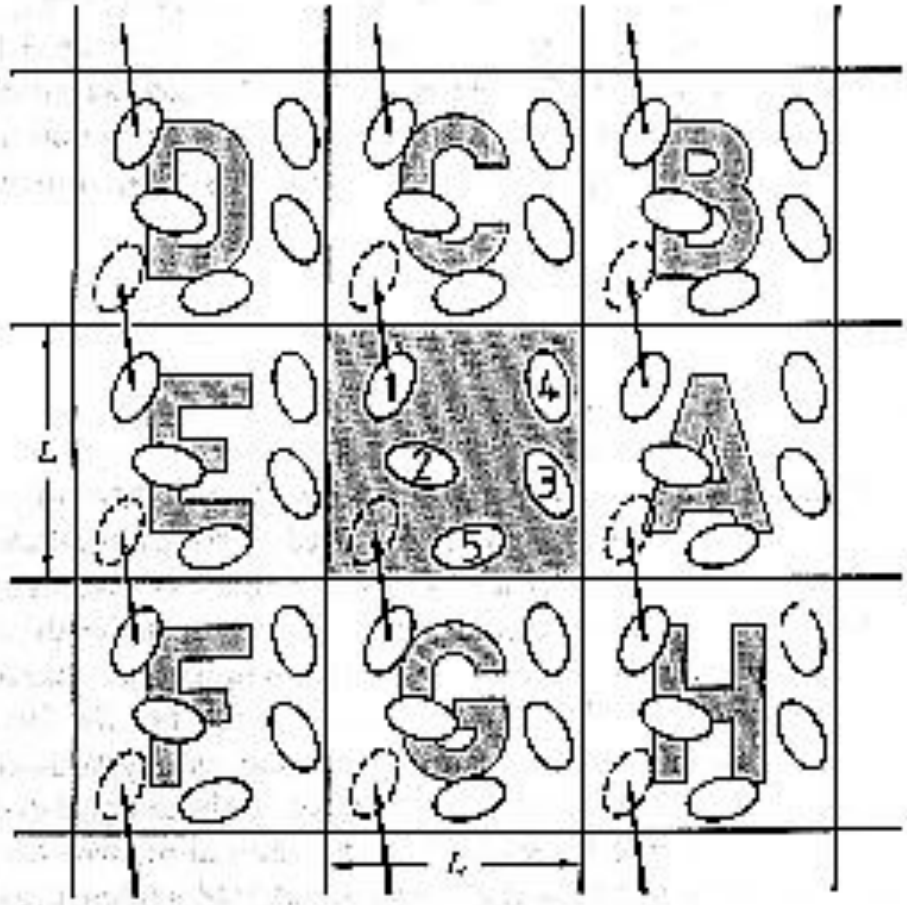

Fig A two-dimensional periodic system. Molecules can enter and leave each box across each of the four edges. In a three-dimensional example, molecules would be free to cross any of the six cube faces.

Les propriétés des systèmes complexes comprenant 10^{23} particules peuvent être aussi précisément calculées à l'aide de systèmes modèles comprenant moins de 10^{3} particules.

Fonctions de corrélation

- Calcul des corrélations de paires

$$RDF(r) = \frac{\sum_{k=1}^{M} N_k(r, \Delta r)}{M \cdot N \cdot V(r, \Delta r)} \qquad (3.11)$$

gaz/liquide

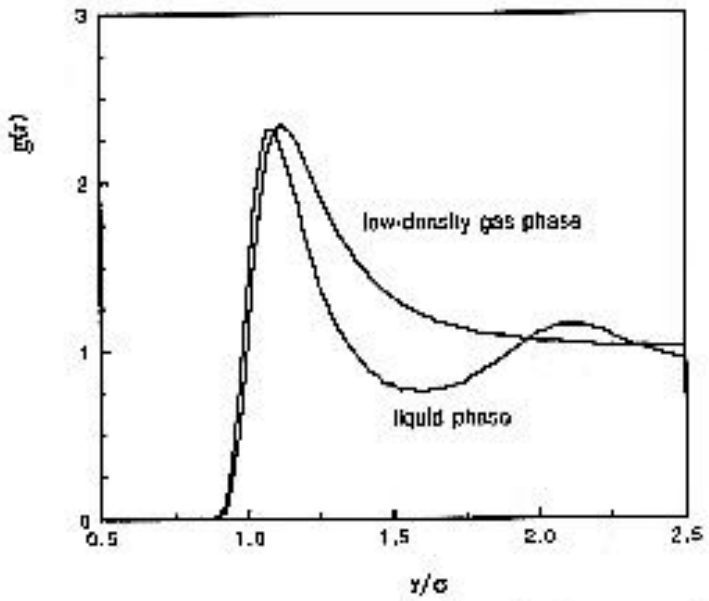

FIGURE Comparison of radial distribution functions for gas and liquid phases of the Lennard-Jones fluid, both at $\langle T^* \rangle = 1.178$. The gas phase curve was obtained from the low-density limit (6.103), while the liquid phase curve was obtained from a molecular dynamics simulation at $\rho^* = 0.7$.

liquide/solide amorphe

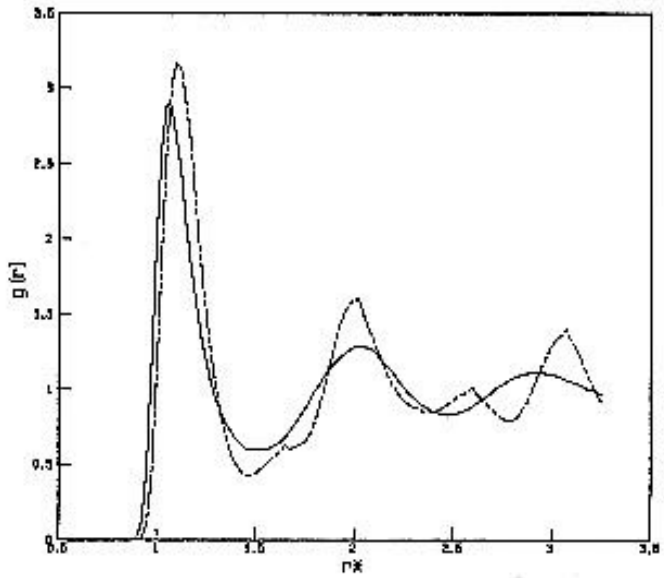

FIGURE The radial distribution function $g(r)$ may often be used to distinguish a fluid state (continuous line) from a metastable solidlike state (broken line). These curves are from simulations that used the Lennard-Jones potential with 256 atoms at a density of $\rho\sigma^3 = 0.9$. The fluid state was at $kT/\varepsilon = 1.087$, while the metastable state was at $kT/\varepsilon = 0.80$

Fonctions de corrélation

•Calcul des corrélations de paires (suite)

cristaux solides parfaits

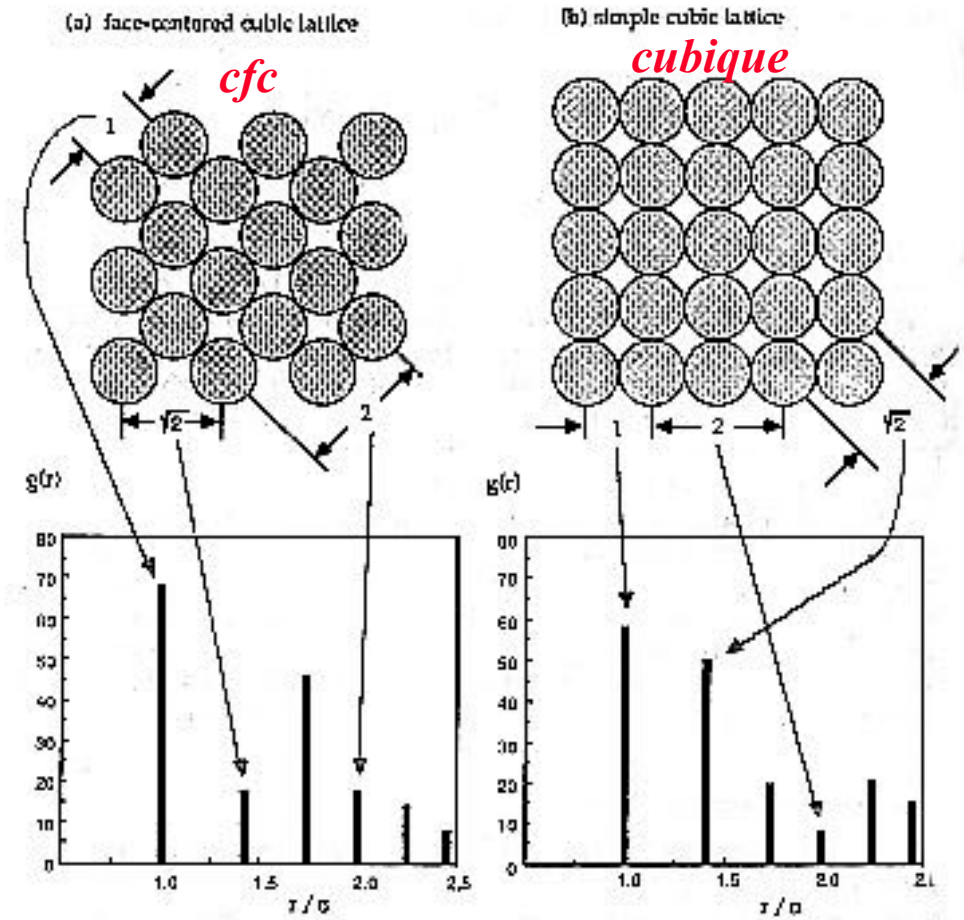

FIGURE Use of the radial distribution function to discriminate between crystal lattice structures. (*a*) Structure of a close-packed ($\rho\sigma^3 = 1.414$) fcc lattice computed for 108 atoms and periodic boundary conditions. (*b*) Structure of a close-packed ($\rho\sigma^3 = 1.953$) simple cubic lattice computed using 125 atoms and periodic boundary conditions. The sketches above the plots show one plane from each three-dimensional lattice.

Fonctions de corrélation

- Calcul des déplacements quadratiques moyens

$$MSD(t) = \frac{1}{N}\left(\sum_{i=1}^{N}[\vec{r}_i(t_0 + t) - \vec{r}_i(t_0)]^2\right)$$

coefficient de diffusion

$$D = \frac{1}{6N}\frac{d}{dt}\left(\sum_{i=1}^{N}[\vec{r}_i(t_0 + t) - \vec{r}_i(t_0)]^2\right)$$

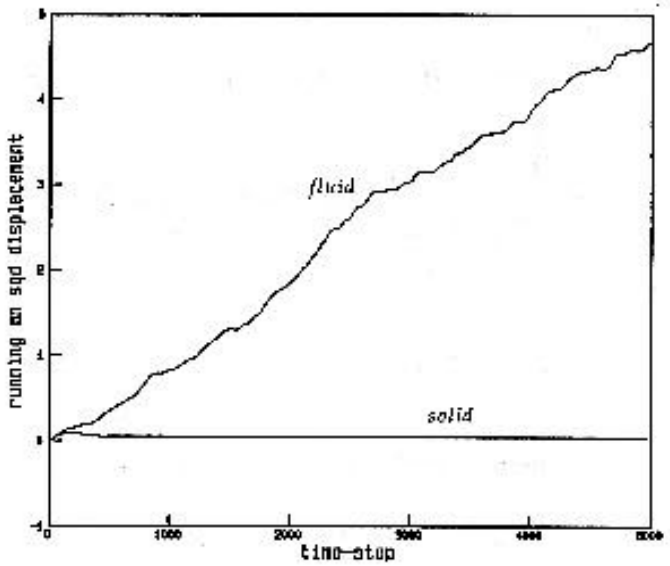

FIGURE The running mean-square displacement (msd) can often be used to distinguish a fluid from a solid. Here the running msd, $\Delta r^{*2}(t)$ from (5.33), of Lennard-Jones atoms in a fluid state (upper line) is compared with that in a solid state (lower line). The simulations were each done using 256 atoms at $\rho\sigma^3 = 0.9$. The fluid state was at $\langle kT/\epsilon \rangle = 1.087$, while the metastable solid was at $\langle kT/\epsilon \rangle = 0.80$.

- Calcul de l'auto-corrélation de vitesses

$$VACF(t) = \frac{1}{N}\left(\sum_{i=1}^{N}\vec{v}_i(t_0)\cdot\vec{v}_i(t_0 + t)\right) \qquad (3.14)$$

Température d'un agrégat

$$\vec{L} = \sum_{i=1}^{N} \vec{r_i} \times \vec{p_i} \tag{3.2}$$

$$\vec{L} = \mathbf{I} \cdot \vec{\omega} \tag{3.3}$$

$$\mathbf{I}_{\alpha\alpha} = \sum_{i=1}^{N} m_i (r_i^2 - \alpha_i^2), \tag{3.4}$$

$$\mathbf{I}_{\alpha\beta} = -\sum_{i=1}^{N} m_i \alpha_i \beta_i \tag{3.5}$$

$$E_{rot} = \frac{1}{2} \vec{\omega} \cdot \vec{L}. \tag{3.6}$$

$$E_{kin} = \frac{1}{2m_i} \sum_{i=1}^{N} p_i^2 \tag{3.7}$$

$$E_{vib} = E_{kin} - E_{rot}. \tag{3.8}$$

$$T_{vib} = 2\langle E_{vib} \rangle / (3N - 6) k_B \tag{3.9}$$

$$T_{rot} = 2\langle E_{rot} \rangle / 3k_B \tag{3.10}$$

Formation et fragmentation d'un agrégat Ar_{13}

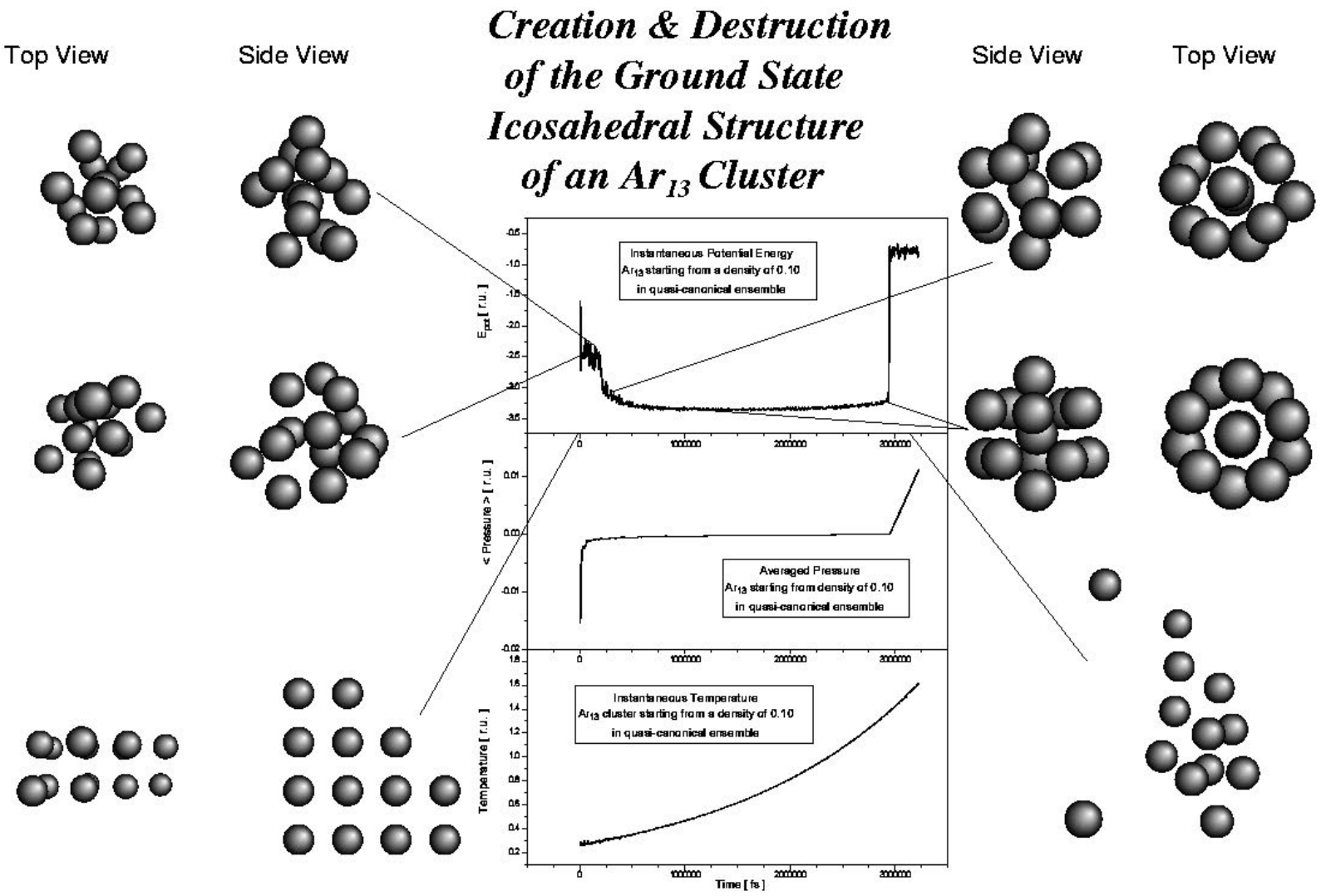

Formation et fragmentation d'un agrégat Ar_{13}

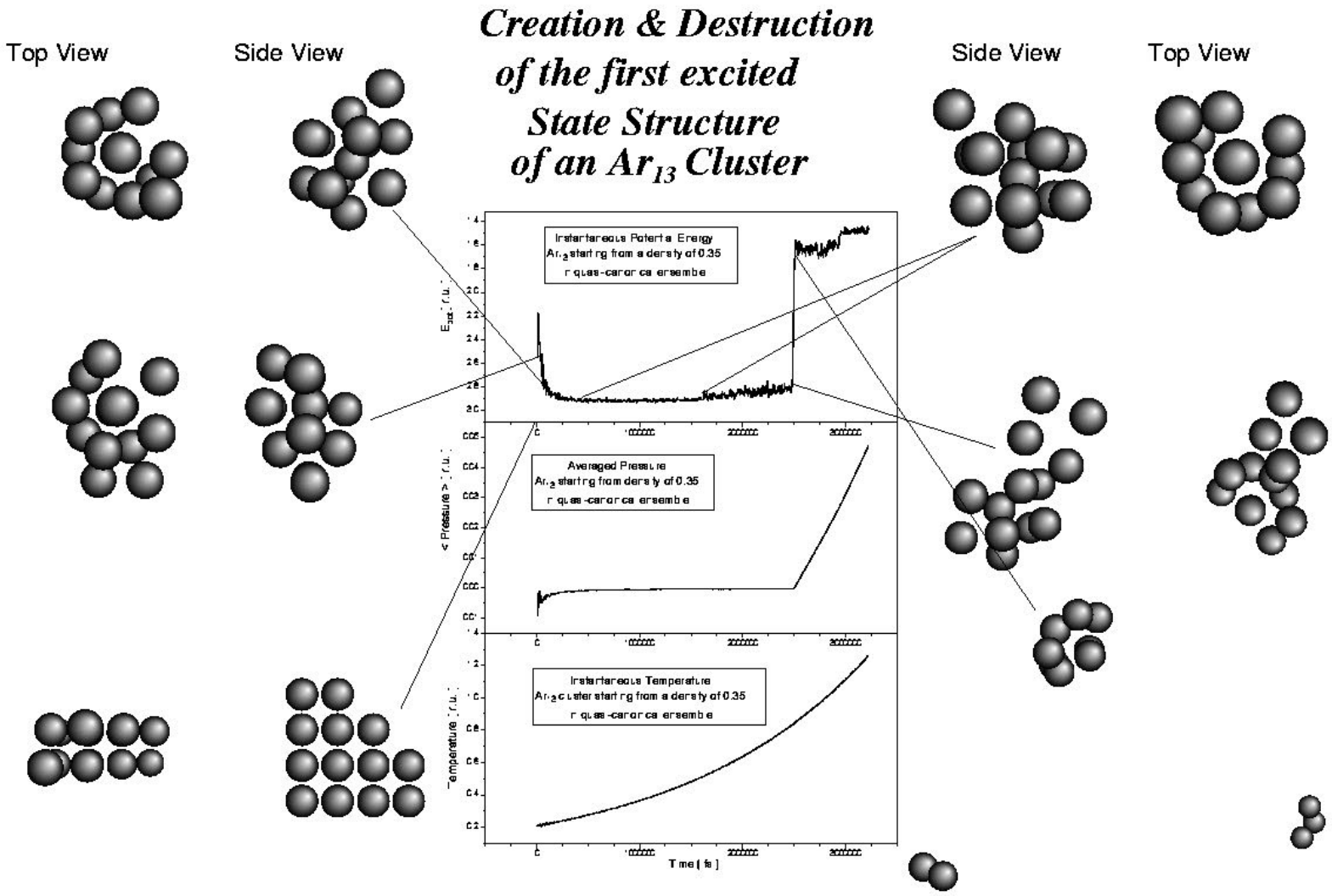

« Toupie symétrique » et « toupie asymétrique »

Trajectoire d'un atome de l'icosaèdre

Ar_{13}

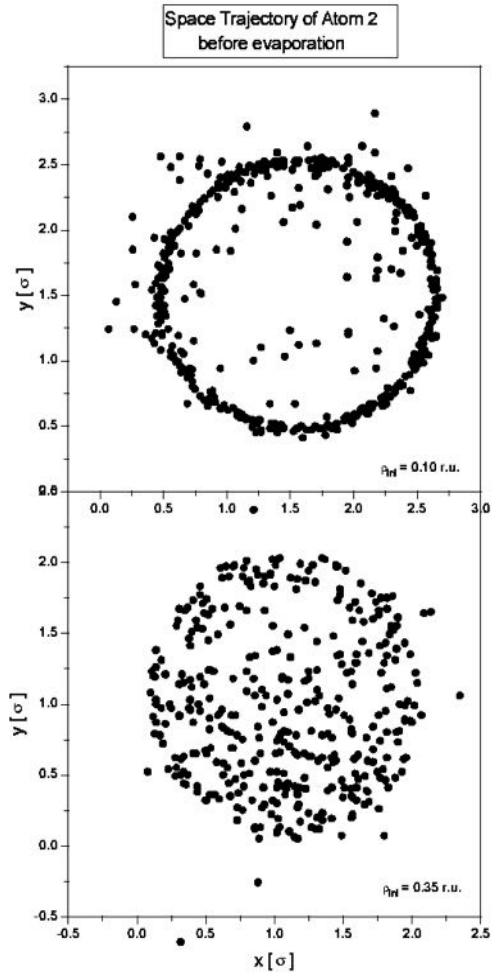

état fondamental

état excité

Formation et fragmentation d'un agrégat Ar_{13}

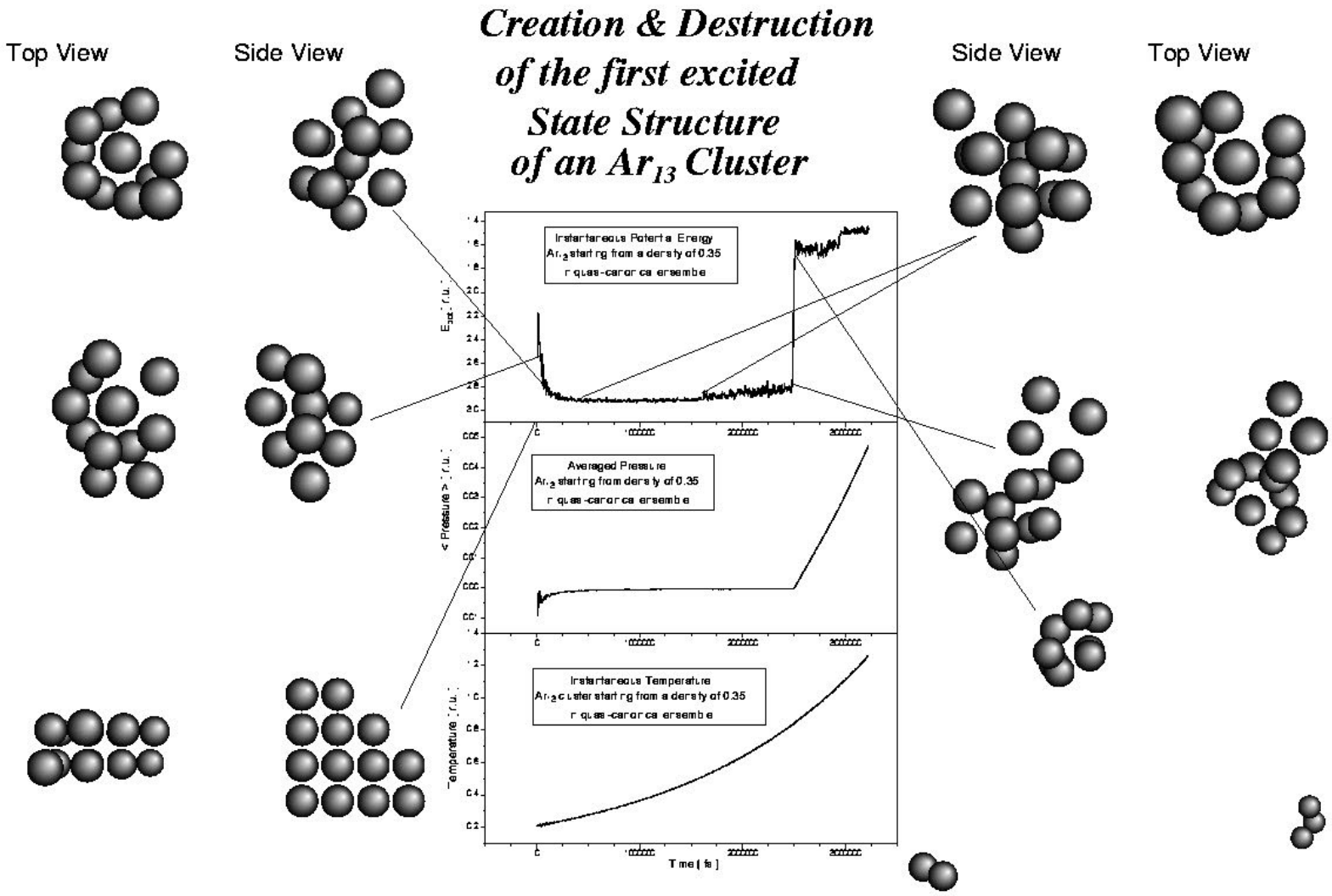

« Mort d'un dimer »

Trajectoire d'un atome du dernier dimer issu de la fragmentation de notre Ar_{13}

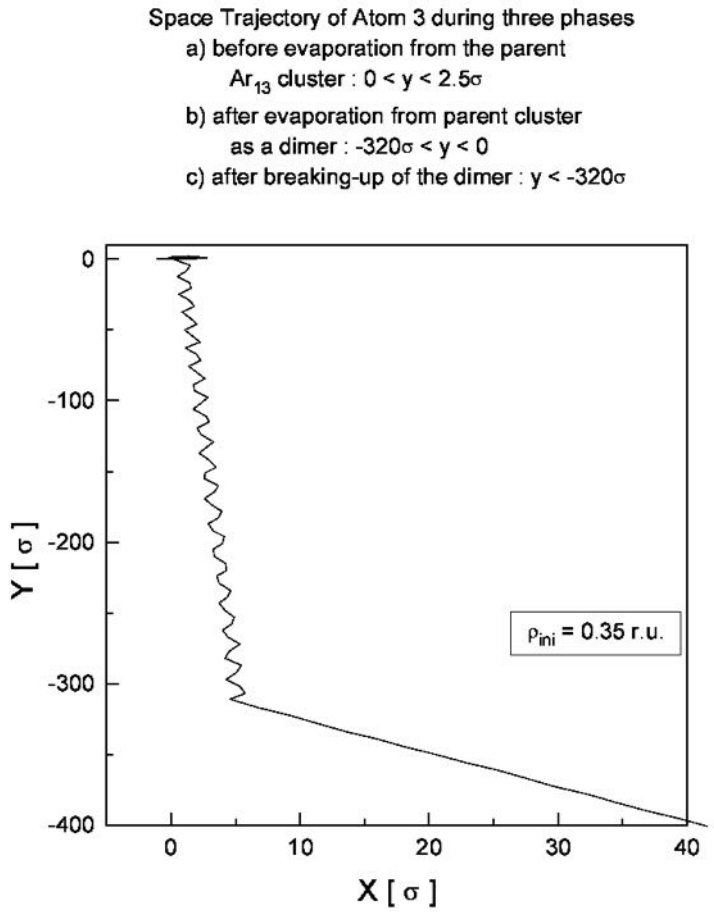

Scattering of mixed rare gas clusters from a graphite surface

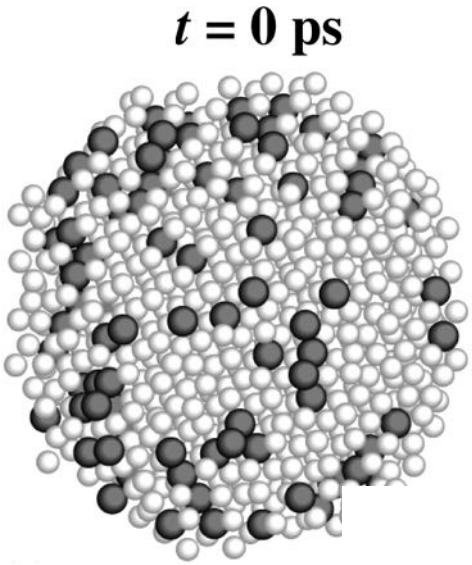

Model of a hard surface:

at $z \leq 0 \Rightarrow v_z = -v_z$

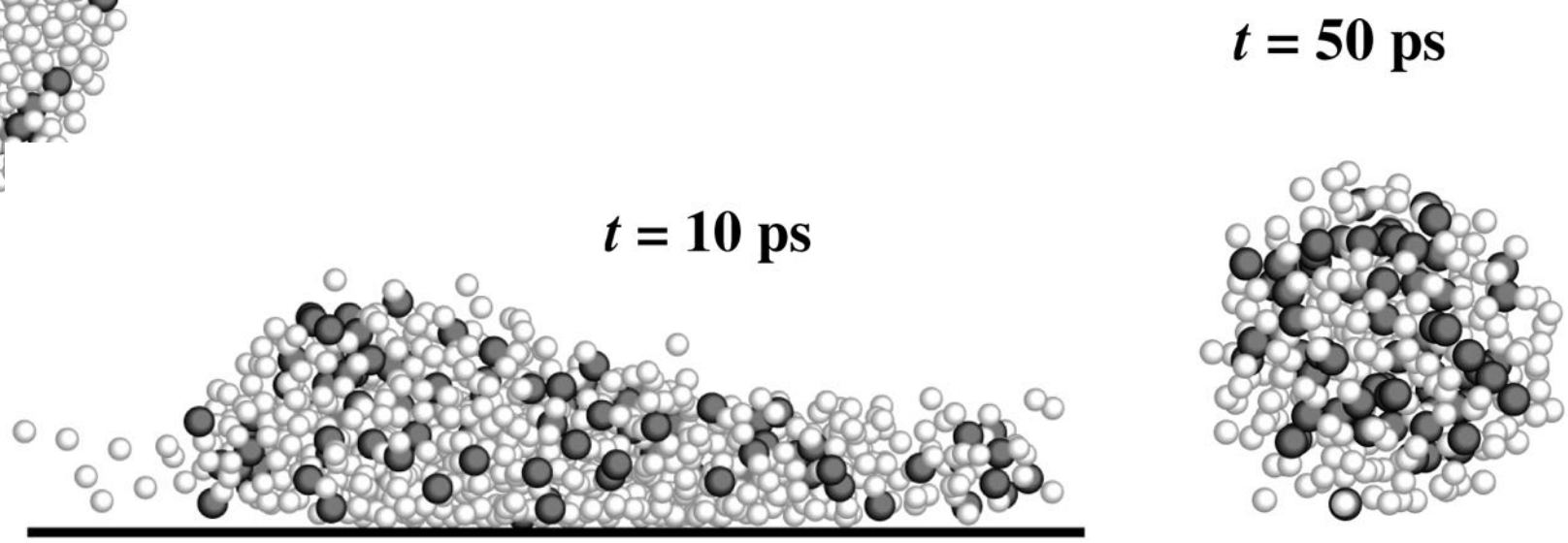

Exemple : « Pick-up »

Cellule de calcul pour le ramassage collisionnel

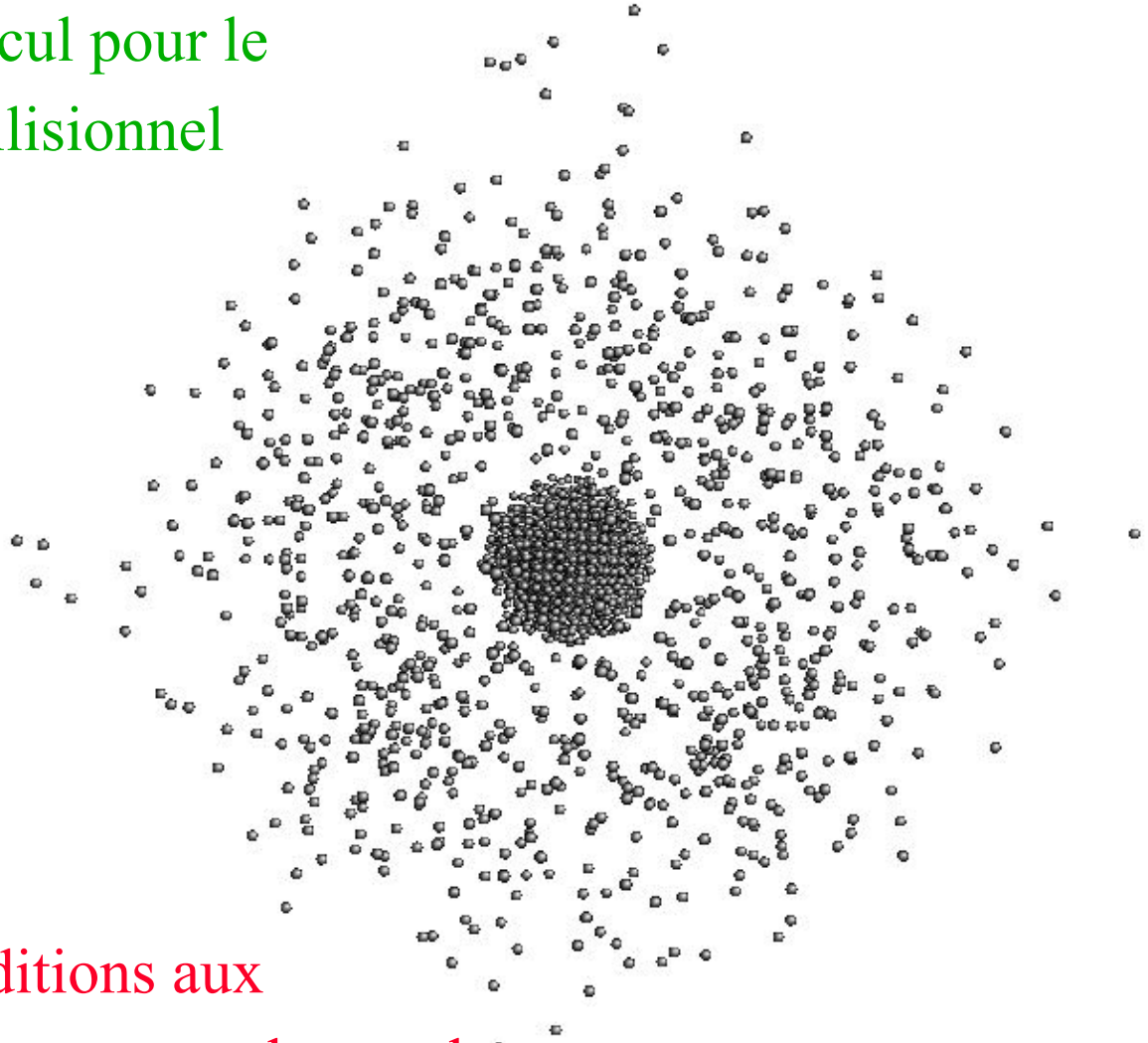

Exemple: conditions aux limites périodiques pour le gaz de tampon

Exemple : « Pick-up »

MD simulation of Kr atom “pick-up” by Ar_{216} under realistic experimental conditions

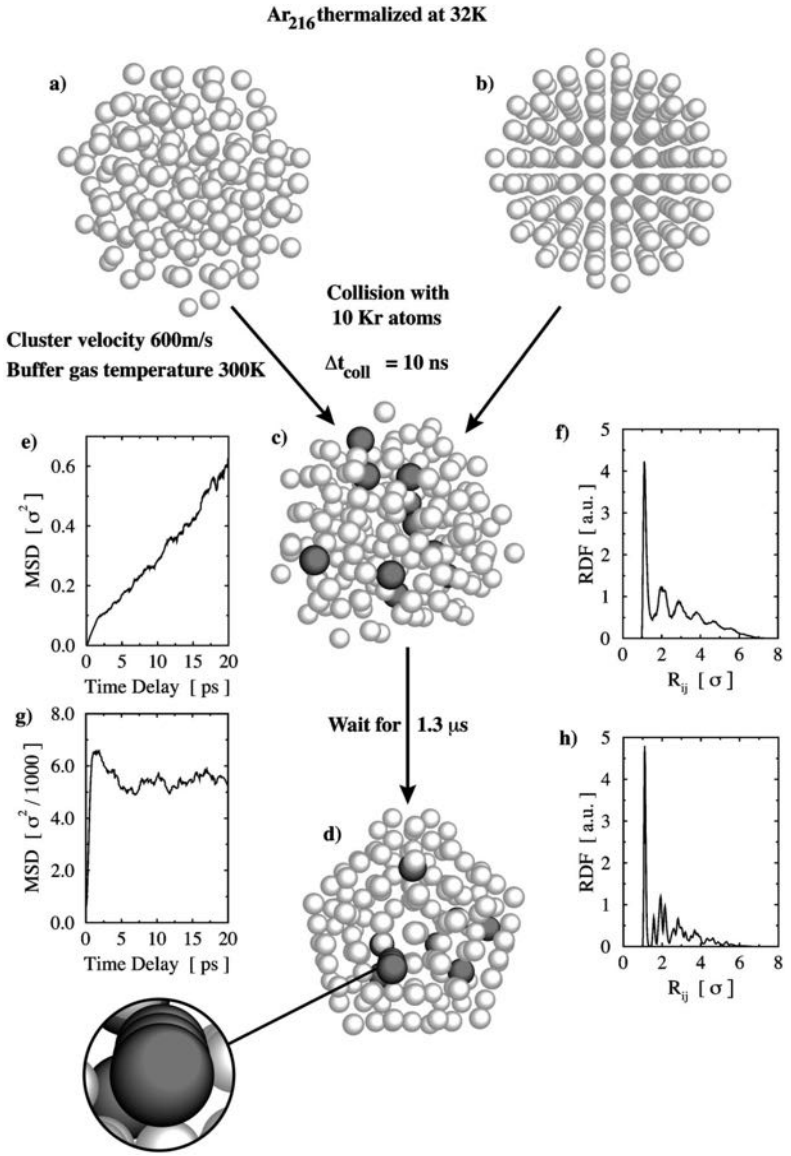

Structure des agrégats mixtes

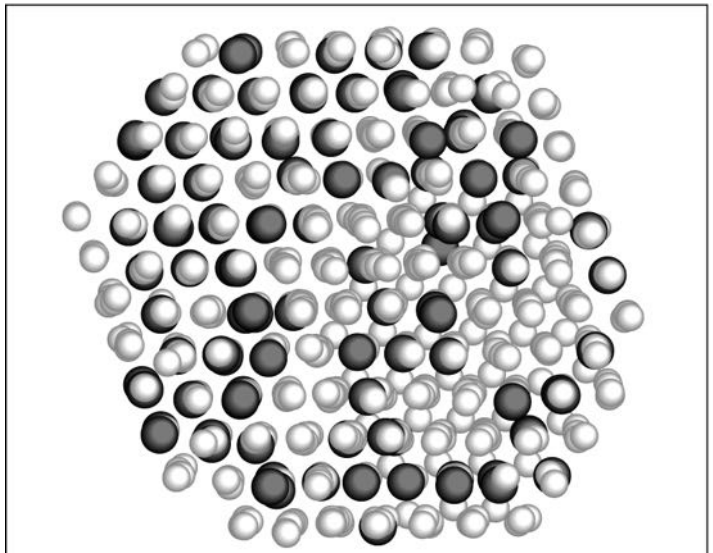

instantané

$Ar_{904}Kr_{140}$

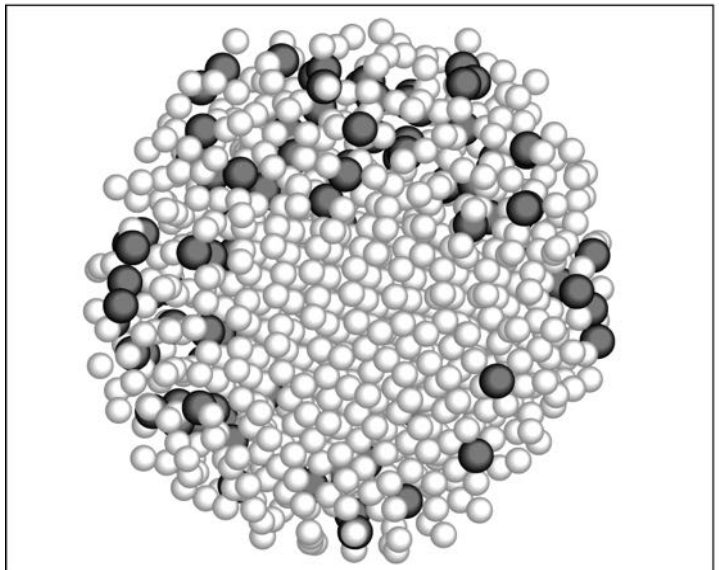

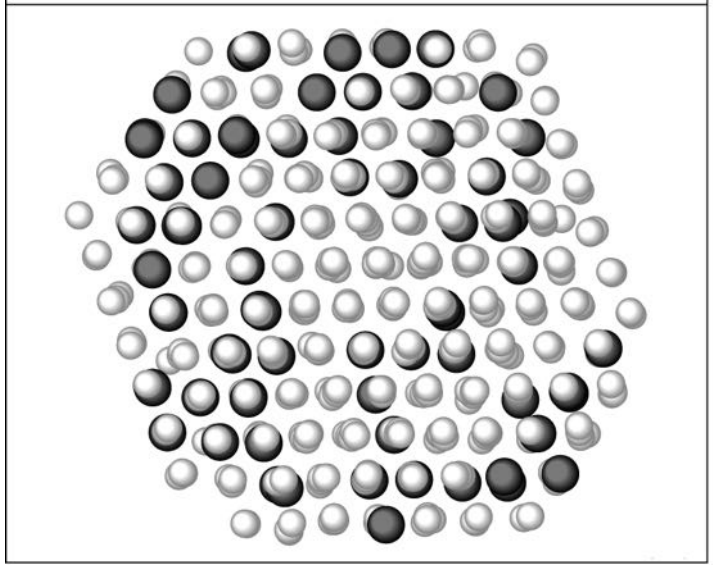

$Ar_{904}Xe_{100}$

coupe

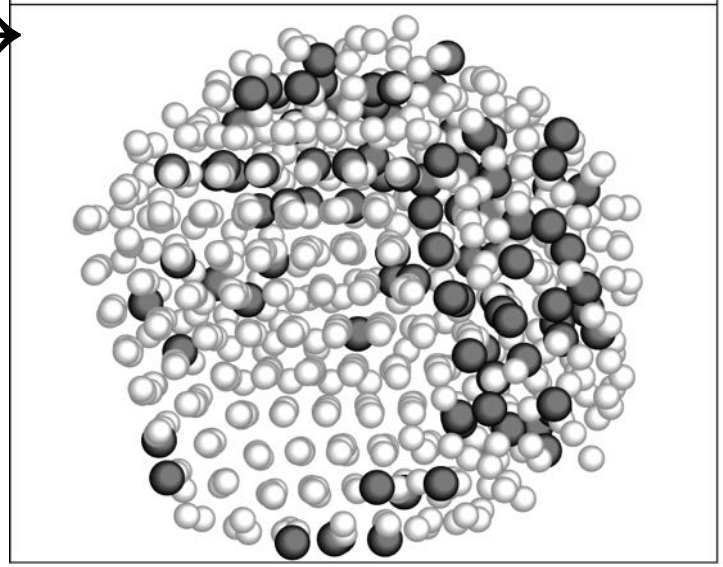

Fonctions de corrélation de paires

$Ar_{904}Kr_{140}$

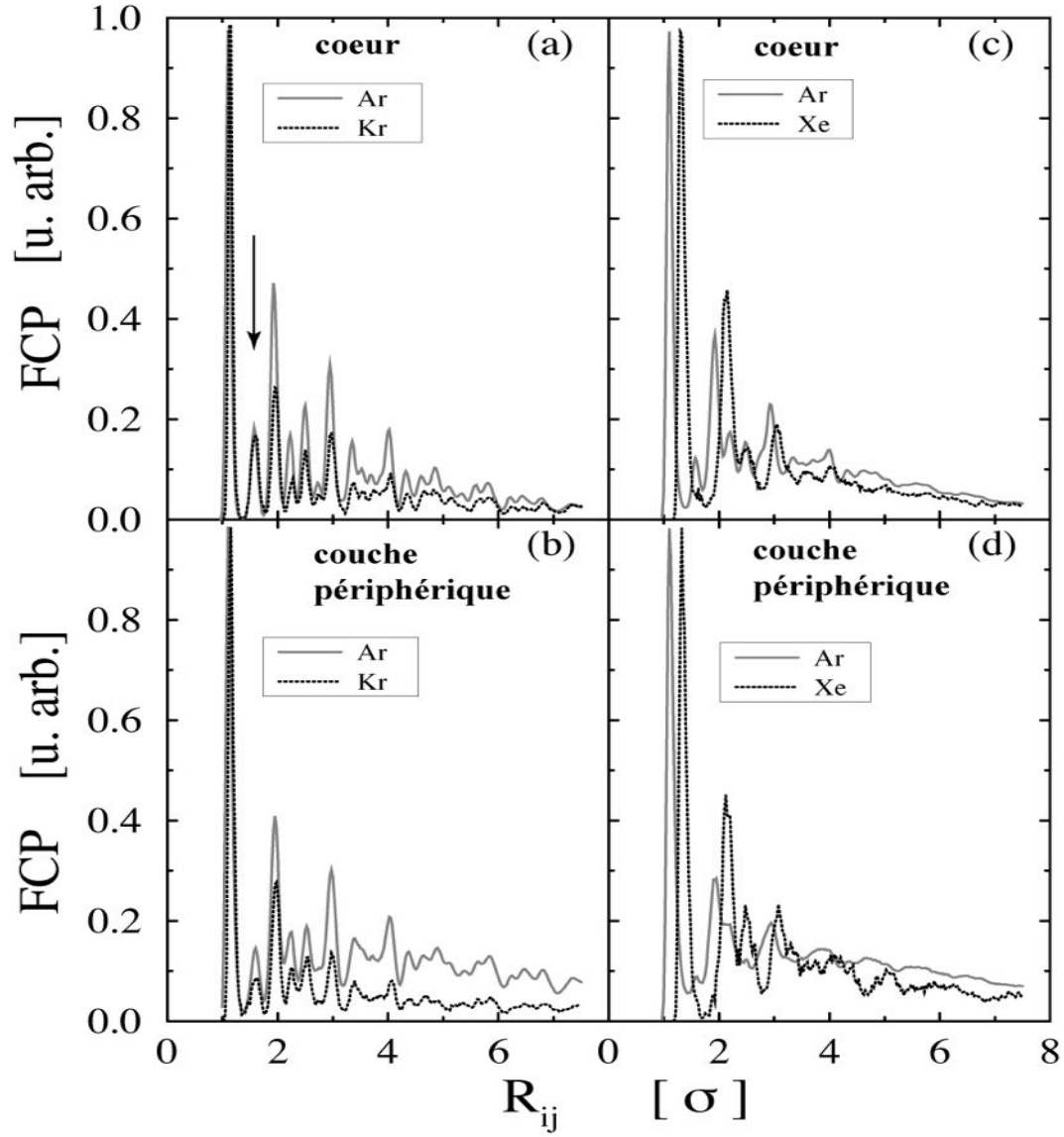

$Ar_{904}Xe_{100}$

Dynamique intra-agrégats

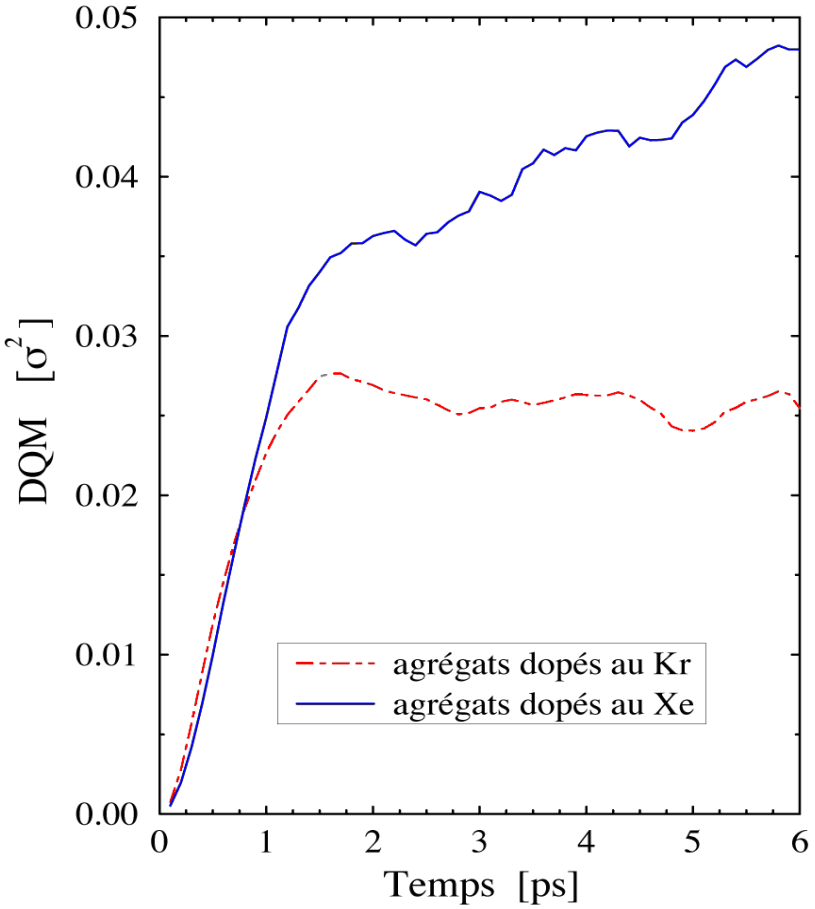

Déplacements quadratiques moyens des atomes de dopant

Dynamique intra-agrégats

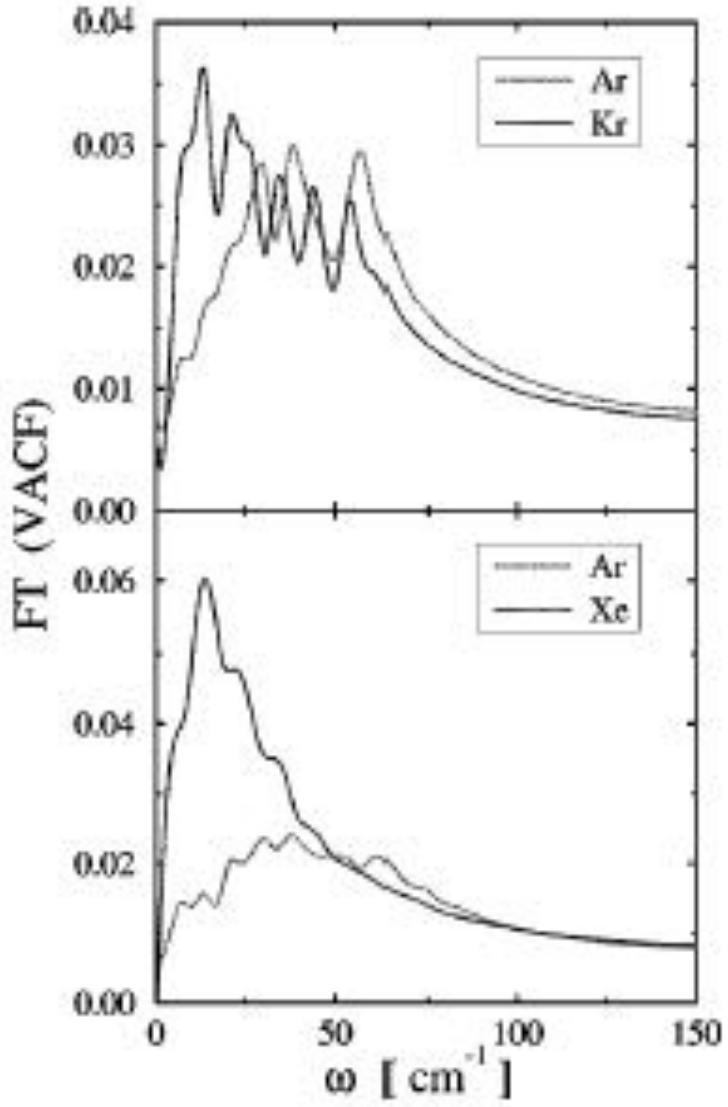

Spectre de fréquence

Model potentials for chemical reactions

Lennard-Jones potential

$$V(r_{ij}) = 4\varepsilon\left[\left(\frac{\sigma}{r_{ij}}\right)^{12} - \left(\frac{\sigma}{r_{ij}}\right)^{6}\right]$$

- Describes well rare gas systems

*Empirical interatomic Ohira-Tersoff potential **

- Describes well pure and hydrogenated c-Si and a-Si bulk materials

$$V = \frac{1}{2}\sum_i \sum_{j\neq i} [a_{ij} V_r(r_{ij}) + b_{ij} V_a(r_{ij})] f_c(r_{ij}),$$

where

$$V_r(r_{ij}) = A_{ij} exp(-\lambda_{ij} r_{ij}), V_a(r_{ij}) = -B_{ij} exp(-\mu_{ij} r_{ij}),$$

$$a_{ij} = \epsilon_{ij}(1 + \beta_i^{n_i} \tau_{ij}^{n_i})^{-1/2n_i}, b_{ij} = \chi_{ij}(1 + \beta_i^{n_i} \xi_{ij}^{n_i})^{-m_i/2n_i},$$

$$\tau_{ij} = \sum_{k\neq i,j} f_c(r_{ik}) \delta_{ik} g(\theta_{ijk}),$$

$$\xi_{ij} = \sum_{k\neq i,j} f_c(r_{ik}) \omega_{ik} g(\theta_{ijk}) exp[\sigma_{ik}(r_{ij} - r_{ik})],$$

$$g(\theta_{ijk}) = 1 + \frac{c_i^2}{d_i^2} - \frac{c_i^2}{d_i^2 + (h_i - cos\theta_{ijk})^2},$$

$$f_c(r_{ij}) = \begin{cases} 1, & r_{ij} < R_{ij} \\ \frac{1}{2} + \frac{1}{2} cos\frac{\pi(r_{ij} - R_{ij})}{S_{ij} - R_{ij}}, & R_{ij} < r_{ij} < S_{ij}. \\ 0, & r_{ij} > S_{ij} \end{cases}$$

* T. Ohira, T. Inamuroa, and T. Adachi, Mat. Res. Spc. Symp. Proc. **34**, 565 (1994).

But sometimes the model potential does not work as it should...

- To describe H_2, SiH_m(m=1,4).

H-H bond stretching in H_2

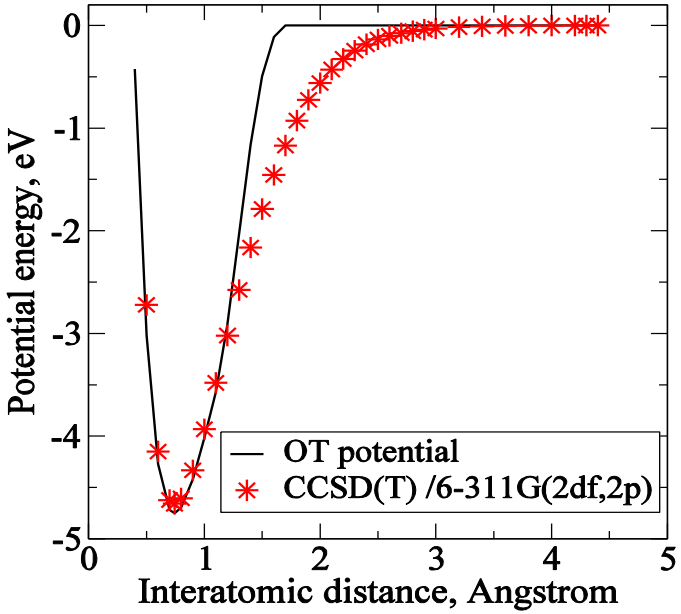

Si-H bond stretching in SiH_3

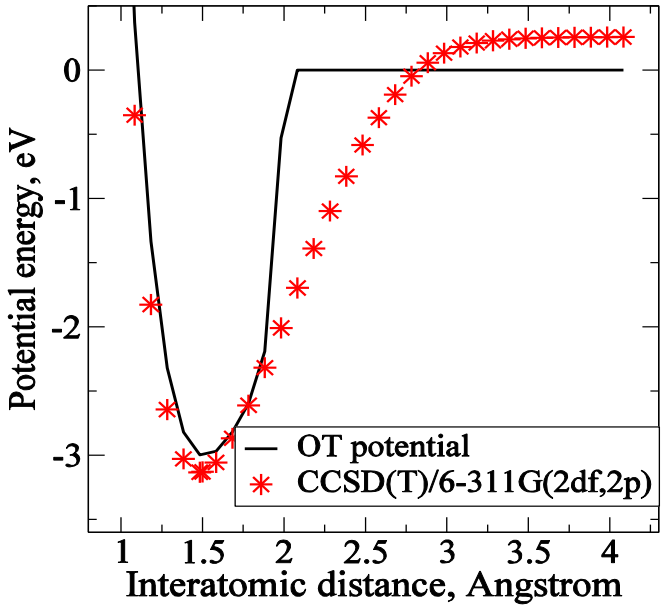

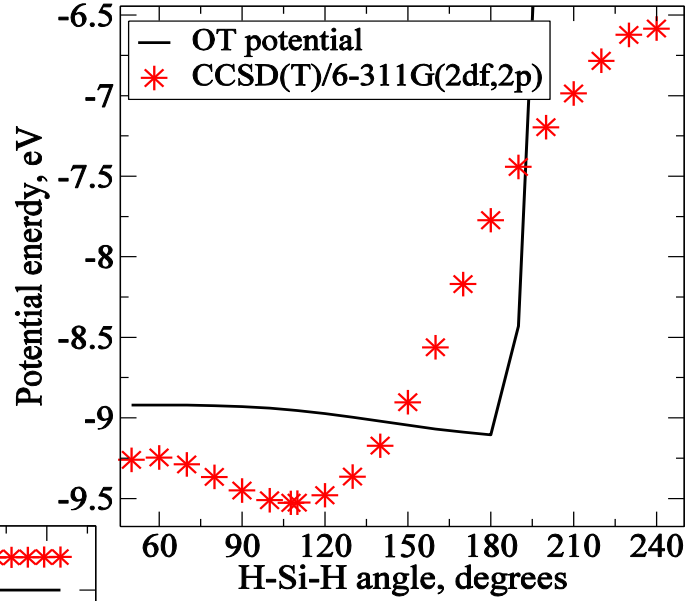

H-Si-H angle bending in SiH_3

Parameter optimization

- Optimization procedure*

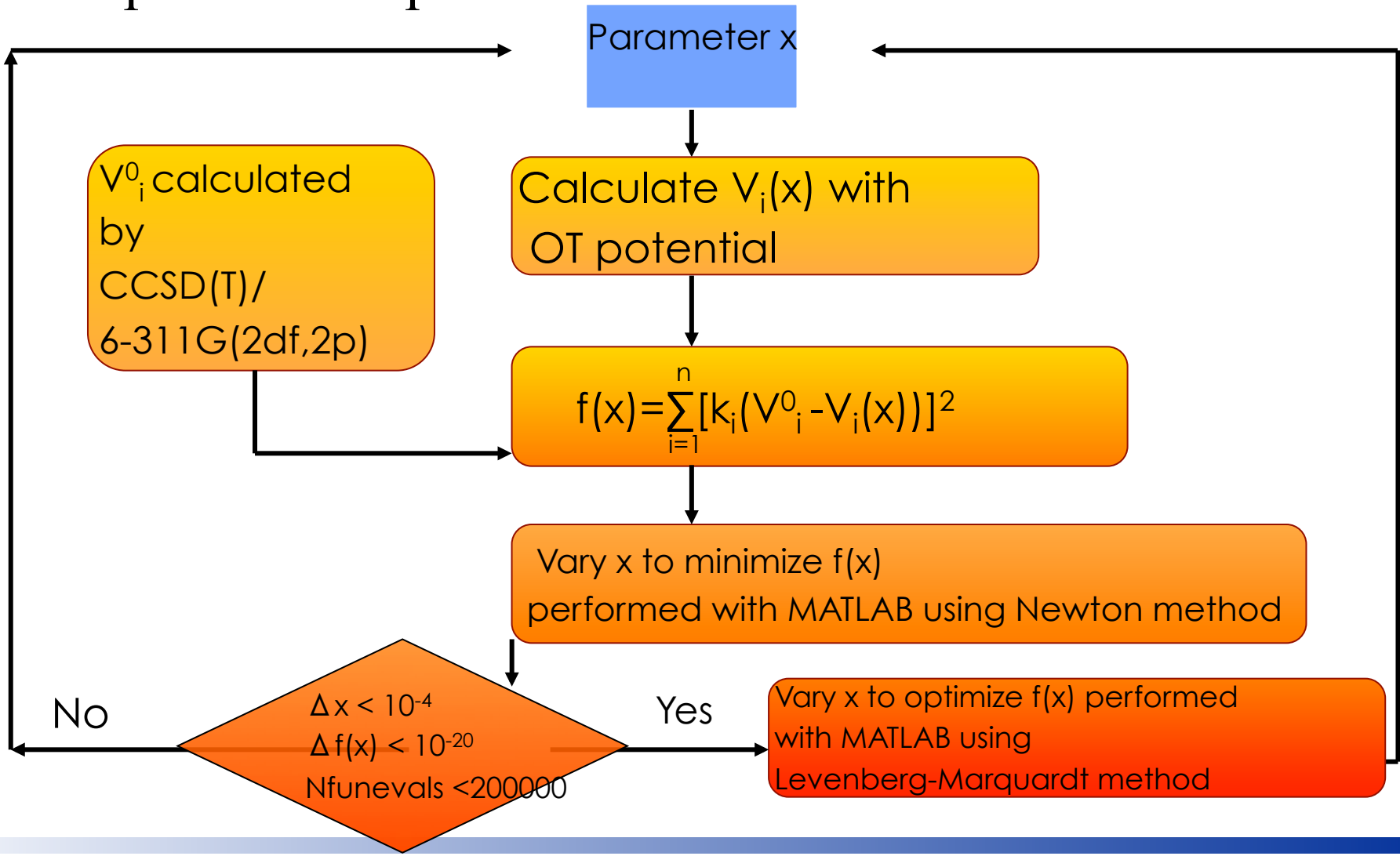

* N. Ning, G. Dolgonos, W. Morscheidt, A. Michau, K. Hassouni, and H. Vach , *Comput. Meth. Sci. Eng.* 1, (2007),

Performance of the mOT potential

- To describe H_2, SiH_m(m=1,4).

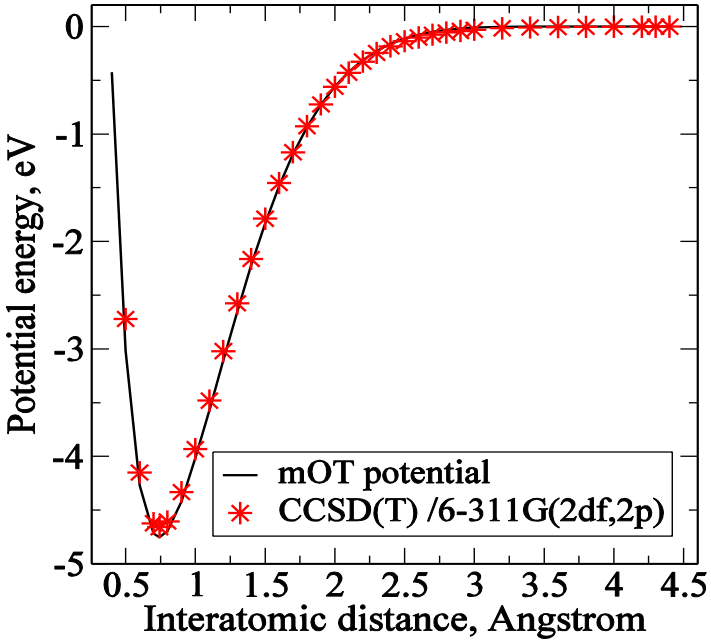

H-H bond stretching in H_2

Si-H bond stretching in SiH_3

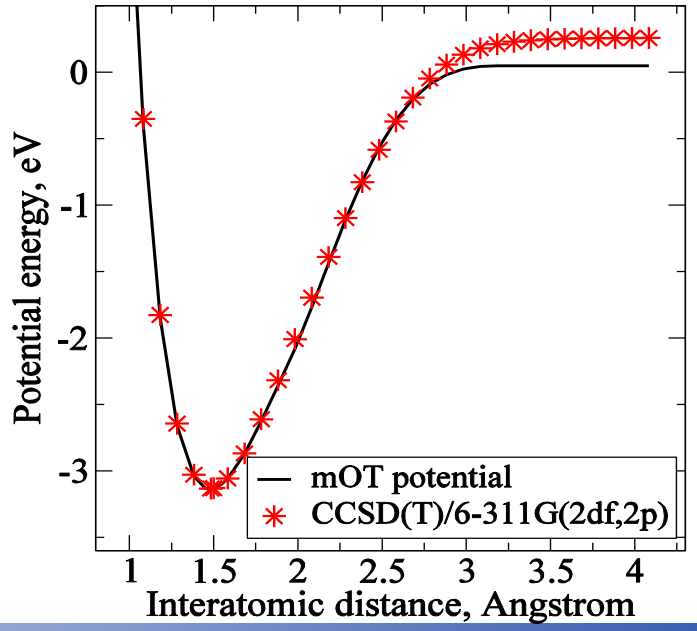

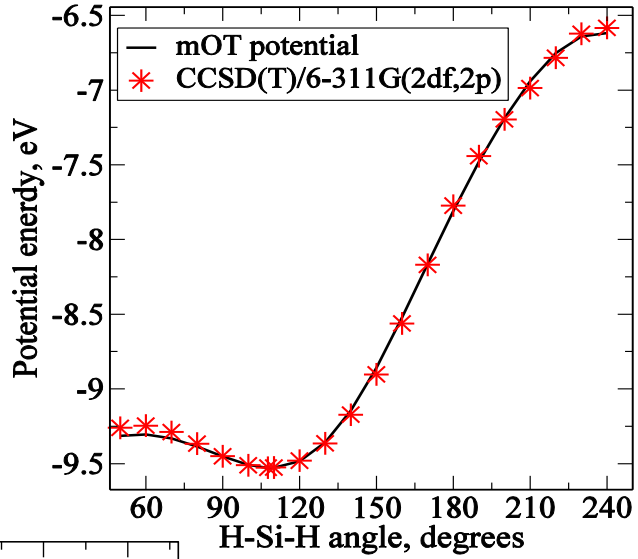

H-Si-H angle bending in SiH_3

What happens to clusters when they interact with H-atoms in the reactor?

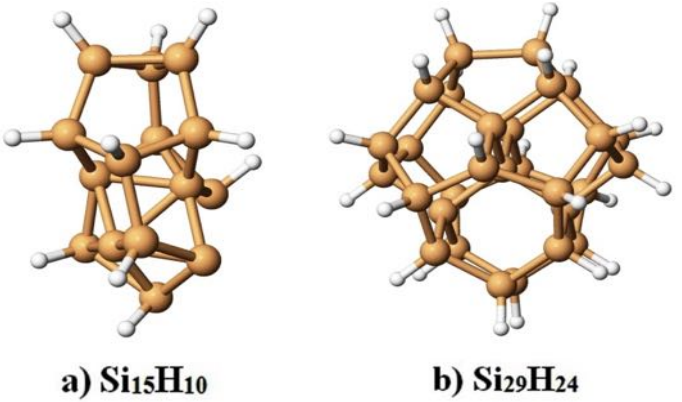

a) $Si_{15}H_{10}$ b) $Si_{29}H_{24}$

- Clusters: $Si_{15}H_{10}$ and $Si_{29}H_{24}$ - initial temperature 300K
- H-atoms are sent to the clusters, one after the other, with a thermal impact energy of 0.025 eV (~ 2225 m/s).
- Each hydrogen-cluster reaction is followed for 10 ps ($Si_{15}H_{10}$) and 30 ps ($Si_{29}H_{24}$) after the reaction took place.
- MD simulations:
  - *ab initio* simulation package VASP*
  - using the Verlet algorithm with a time step of 1.0 fs.
- To determine the vibrational temperature of the cluster, we eliminate the collective translational and rotational motion of the cluster after the reaction with atomic hydrogen

* G. Kresse and J. Hafner, Phys. Rev. B, **47**, 558 (1993); G. Kresse and J. Furthmüller, Comput. Mat. Sci., **6**, 15 (1996); G. Kresse and D. Joubert, Phys. Rev. B, **59**, 1758 (1999).

Hydrogen-induced heating of hydrogenated silicon nanoparticles

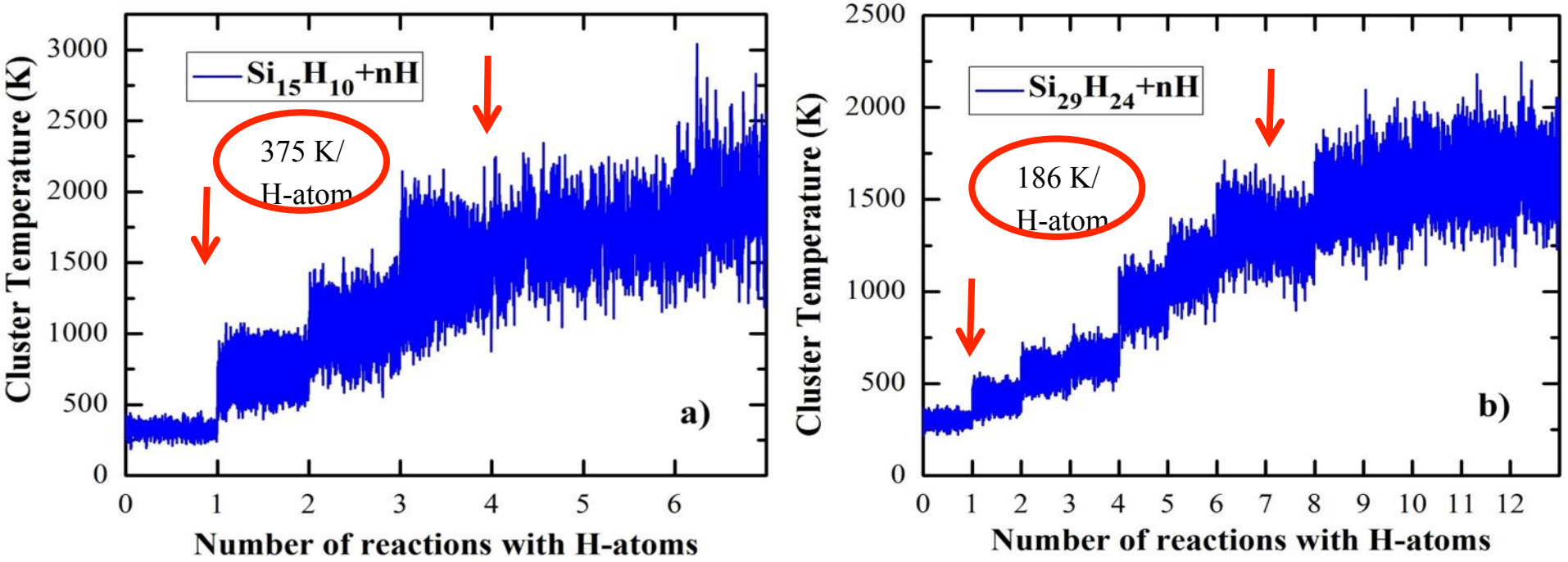

The evolution of the instantaneous temperature of clusters with the number *n* of reactions with H-atoms: a) $Si_{15}H_{10}$; b) $Si_{29}H_{24}$.

The average energy resulting from each H-atom reaction is about the same for both the amorphous and the initially crystalline clusters before the clusters start undergoing their structural transition from the solid to the liquid state.

Melting dynamics

Mean square displacement function

$$MSD(t) = \frac{1}{N}\left\langle \sum_{i=1}^{N} [\mathbf{r}_i(t_0 + t) - \mathbf{r}_i(t_0)]^2 \right\rangle$$

Einstein relation

Self-diffusion coefficient

$$D = \frac{1}{6}\frac{d}{dt}(MSD(t))$$

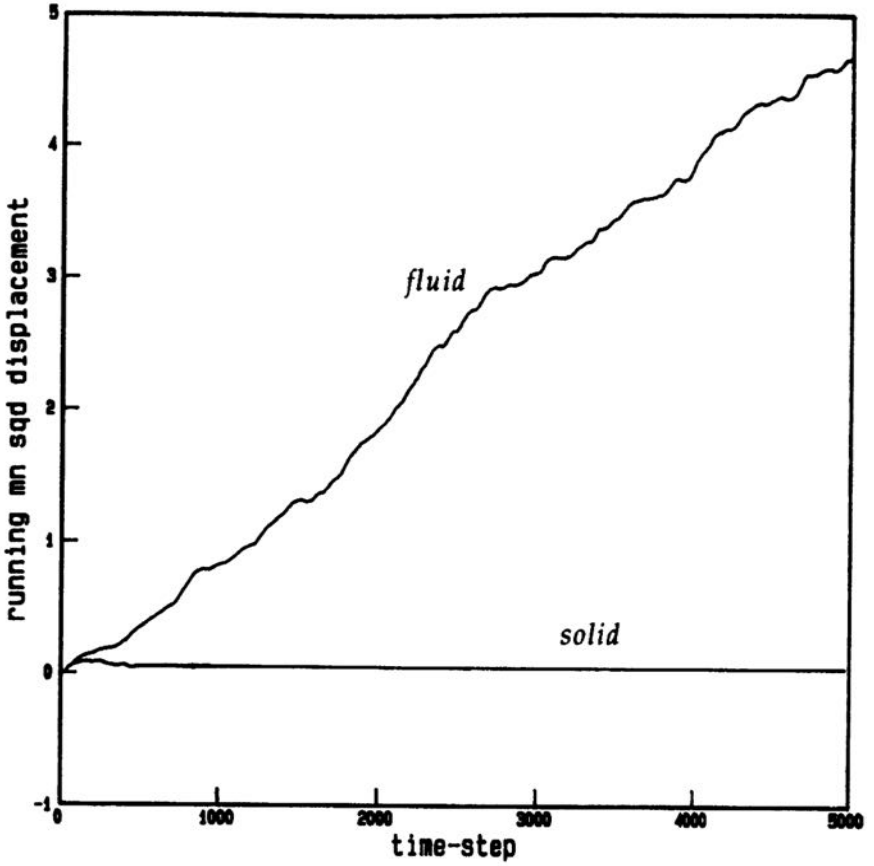

FIGURE 5.12 The running mean-square displacement (msd) can often be used to distinguish a fluid from a solid. Here the running msd, $\Delta r^{*2}(t)$ from (5.33), of Lennard-Jones atoms in a fluid state (upper line) is compared with that in a solid state (lower line). The simulations were each done using 256 atoms at $\rho\sigma^3 = 0.9$. The fluid state was at $\langle kT/\varepsilon \rangle = 1.087$, while the metastable solid was at $\langle kT/\varepsilon \rangle = 0.80$. See Figure 5.7 for the location of these states on the Lennard-Jones phase diagram.

Melting dynamics

Mean square displacement functions

$Si_{29}H_{24}$

a) First six reactions with H-atoms

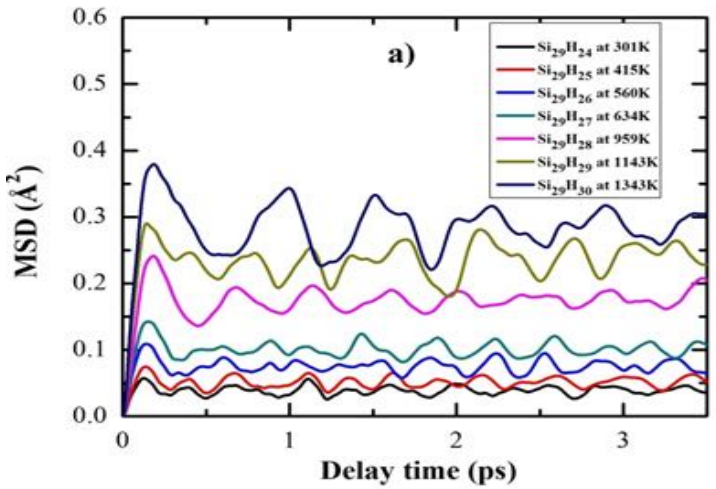

b) Last six reactions with H-atoms

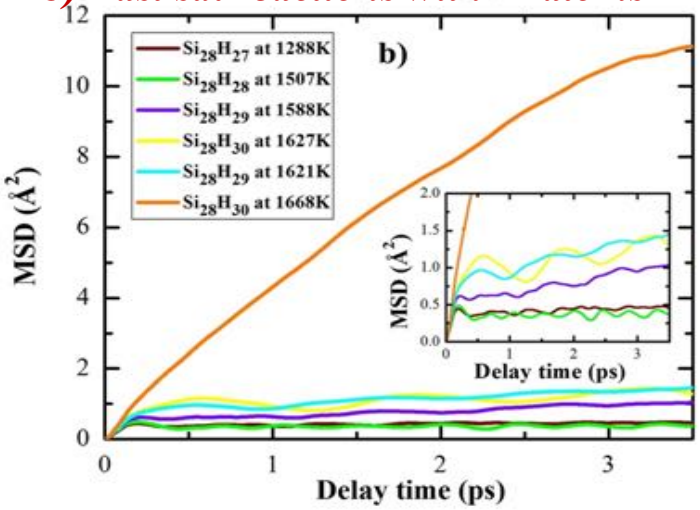

Melting dynamics

Self-diffusion coefficients

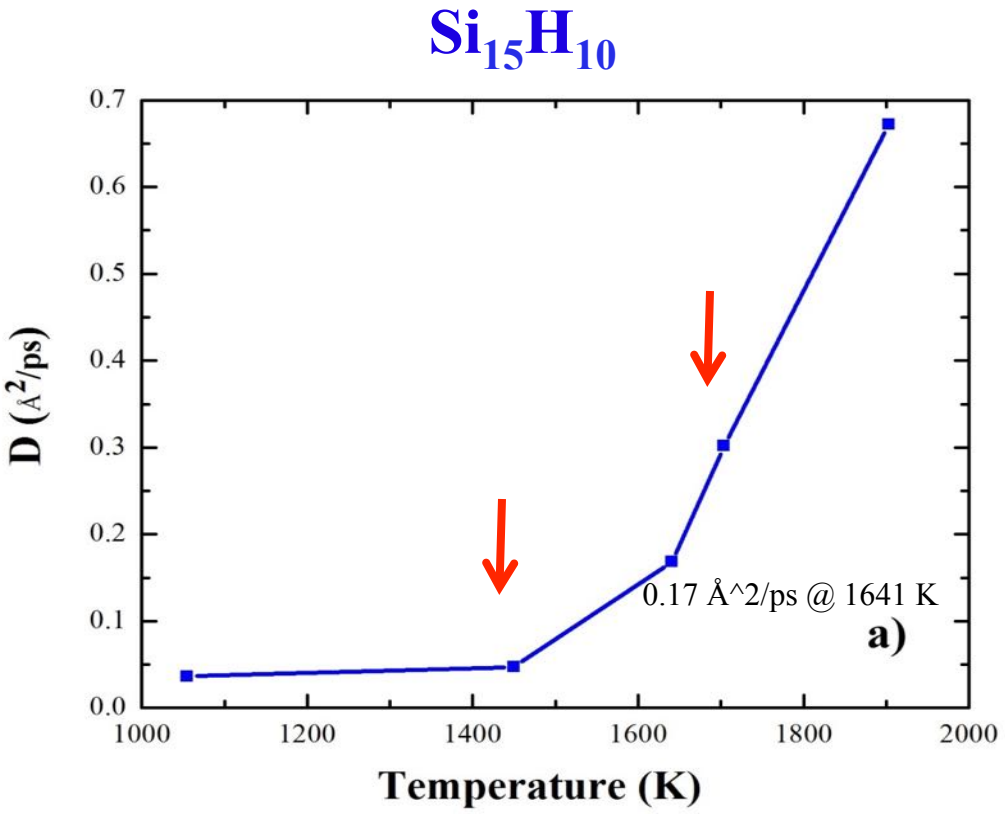

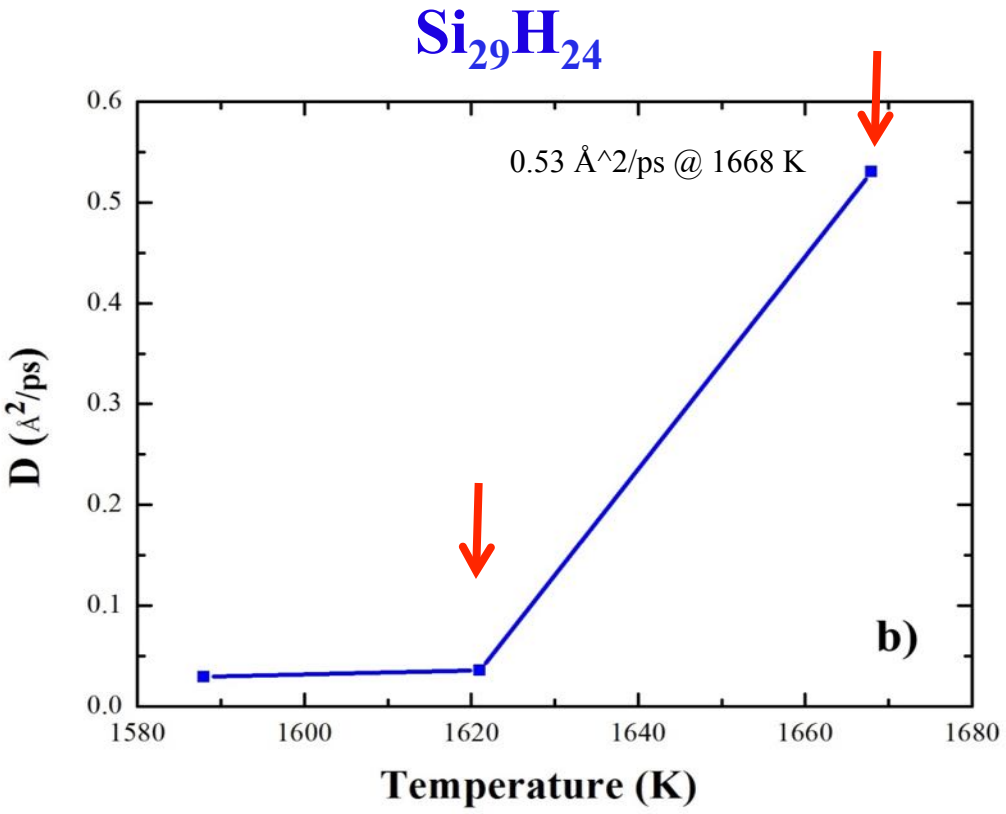

Bulk silicon: 2.52 Å^2/ps @ 1687 K

Temperature region of the phase transition from the solid to the liquid state:

1450 to 1704 K for $Si_{15}H_{10}$ 1621 to 1668 K for $Si_{29}H_{24}$

Epitaxial silicon thin films

- Various deposition techniques: MBE, HW CVD, Atmospheric Pressure CVD, PECVD, etc.
- MBE: perfect crystalline structure

  requires an ultra high vacuum system

  low deposition rates since one atom is deposited after the other

- Other CVD techniques: high deposition rates, but high temperatures

- PECVD: low temperatures, low cost and flexible substrate materials, large areas

  Recent experiments: 1.5 - 2 Å/s growth rate for cluster-induced epitaxy

A task for MD simulations !

Which experimental conditions can lead to high-speed epitaxial growth of thin silicon films from the deposition of plasma-born hydrogenated silicon nanoparticles at low substrate temperatures in PECVD reactors?

MD simulations of the deposition processes of hydrogenated silicon clusters on a crystalline silicon substrate

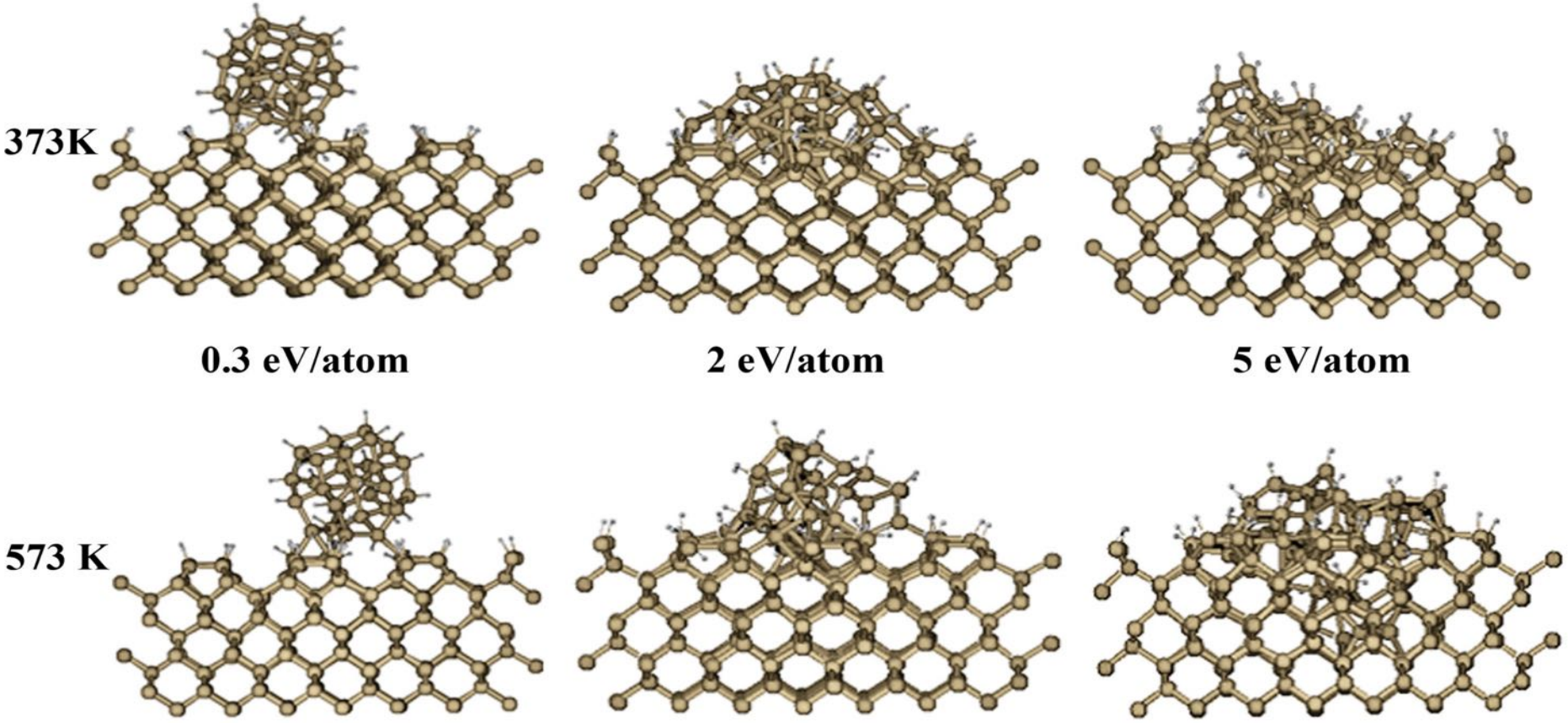

Snapshots at t = 10 ps of various trajectories with different impact energies and at different substrate temperatures to illustrate various deposition mechanisms, from soft-landing to destructive deposition of clusters*

Q: What happens if we expose the cluster-damaged surfaces to atomic hydrogen?

* N. Ning and H. Vach, J. Phys. Chem. A **114**, 3297 (2010).

Results

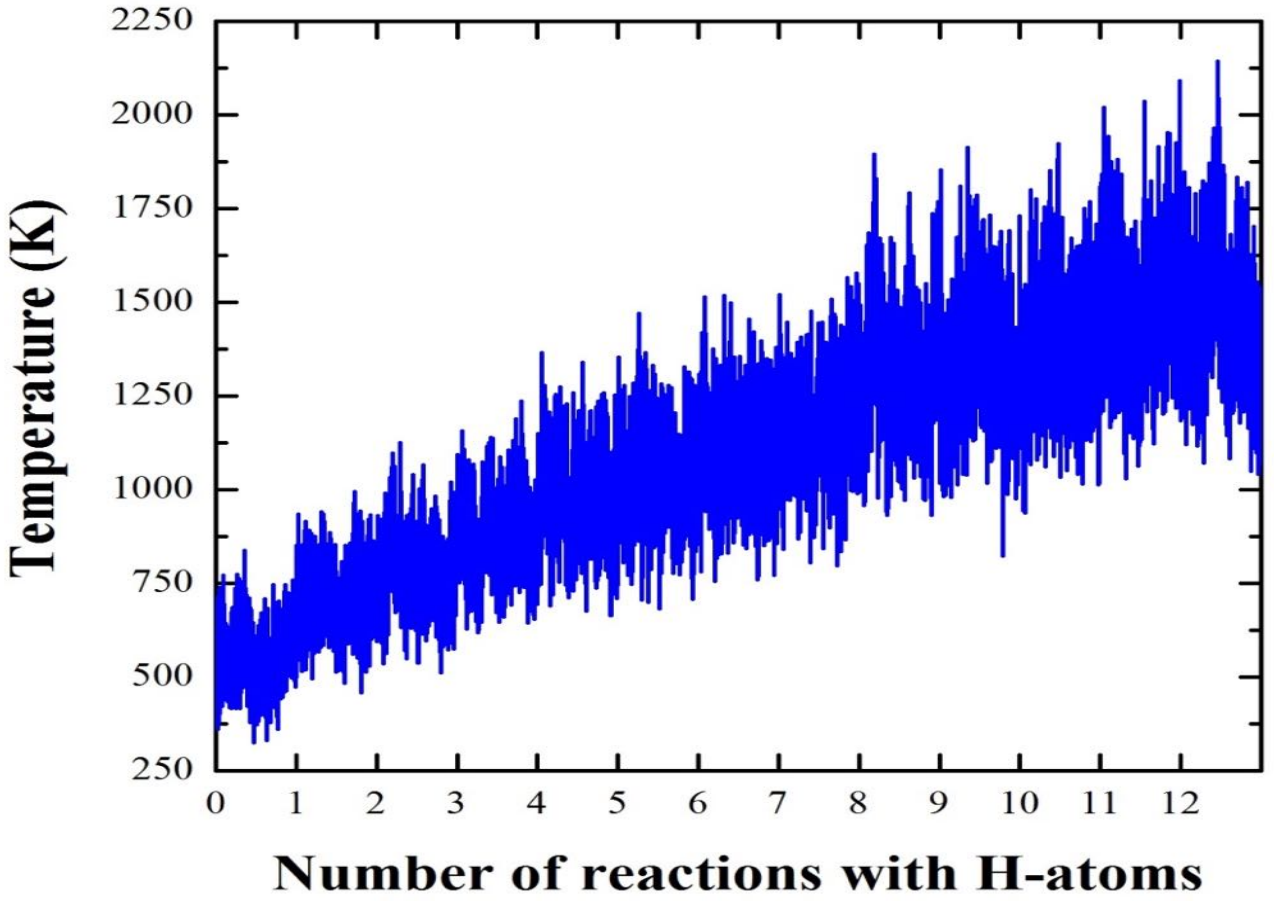

The evolution of the instantaneous temperature of the cluster atoms together with the substrate atoms touching the cluster with the number of reactions with H-atoms.

Result of H-atom treatment

- After 9 H-atom exposure

Surface temperature at 1371 K

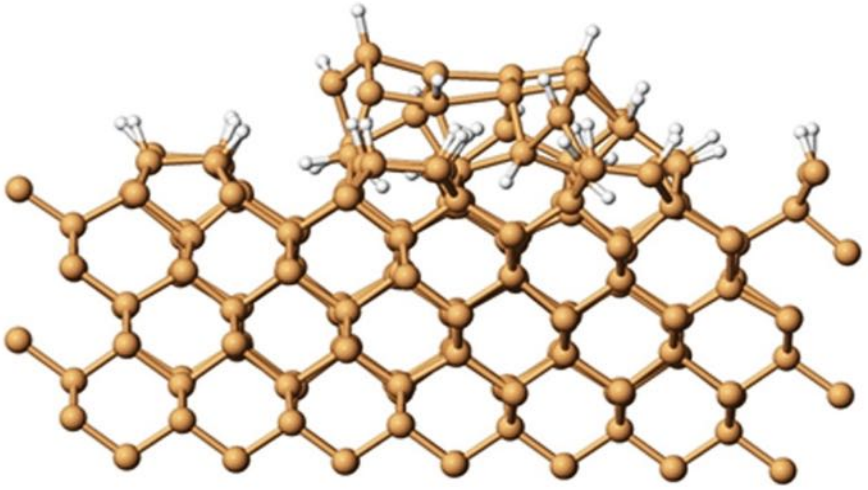

a) Before hydrogen exposure

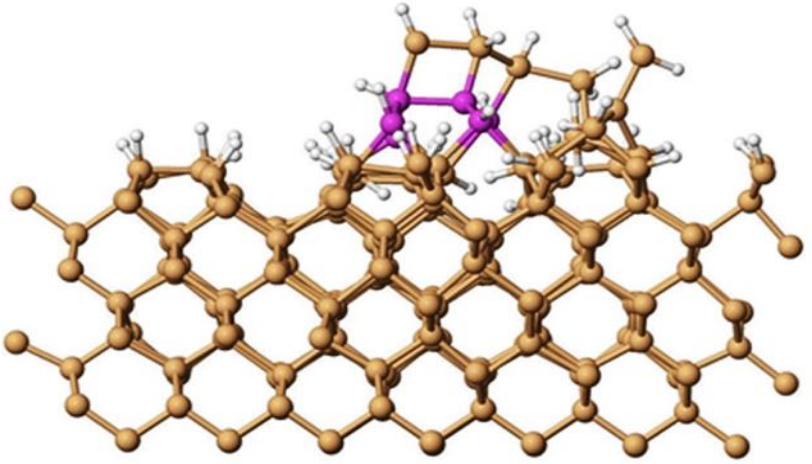

b) After 9 H-atom exposure

Results of H-atom treatment

- After 12 H-atom exposure

Surface temperature at 1616 K

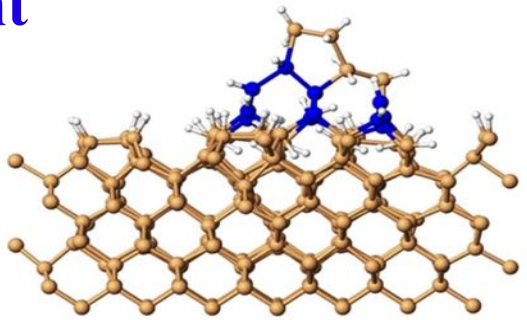

a) 35.50 ps

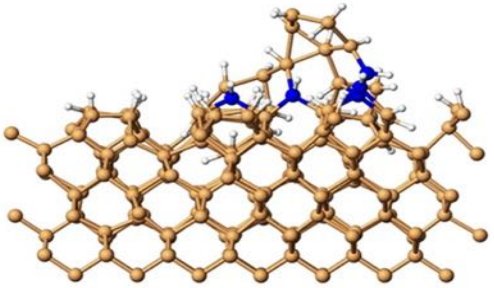

b) 114.98 ps

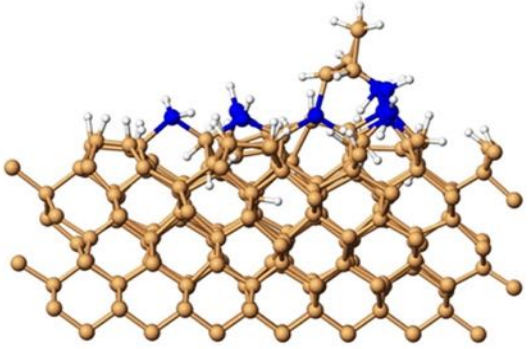

c) 250.54 ps

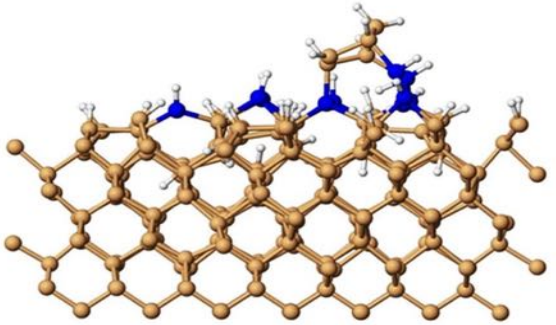

d) 266.48 ps

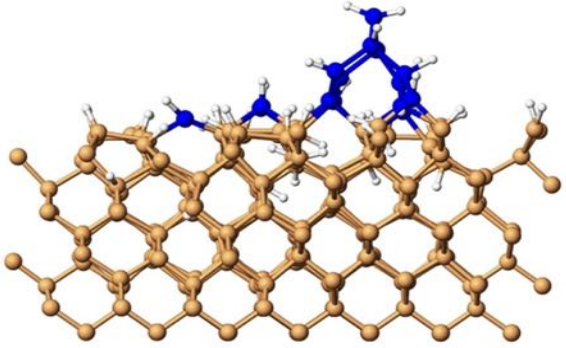

e) 312.28 ps

Results of H-atom treatment

Atomic configuration after cooling down to 573 K

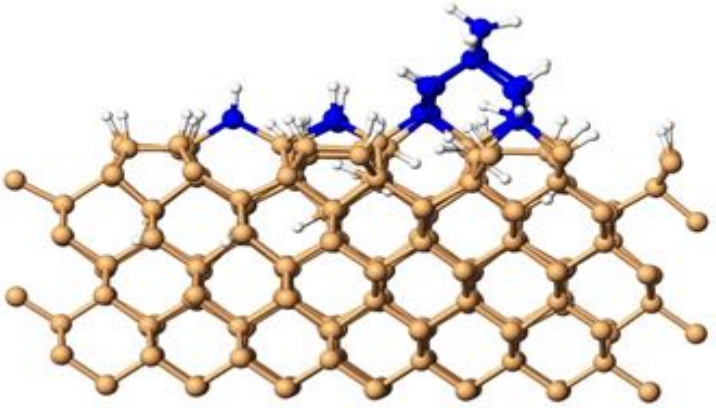

Side view

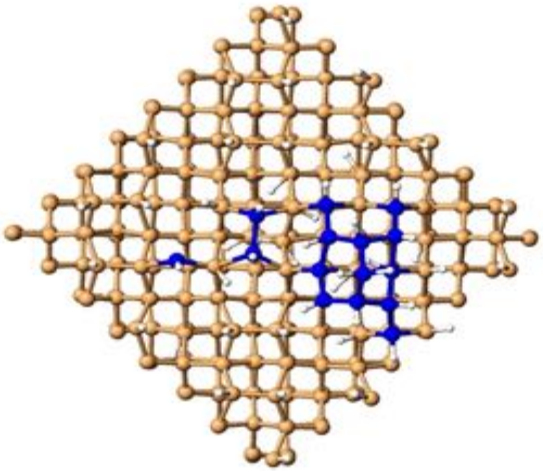

Top view

Radial distribution functions

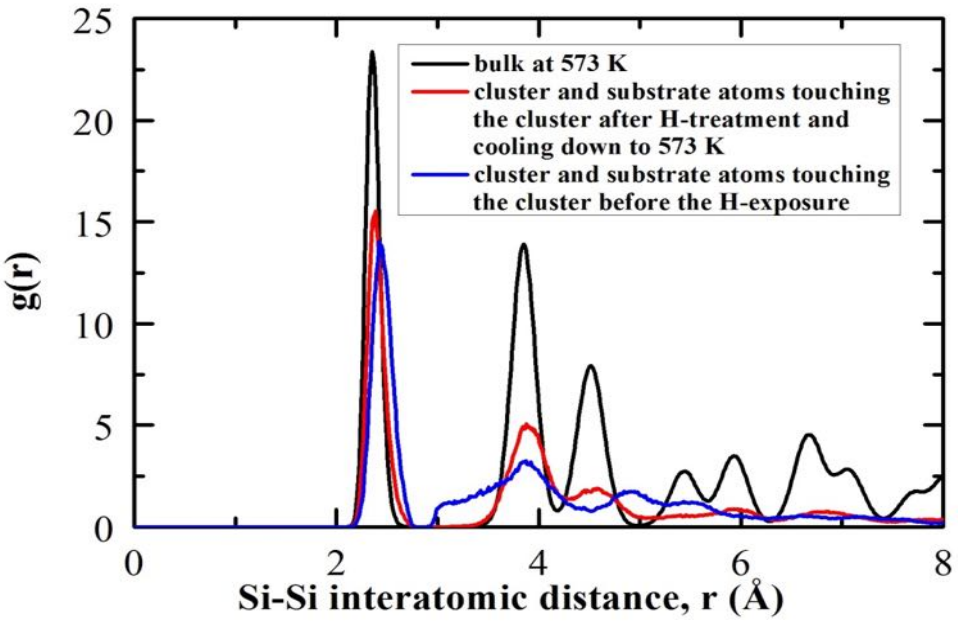

Proposal #1 for the experimentalist

Exposure to hydrogen plasma "after" epitaxial deposition to repair local damages due to non-perfect epitaxial deposition conditions.

Q: Amorphous or crystalline?

The formation of the polymorphous material is related to the powder formation in the SiH_4 plasma.

⇩

Incorporation of nanometric particles in the film

(polymorphous films)

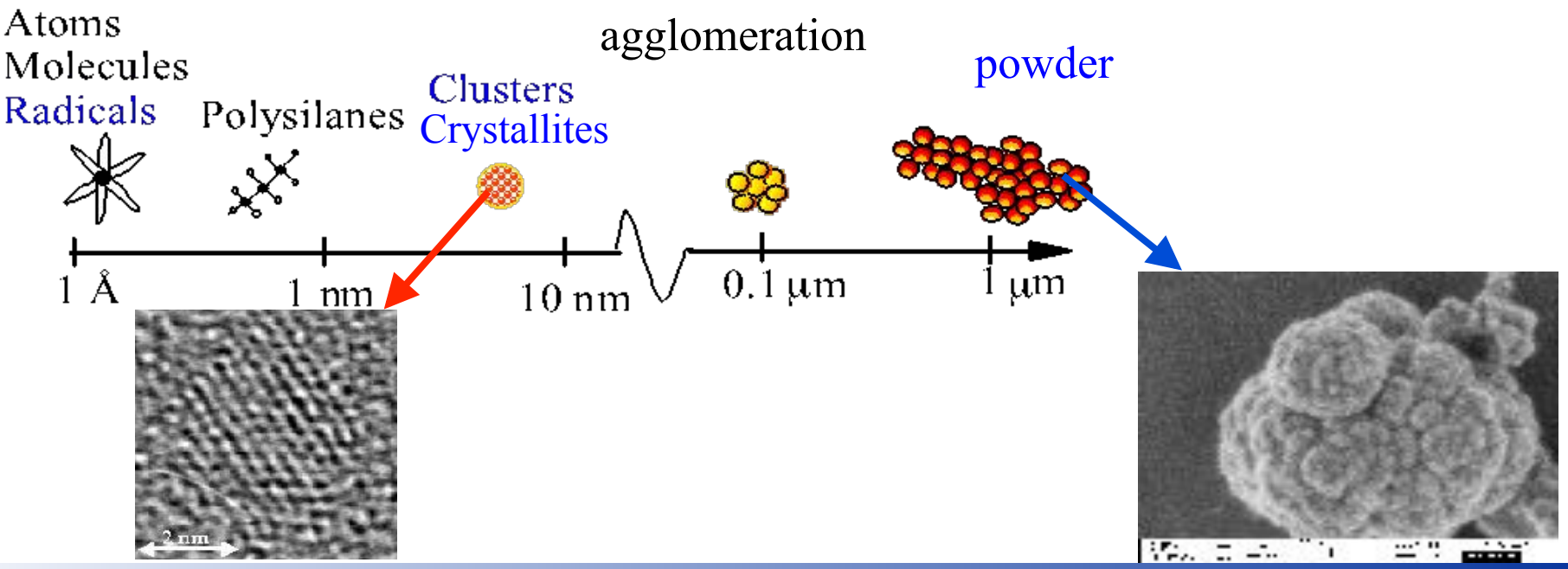

Growth of hydrogenated silicon nanoparticles in a plasma reactor

Fluid dynamics models for an H_2/SiH_4 discharge*

2% SiH_4, 98% H_2

Excitation voltage : 300 V

Pressure : 1 Torr

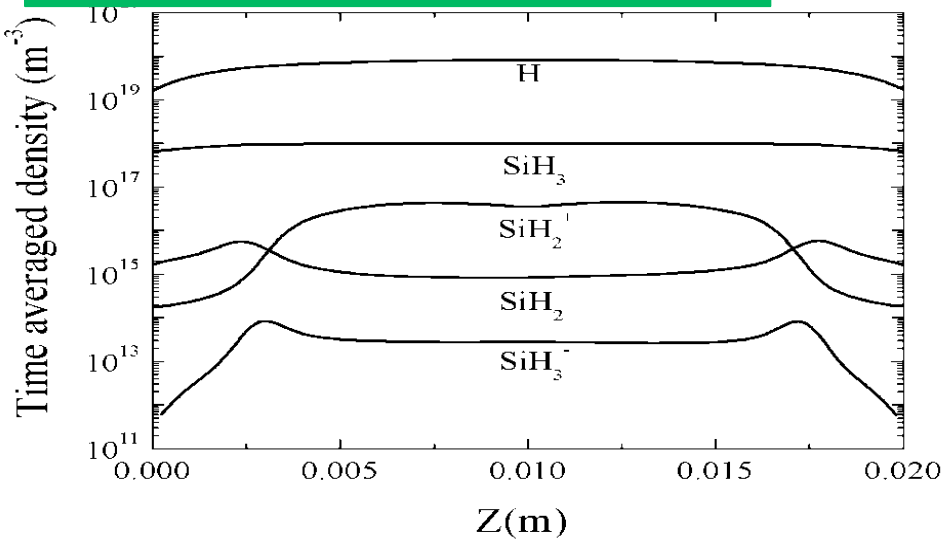

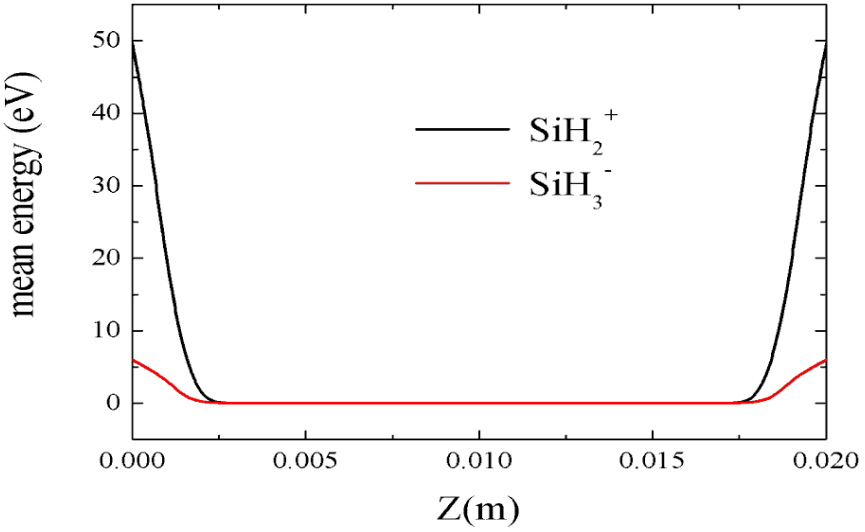

- Atomic H and SiH_3 radicals are the dominant dissociation products.
- H_2 and SiH_4 molecules are still the major plasma species.
- All species are found to have a room temperature energy distribution.

* H. Vach, Q. Brulin, N. Chaâbane, T. Novikova, P. R. i Cabarrocas, B. Kalache, K. Hassouni, S. Botti, and L. Reining, Comput. Mat. Sci., **35**, 216 (2006).

Growth of Si_nH_m clusters in a plasma reactor

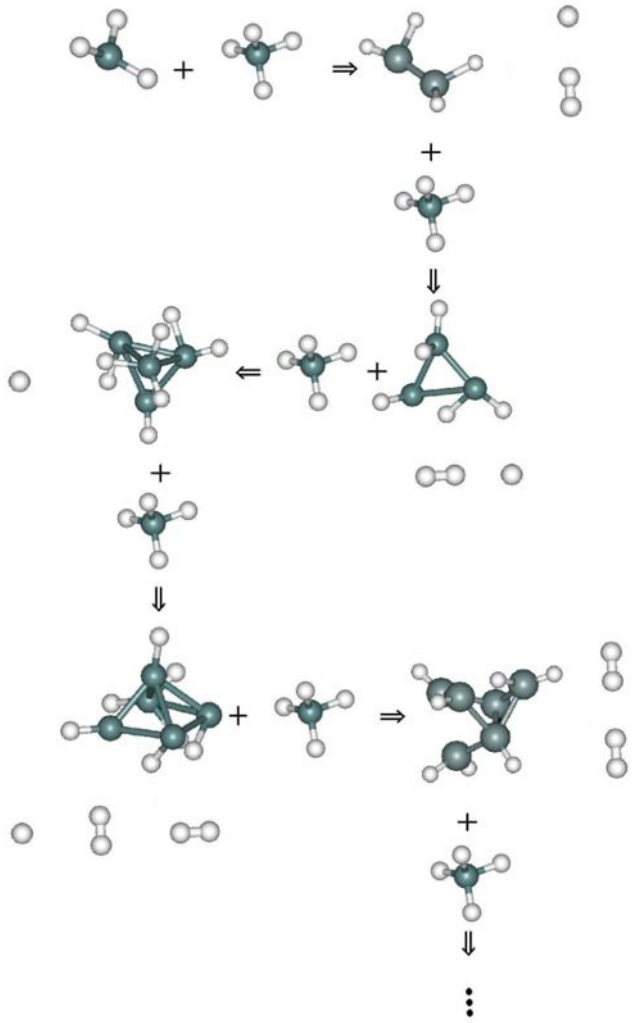

We use ab initio molecular dynamics simulations to simulate the growth of silicon nanoparticles in a plasma reactor.

<u>NOTE:</u> We do NOT look for global minimum energy structures, but for stable structures that form by self-assembly in a plasma reactor!

Using our results from the plasma modeling, we now can follow the dynamics of the cluster growth as a result of the consecutive capture of plasma radials (SiH_4, SiH_3, SiH_2…).

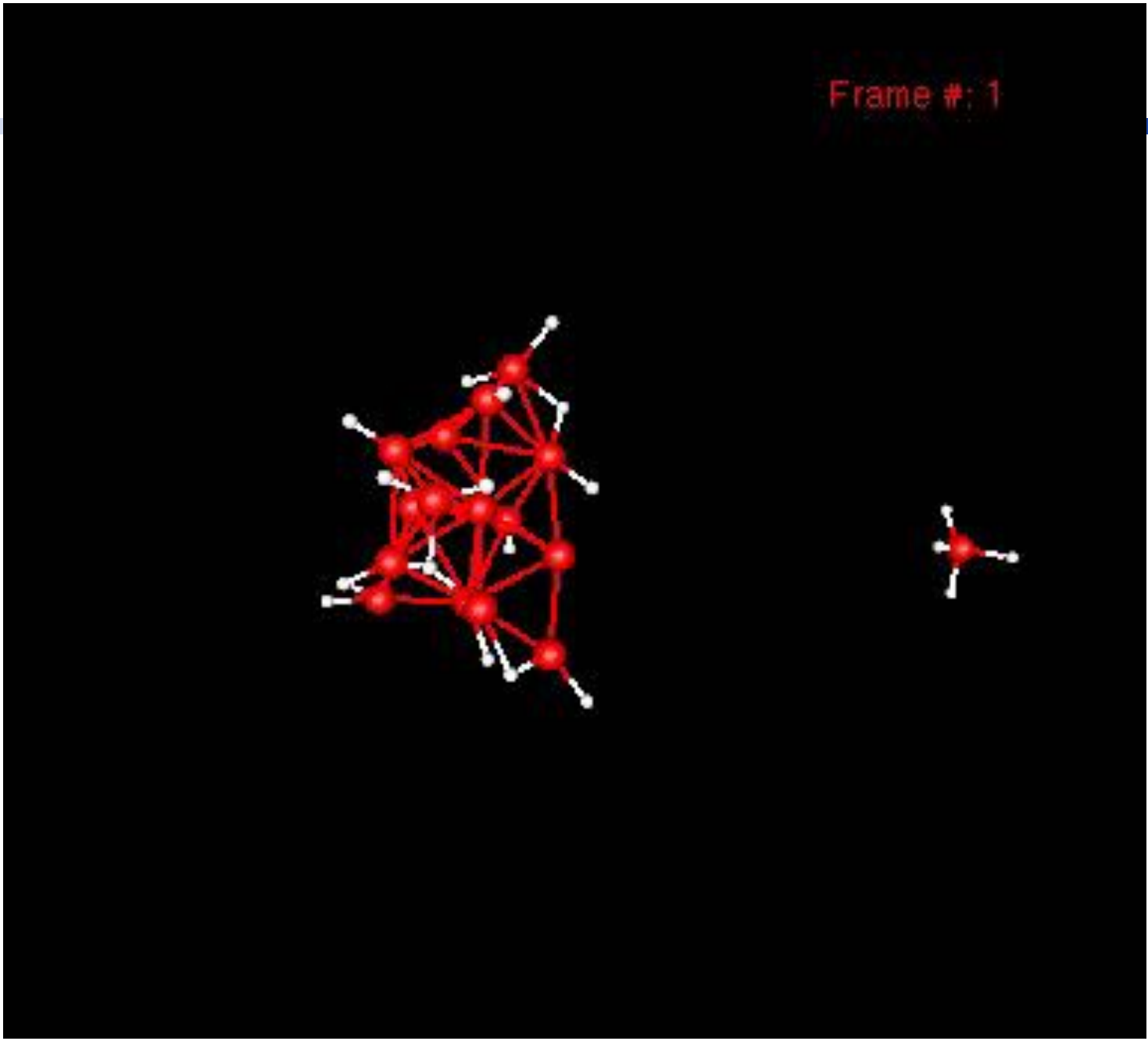
Frame #: 1

Growth of $Si_n H_m$ clusters in a plasma reactor

Role of atomic H for the crystallization of an amorphous $Si_{24}H_{25}$ nanoparticle

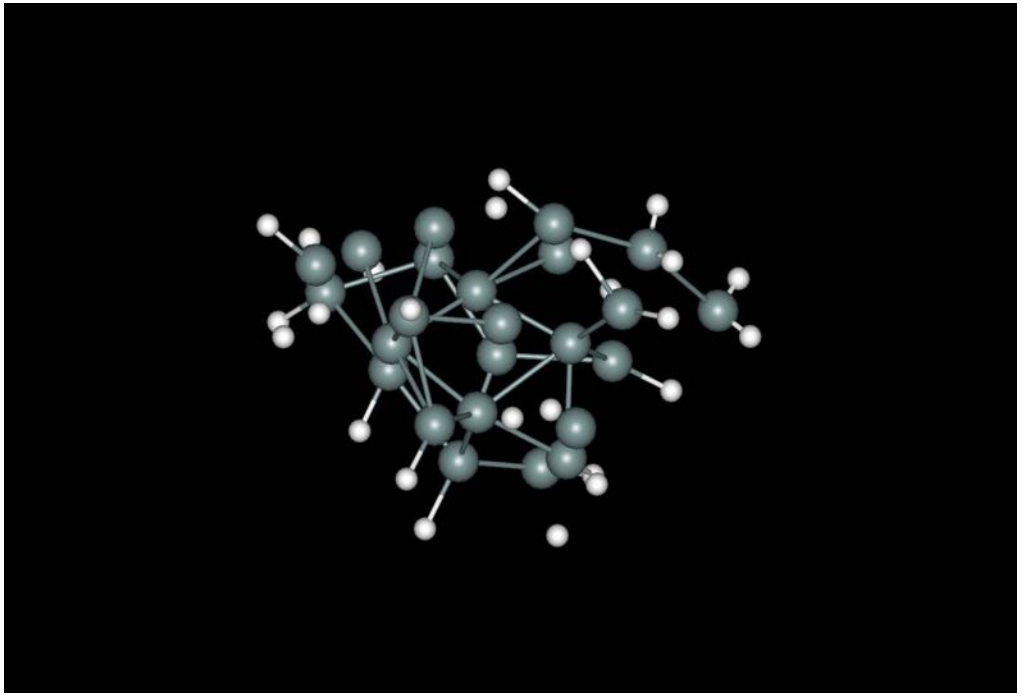

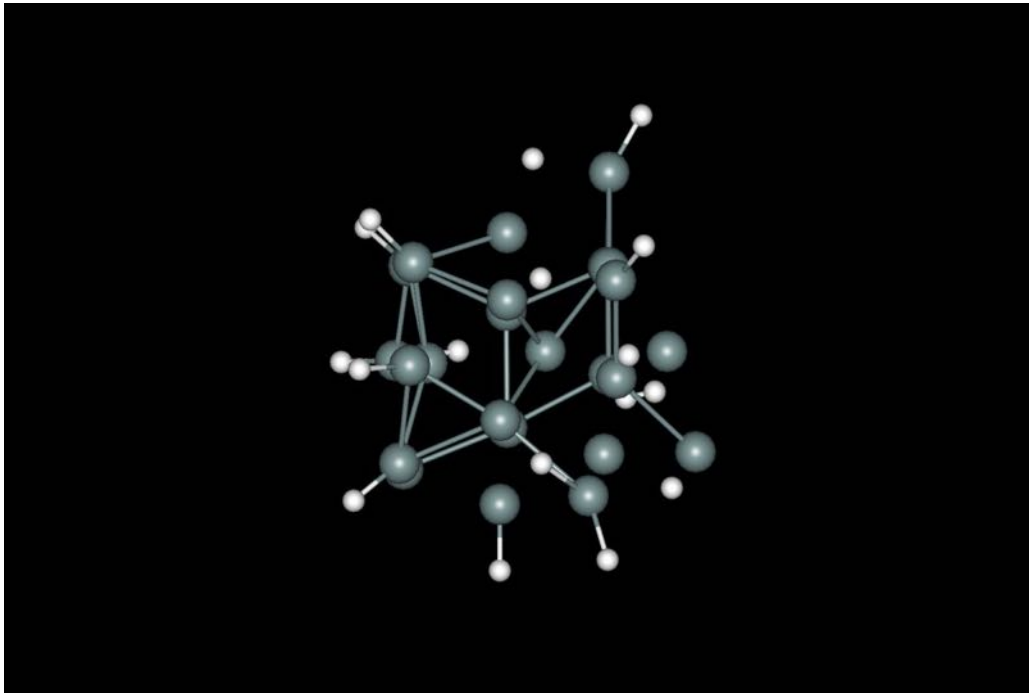

BEFORE … ***AFTER …***

… the collision with 10 thermal H atoms

Growth of $Si_n H_m$ clusters in a plasma reactor

Role of atomic H for the crystallization of an amorphous $Si_{24}H_{25}$ nanoparticle

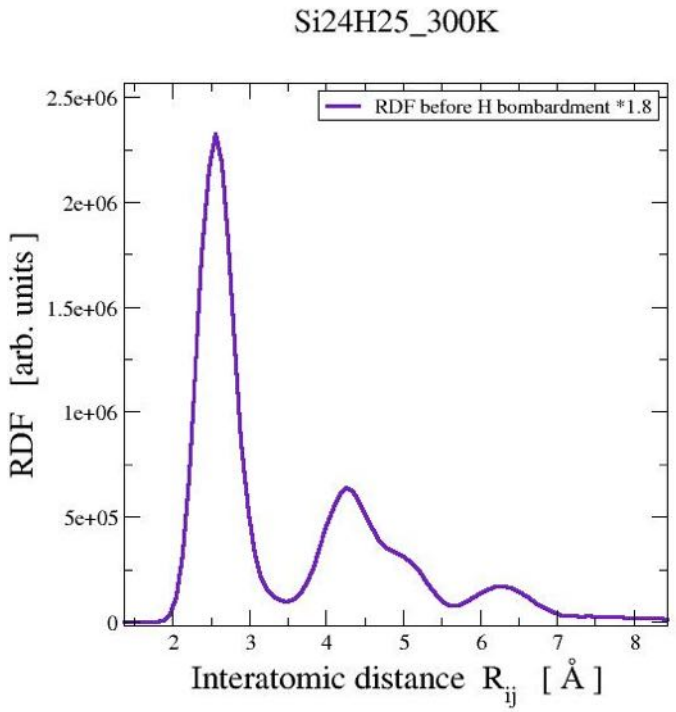

BEFORE …

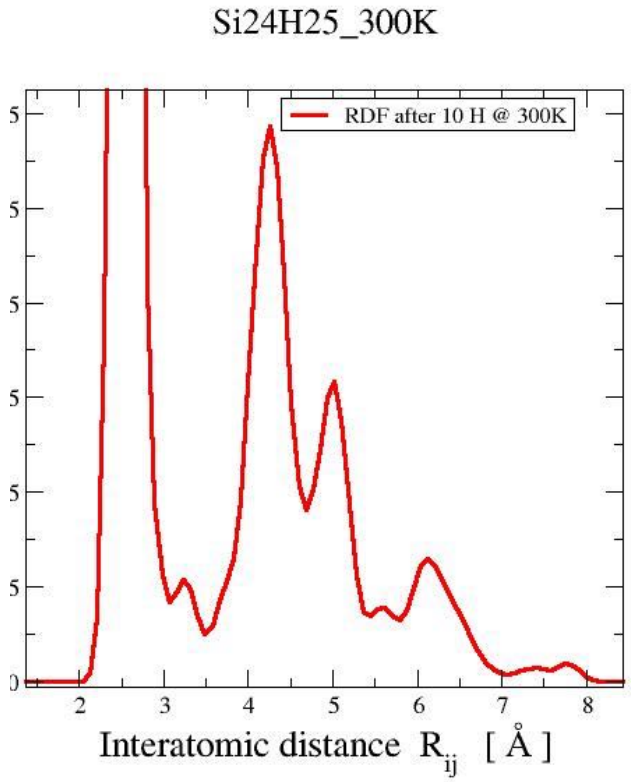

AFTER …

… the collision with 10 thermal H atoms

Growth of $Si_n H_m$ clusters in a plasma reactor

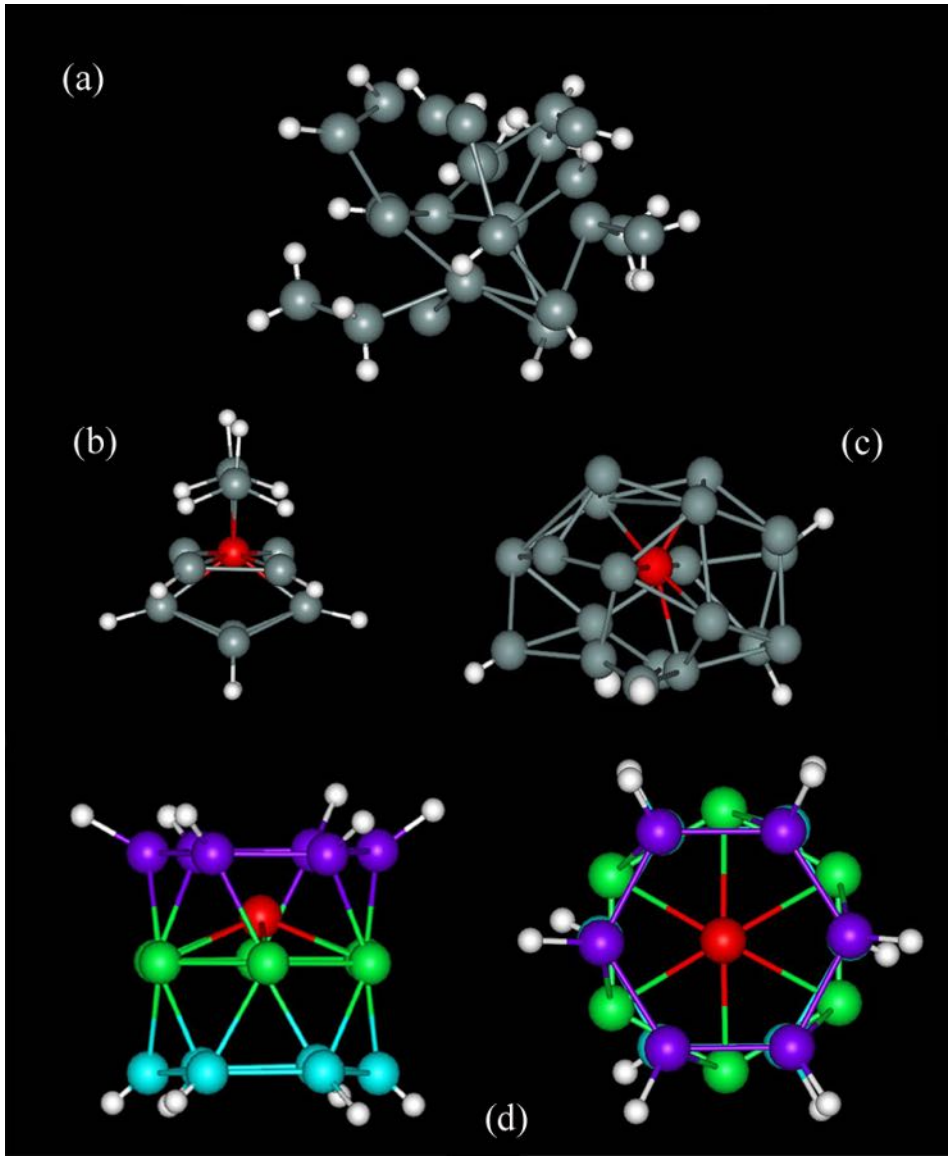

(a) Typical structure before atomic H exposure

(b) Typical structure after low H-flux exposure

(c) Typical structure after high H-flux exposure

(d) Structure after intermediate H-flux exposure

Vach & Brulin, Phys. Rev. Lett. **95**, 165502 (2005).
Highlighted in: Nature Materials **4**, 878 (2005).

Th. Nguyen-Trana, P. Roca i Cabarrocas, G. Patriarche, Appl. Phys. Lett. **91**, 111501 (2007).

Do different levels of theory give the same results?

Starting out from final MD structure, we optimized geometry at different levels of theory:

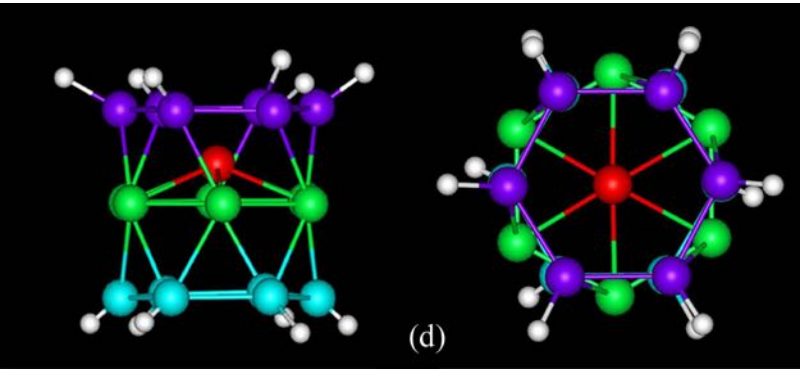

PM3

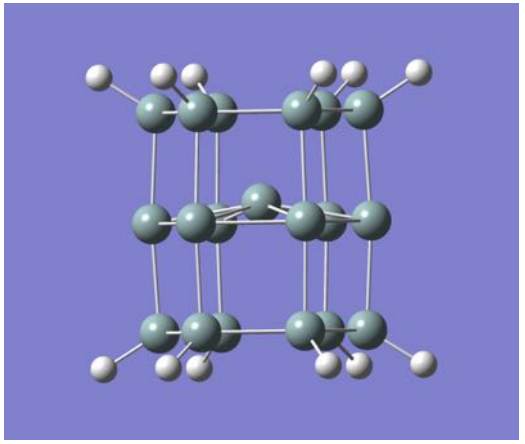

MP2 FULL/6-311++G**

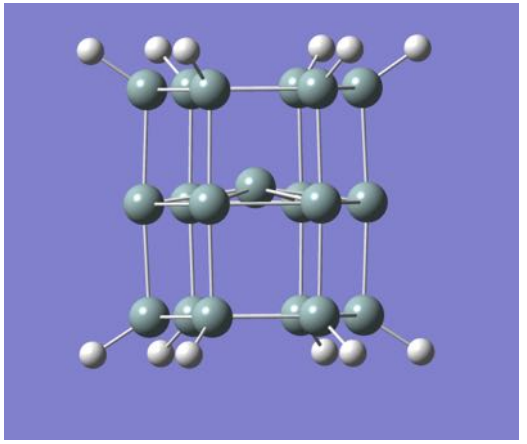

B3LYP 6-311++G**

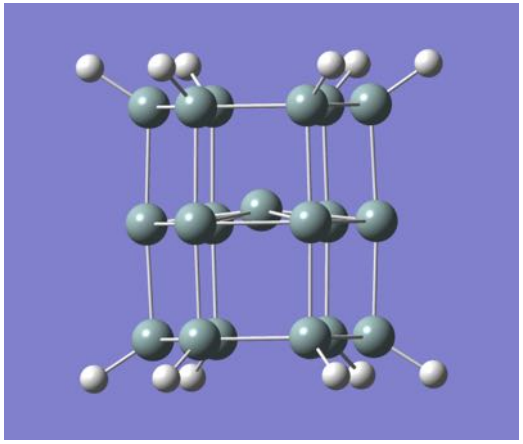

PBE aug-cc-pVTZ

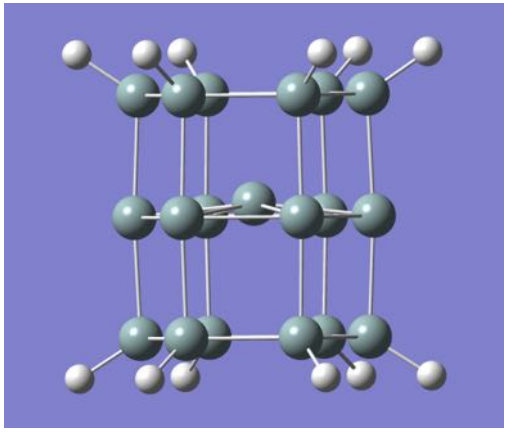

M06 6-311++G**

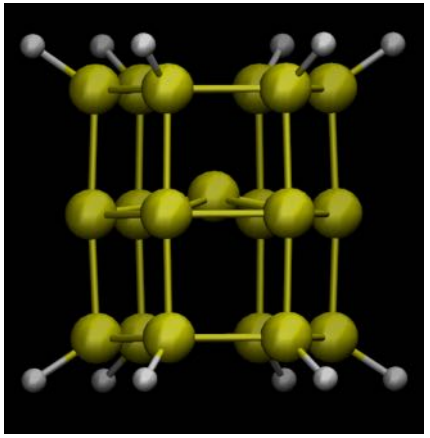

PBE-PAW plane-wave 500eV

Si19H12 @ 1200K

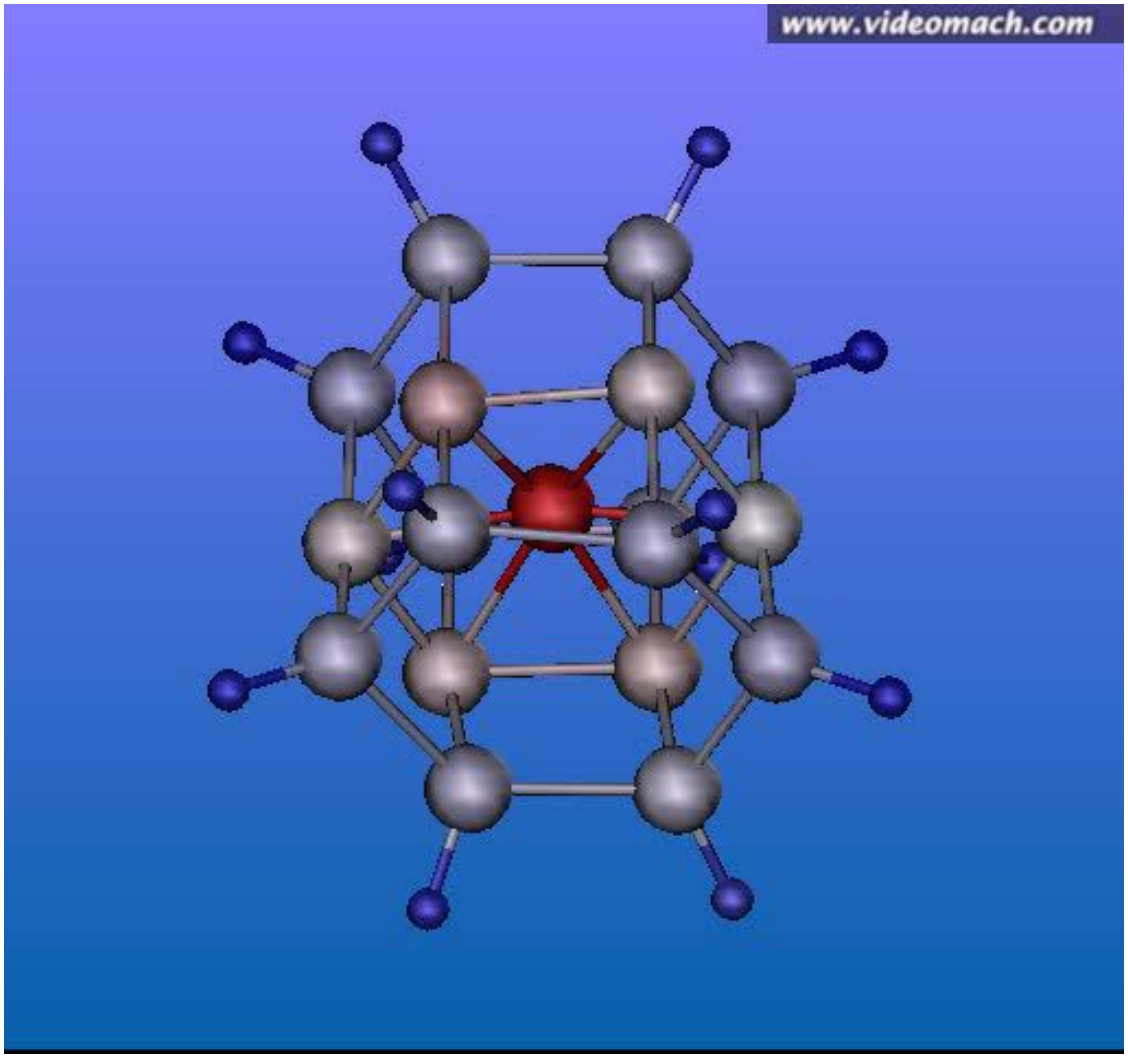

Adding just ONE silicon atom…

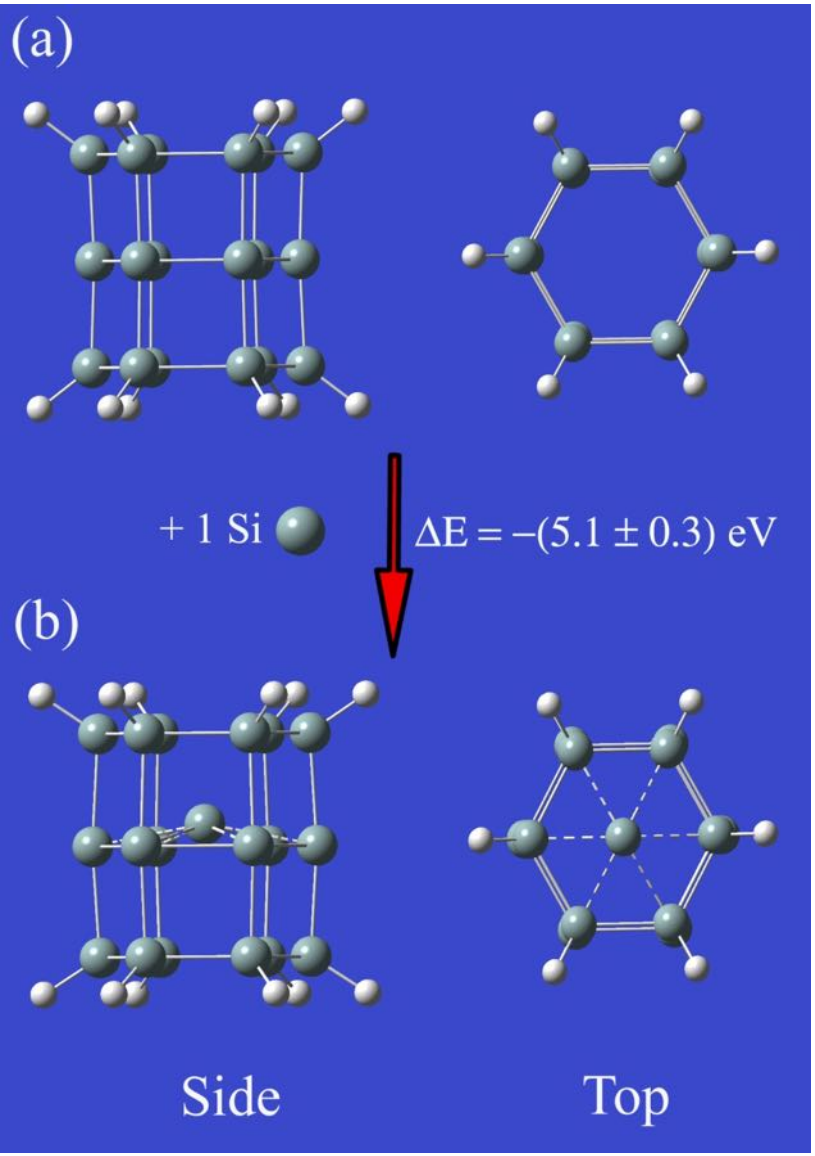

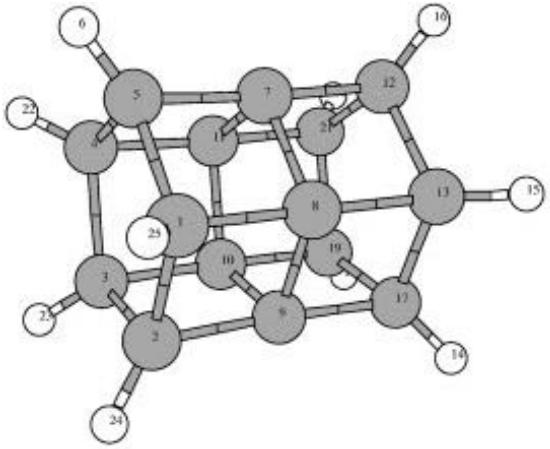

Bai, J.; Zeng, X. C.; Tanaka, H.; Zeng, J. Y. *Proc. Nat. Acad. Sci. USA* **2004**, *101*, 2664-2668.

- Normal clusters of this size: -3.8eV
- Crystalline bulk silicon: -4.6 eV
- $Si_{19}H_{12}$: (-5.1+/-0.3)eV

How can it be so stable?

- 5.1eV > Cohesive energy of bulk silicon
- => cannot be understood in terms of classical covalent Si-Si bonds…
- Look where the electrons are:

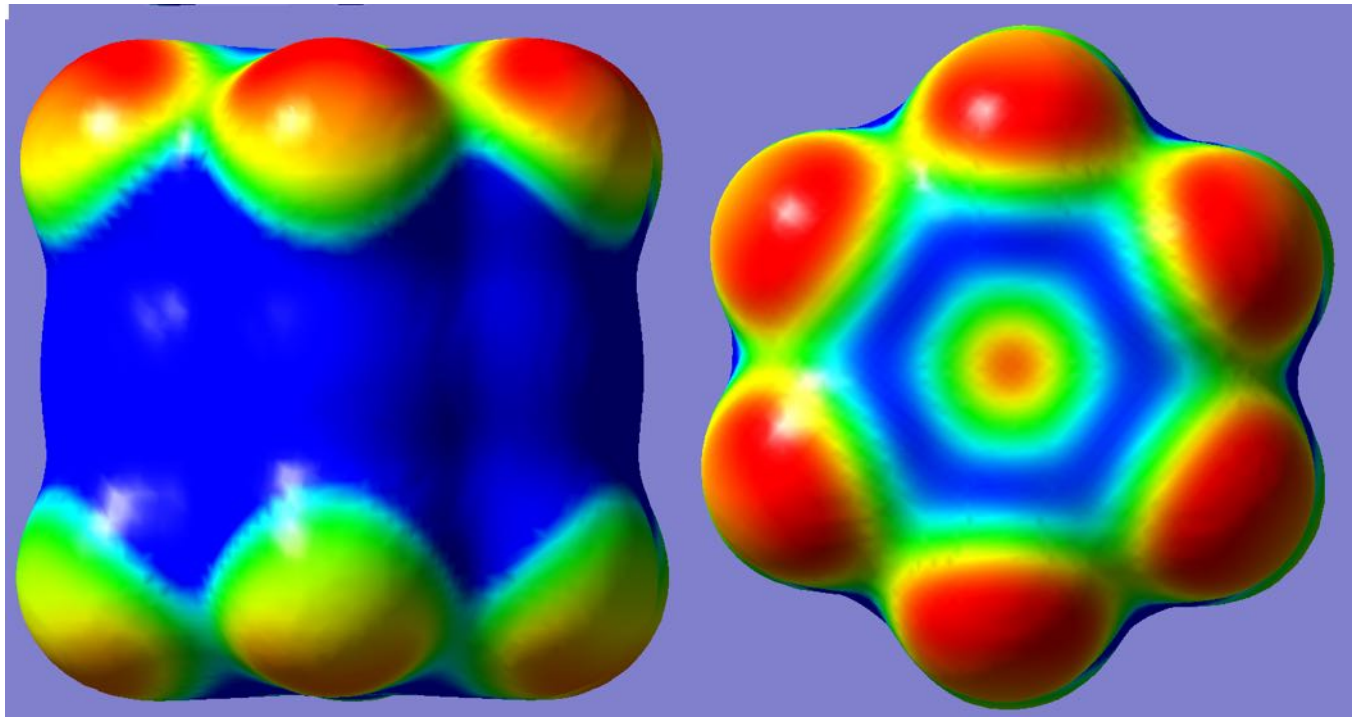

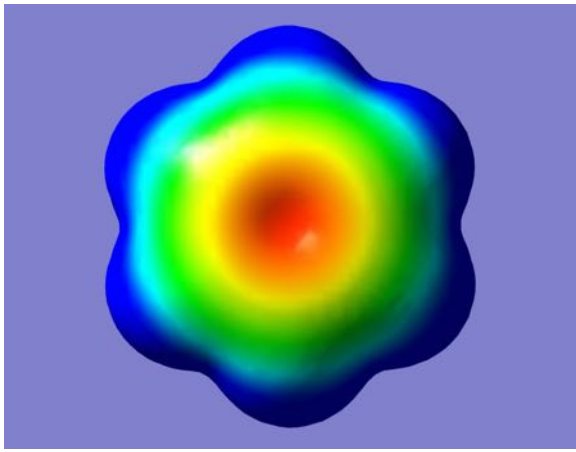

The electron density is calculated from the total self-consistent field density mapped with the corresponding electrostatic potential in atomic units; the shown color differences correspond to a permanent dipole moment of 1.9 D

How can $Si_{19}H_{12}$ be so stable?

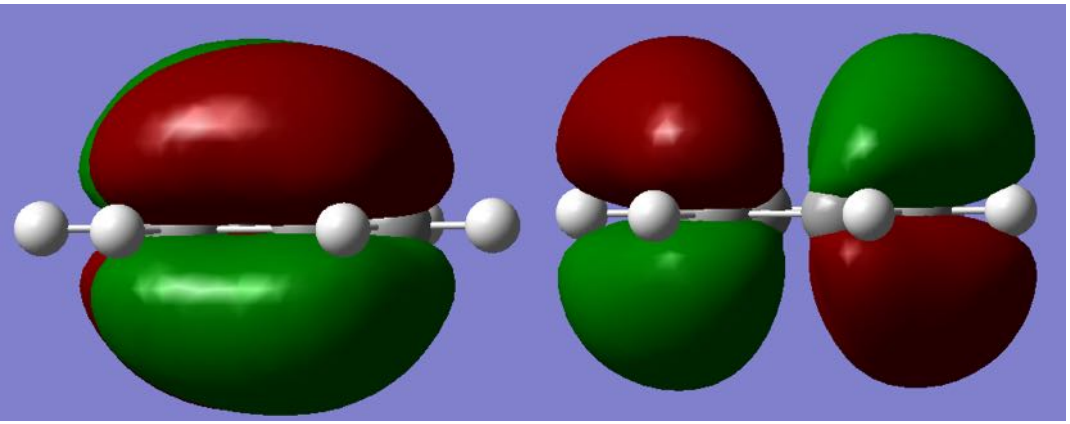

HOMO1 HOMO2

C_6H_6

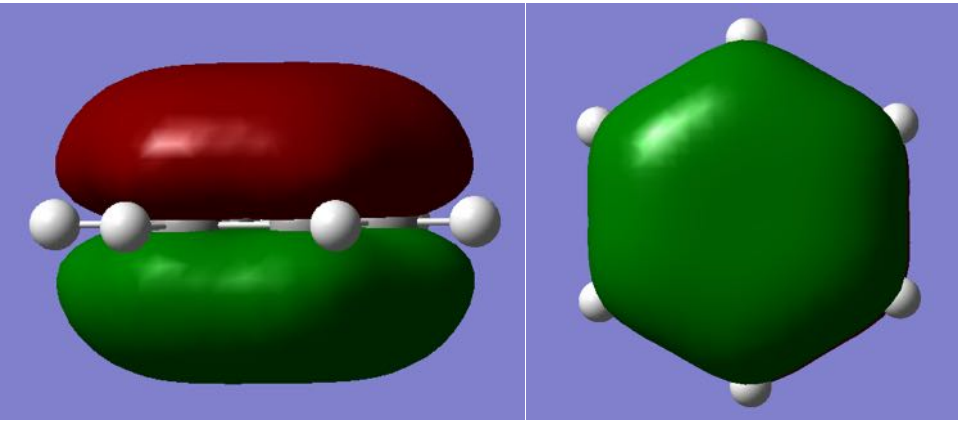

HOMO-4

HOMO

$Si_{19}H_{12}$

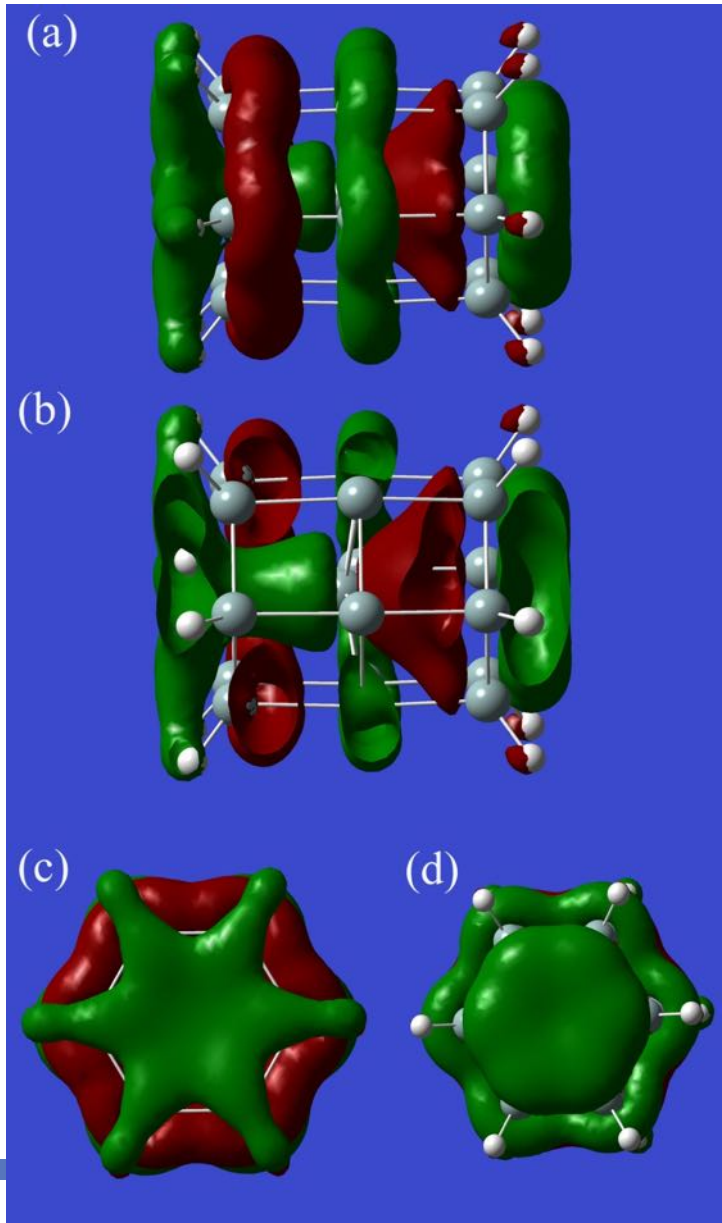

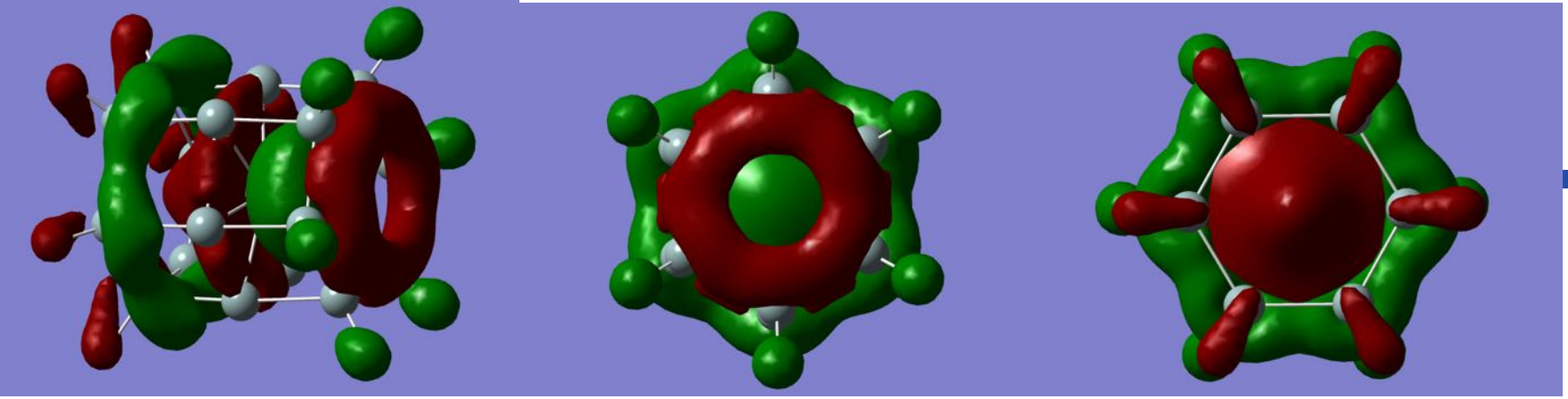

HOMO-1

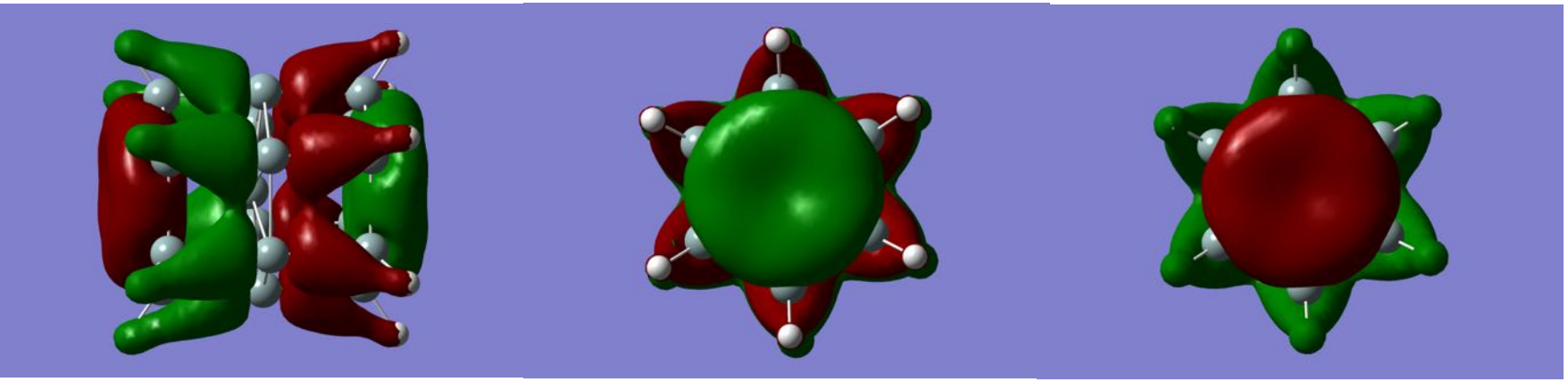

MO124

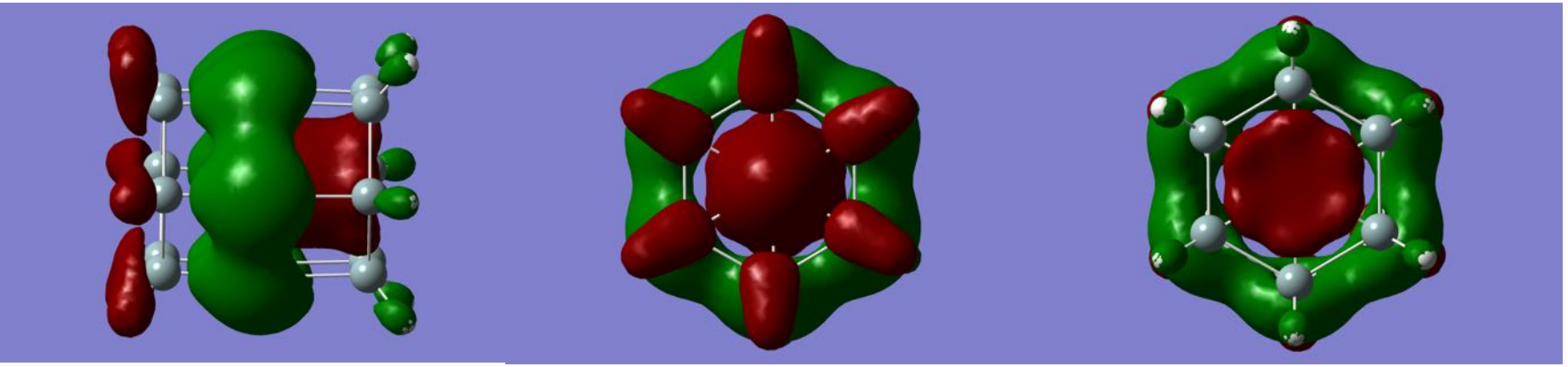

MO113

Magnetic Shielding

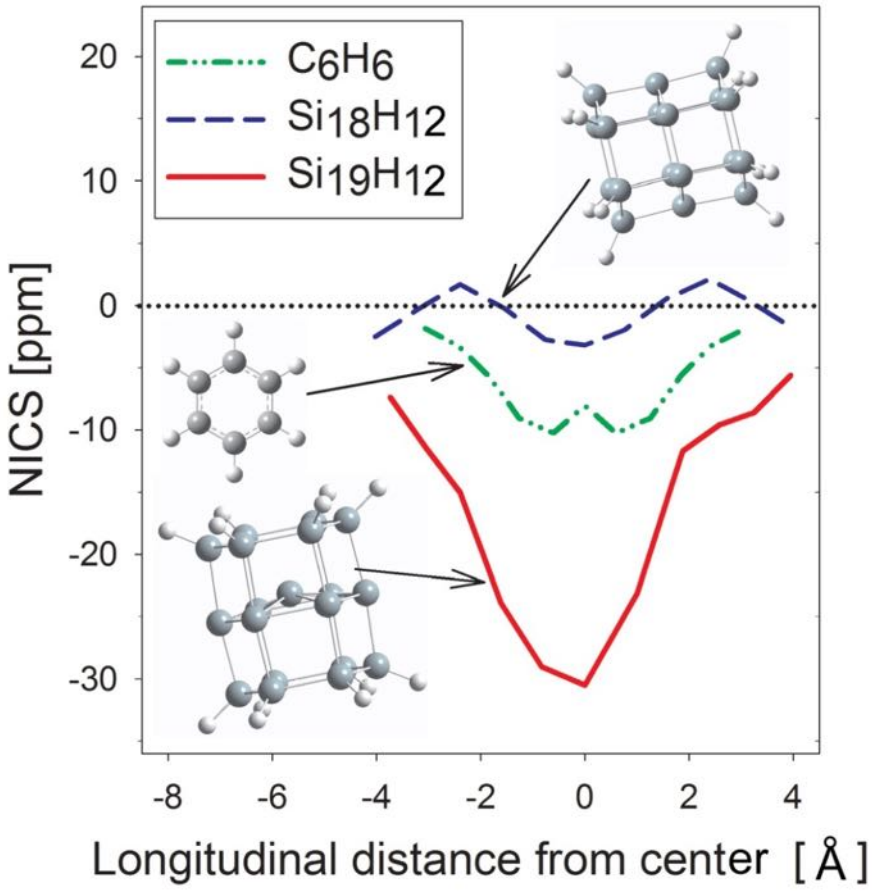

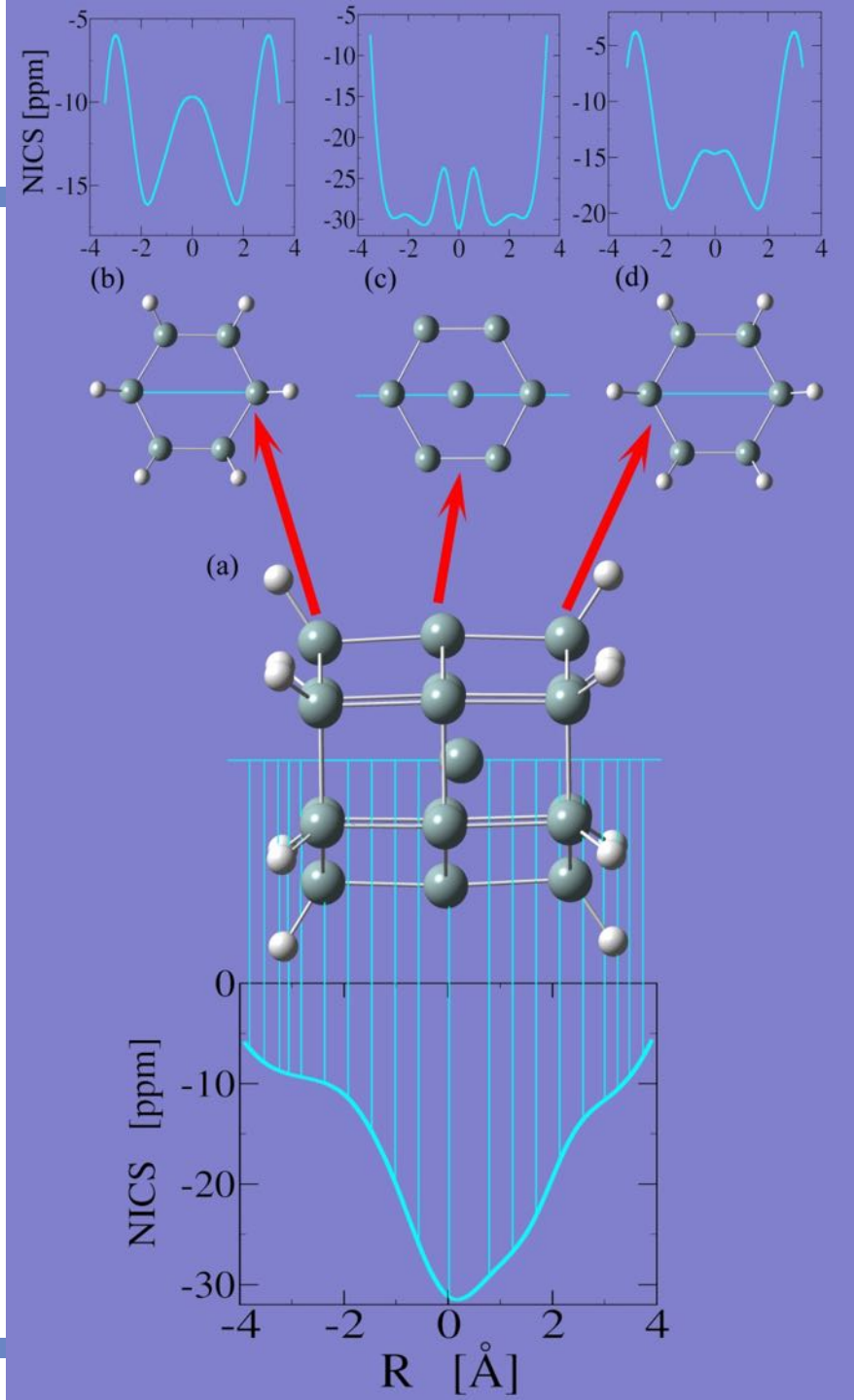

$Si_{19}H_{12}$ exhibits stronger aromatic behavior than C_6H_6!

Electron-defiency aromaticity

J. Chem. Theory Comput. **8**, 2088-2094 (2012).

Aromatic Ring Currents

An aromatic ring current is an effect observed in aromatic molecules such as benzene and naphthalene. If a magnetic field is directed perpendicular to the plane of the aromatic system, a ring current is induced in the delocalized π electrons of the aromatic ring. This is a direct consequence of Ampère's law; since the electrons involved are free to circulate, rather than being localized in bonds as they would be in most non-aromatic molecules, they respond much more strongly to the magnetic field.

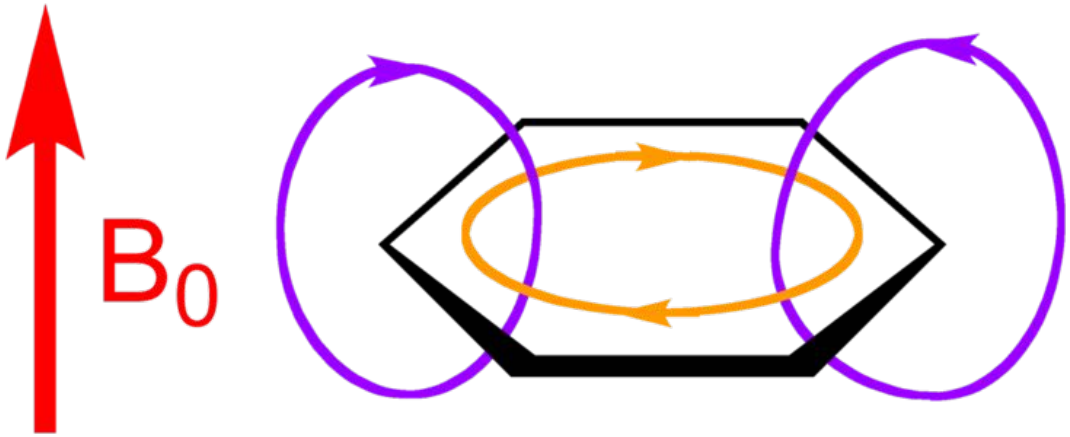

A diagram of an aromatic ring current. B0 is the applied magnetic field, the **red arrow** indicating its direction. The **orange ring** shows the direction of the ring current, and the **purple rings** show the direction of the induced magnetic field.

Aromatic Ring Currents

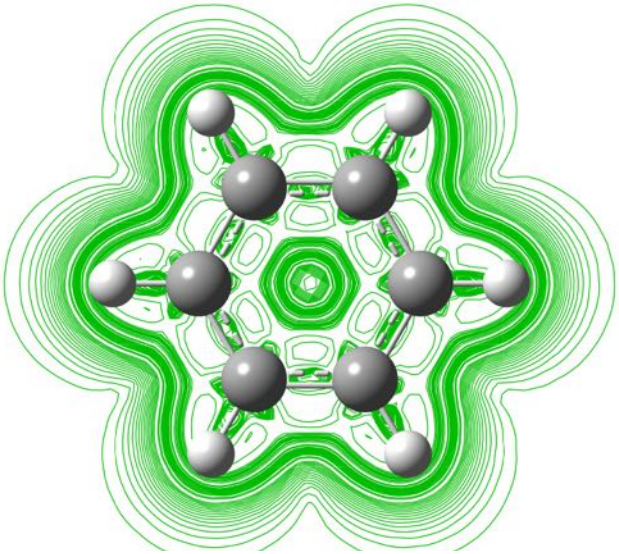

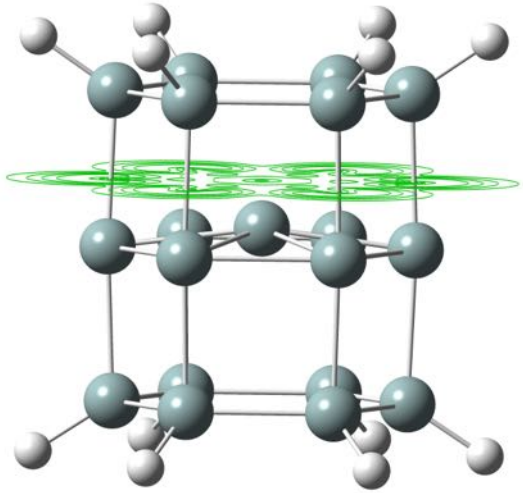

Central hexagon

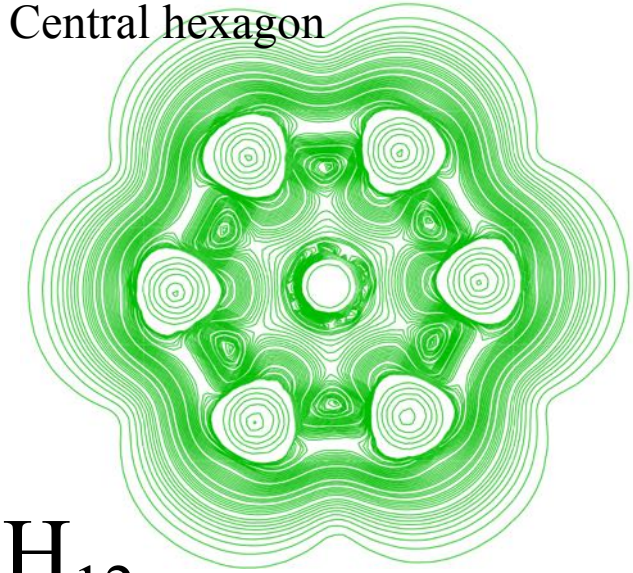

$Si_{19}H_{12}$

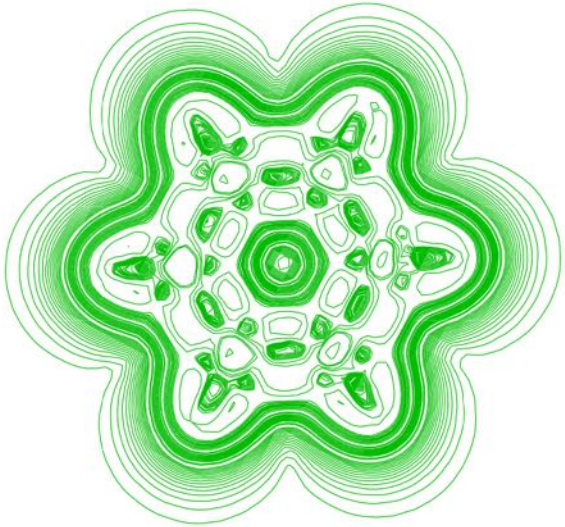

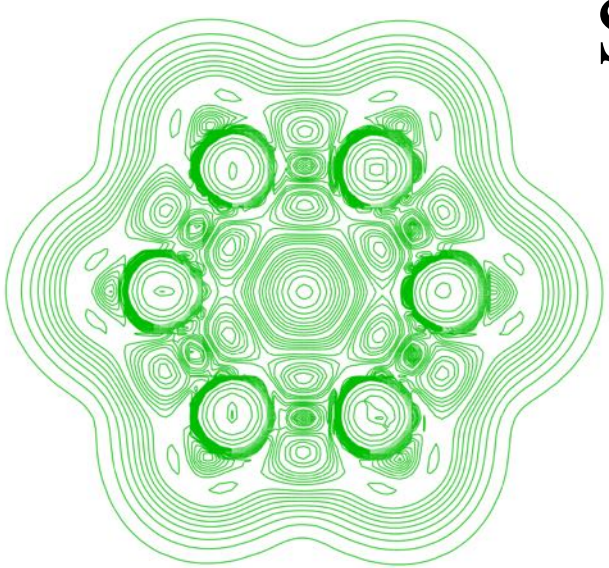

Upper hexagon

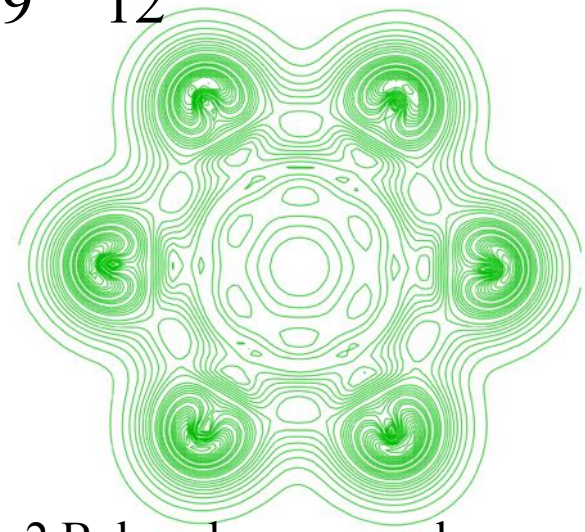

2 Bohrs above upper hexagon

C_6H_6

Heating $Si_{19}H_{12}$ to 600K

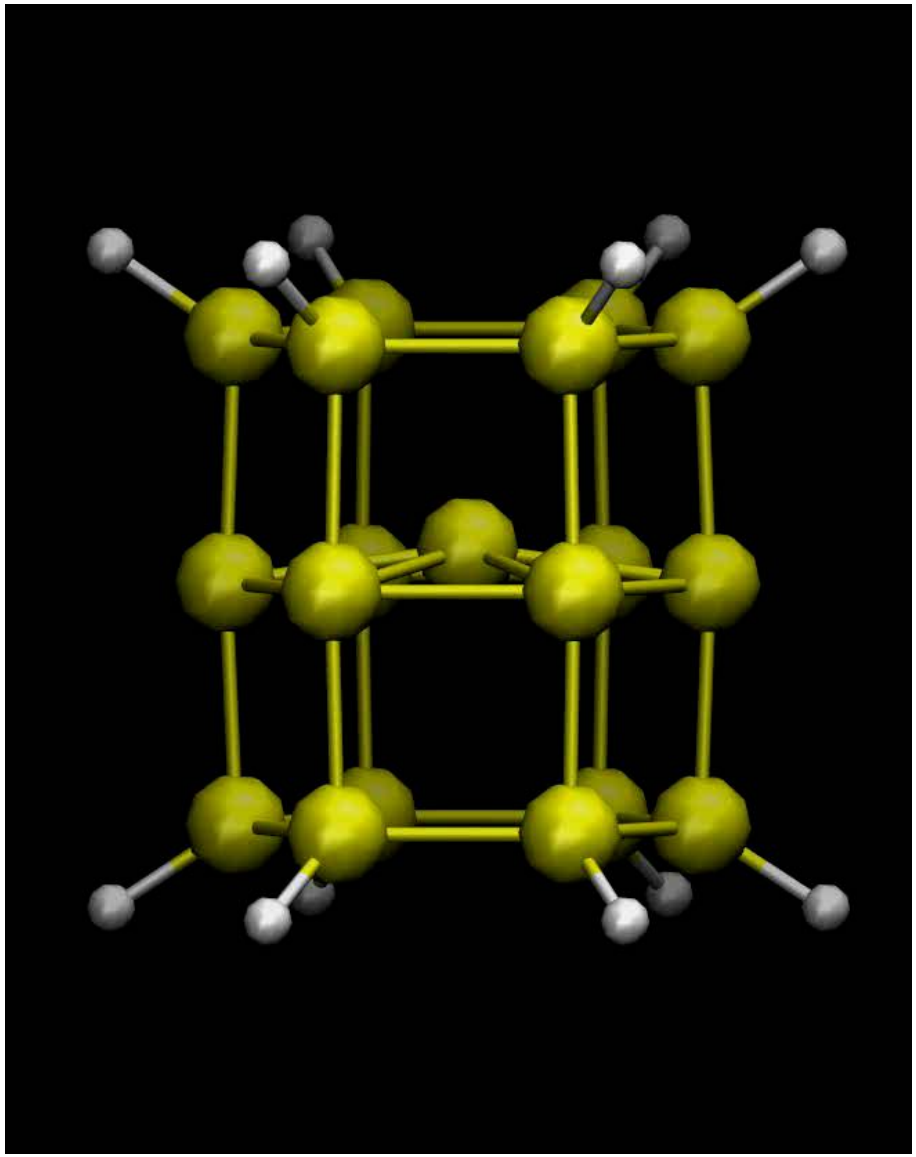

Spontaneous THz oscillations

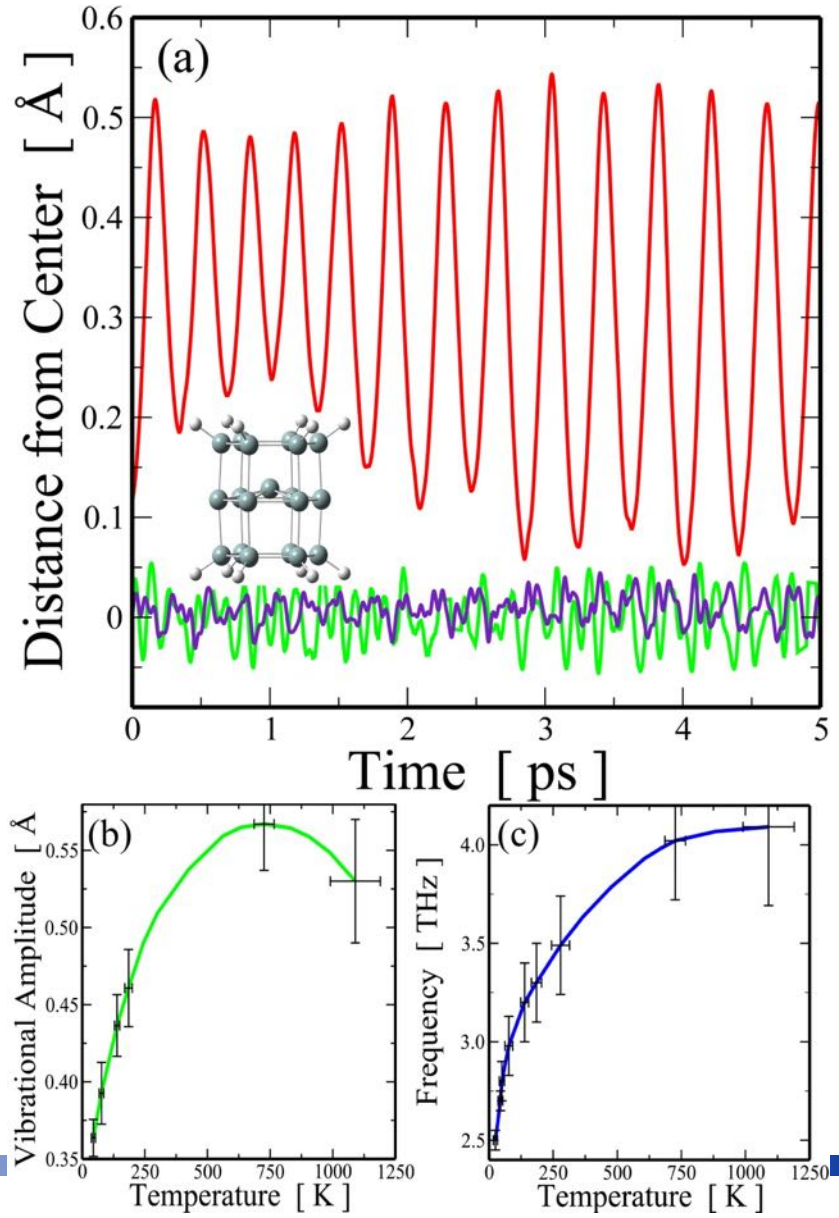

Typical example of spontaneous oscillations at 44 K. (a) red curve: typical movement of the inner Si atom; green curve: typical movement of one of the other Si atoms around its equilibrium position; violet curve: movement of the center Si atom in the Si29H24 nanocrystal under the same conditions;

(b) peak-to-peak amplitude and

(c) oscillation frequency of the inner silicon atom as function of the NC temperature.

THz oscillations excited by external pulse

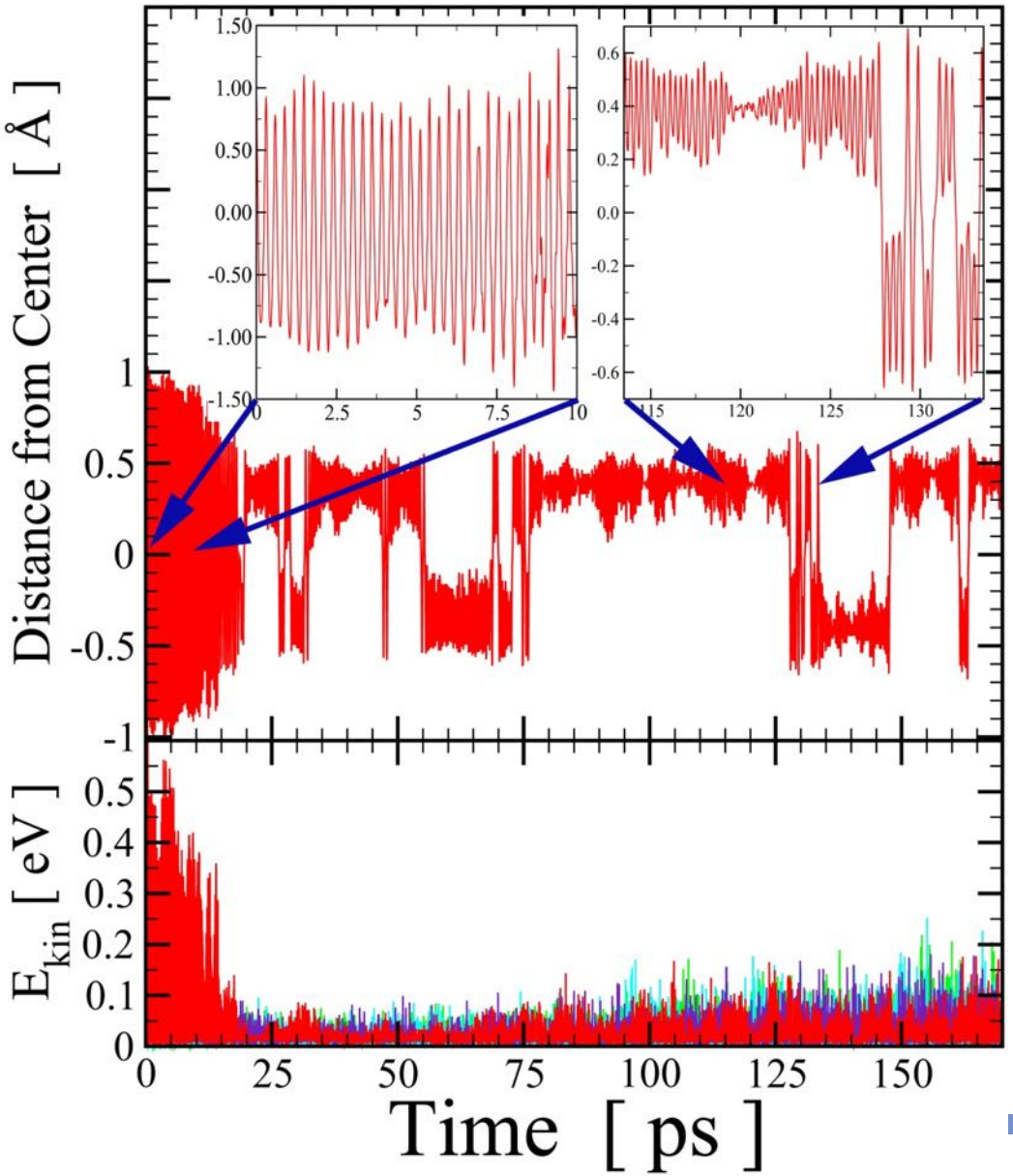

Large amplitude oscillations of the inner Si atom can be excited by an external source (e.g., an electric field or laser pulse) leading to oscillations through the center hexagon.

Upper panel: Movement of inner Si atom relative to central hexagon plane. The two insets illustrate the dynamic behavior during the nonequilibrium oscillations until about 20 ps after the exciting trigger, and the equilibrium behavior thereafter. Lower panel: Kinetic energy of inner Si atom (in red) in comparison to kinetic energies of all other Si atoms (all other colors).

Phys. Rev. Lett. **112**, 197401 - 14 May 2014

Highlights in

Volume 36 | Issues 27–28 | 2015
Included in this print edition:
Issue 27 (October 15, 2015)
Issue 28 (October 30, 2015)
Journal of COMPUTATIONAL CHEMISTRY
Organic • Inorganic • Physical
Biological • Materials

- *NATURE NANOTECHNOLOGY*
  vol. **6**, p. 756, DECEMBER 2011 (Editor's Choice)
- *SCIENTIFIC AMERICAN*
  p. 5, FEBRUARY 2012 (Briefings in Nanotechnology)

- "***A la Une...***", Actualités du CNRS du 17.07.2014
- "***A la Une...***", Actualités du CNRS du 27.06.2012
- "*La Jaune et la Rouge*"
  Magazine N699, Novembre 2014

Applications aux autres systèmes moléculaires par exemple, aux perhalocyclohexasilanes dihalogénés (J. Phys. Chem. A, 2013, 117, pp 3529-3538), aux systèmes de silabiphenyl (Comput. Theo. Chem., 1052, 15 January 2015, Pages 6-11), aux composés de silicium-pyrrolil (J Phys Chem A. 2015 Jul 9 ; 119 (27),7038-51) et même aux agrégats de **H2O** (Phys. Chem. Chem. Phys., 2015, 17, 2987-2990).

Use much more atomic hydrogen

To obtain the above structure, we used a low-temperature low-pressure silane/ hydrogen plasma with a very specific ratio between H-atoms and H2-molecules.

What happens if there were much more H-atoms?

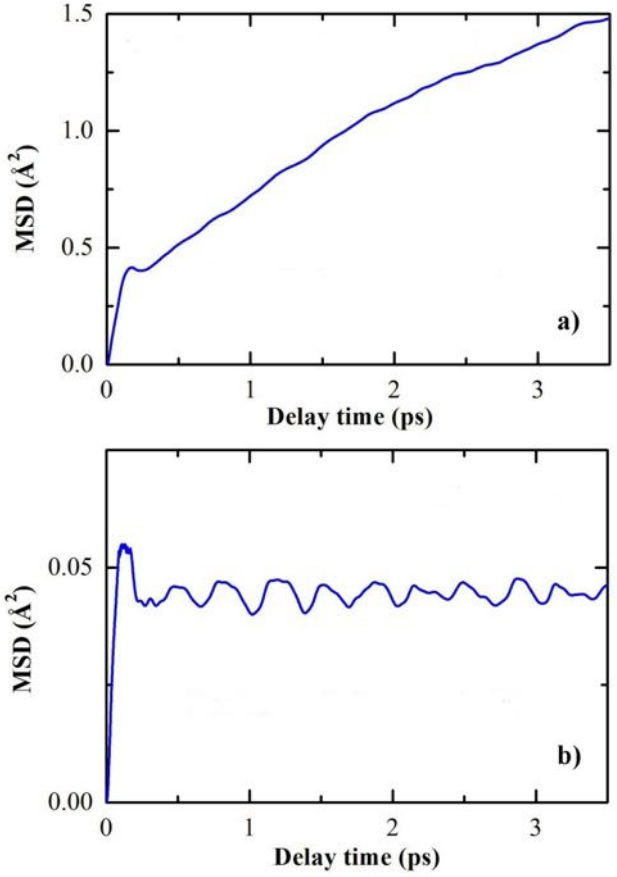

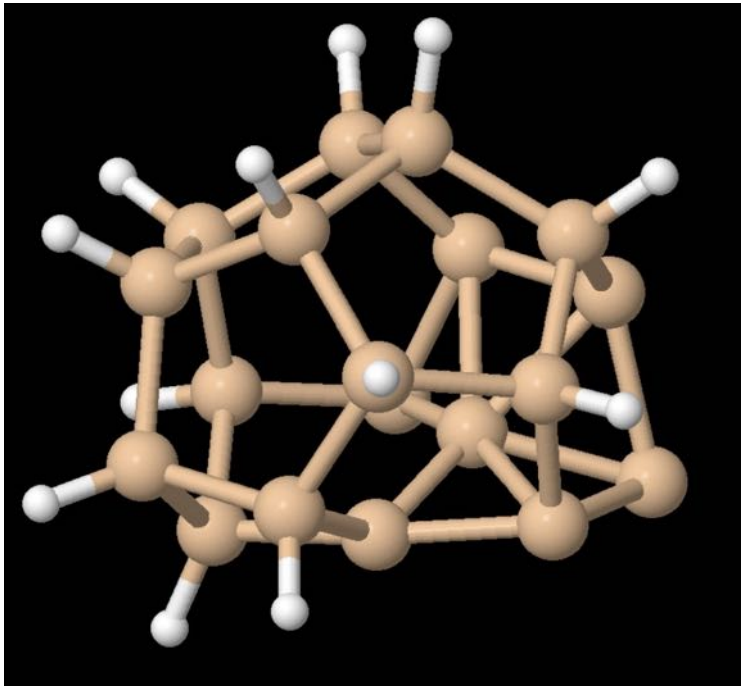

Despite its irregular structure, this nanocluster is still about 2.8eV more stable than its highly symmetric counterpart that was already ultrastable.

How can this irregular cluster be so stable?

A detailed natural bond orbital (NBO) analysis reveals

- the presence of one six-times coordinated silicon atom
- severely electron-deficient bonds (down to 1.66 electrons per bond)
- different hybridization states (between sp^1 and sp^{17})
- extremely strong stabilization energies (up to 500 kcal/mol involving the overcoordinated silicon atom) and
- very high NICS values (up to -42ppm)

All these characteristics suggest that it this cluster might also experience a high degree of electron delocalization.

Instead of relying on very local information (as the NICS values), measure the net induced aromatic current as function of an applied magnetic field. Aromatic molecules and nanostructures sustain a net diamagnetic ring current when exposed to an external magnetic field.

Integrating all induced currents going through a sample surface perpendicular to the induced current direction, we directly obtain the quantitative total difference between all para- and diamagnetic components

Magnetically induced ring currents

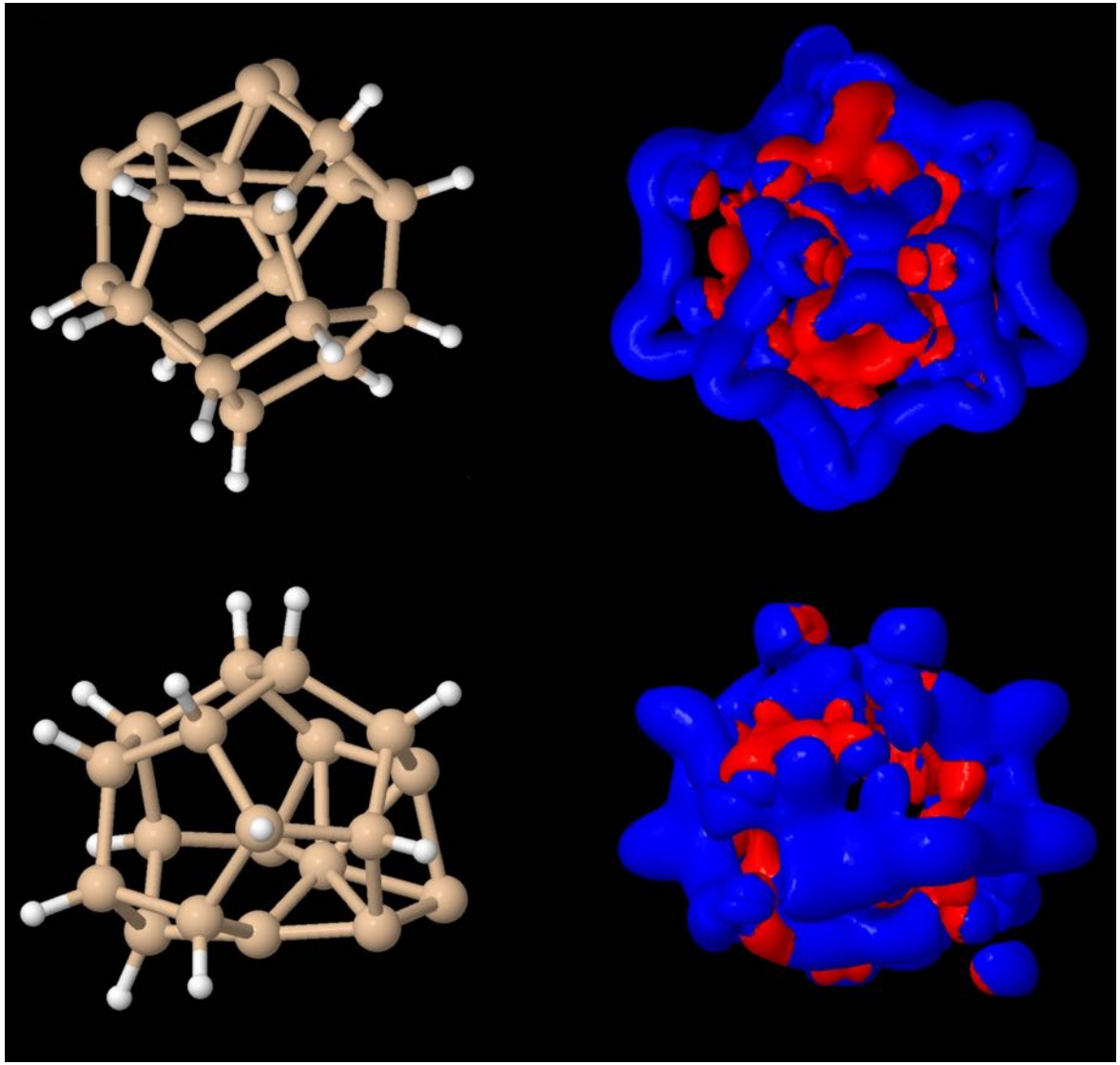

Red: paramagnetic contribution

Blue: diamagnetic contribution

Asymmetric $Si_{19}H_{12}$: Despite the apparently unruly mixing of para- and diamagnetic components in space, integration over all currents yields

a net diamagnetic aromatic ring current of **+41.2nA/T**

=> 3 times higher than in benzene

Magnetically induced ring currents

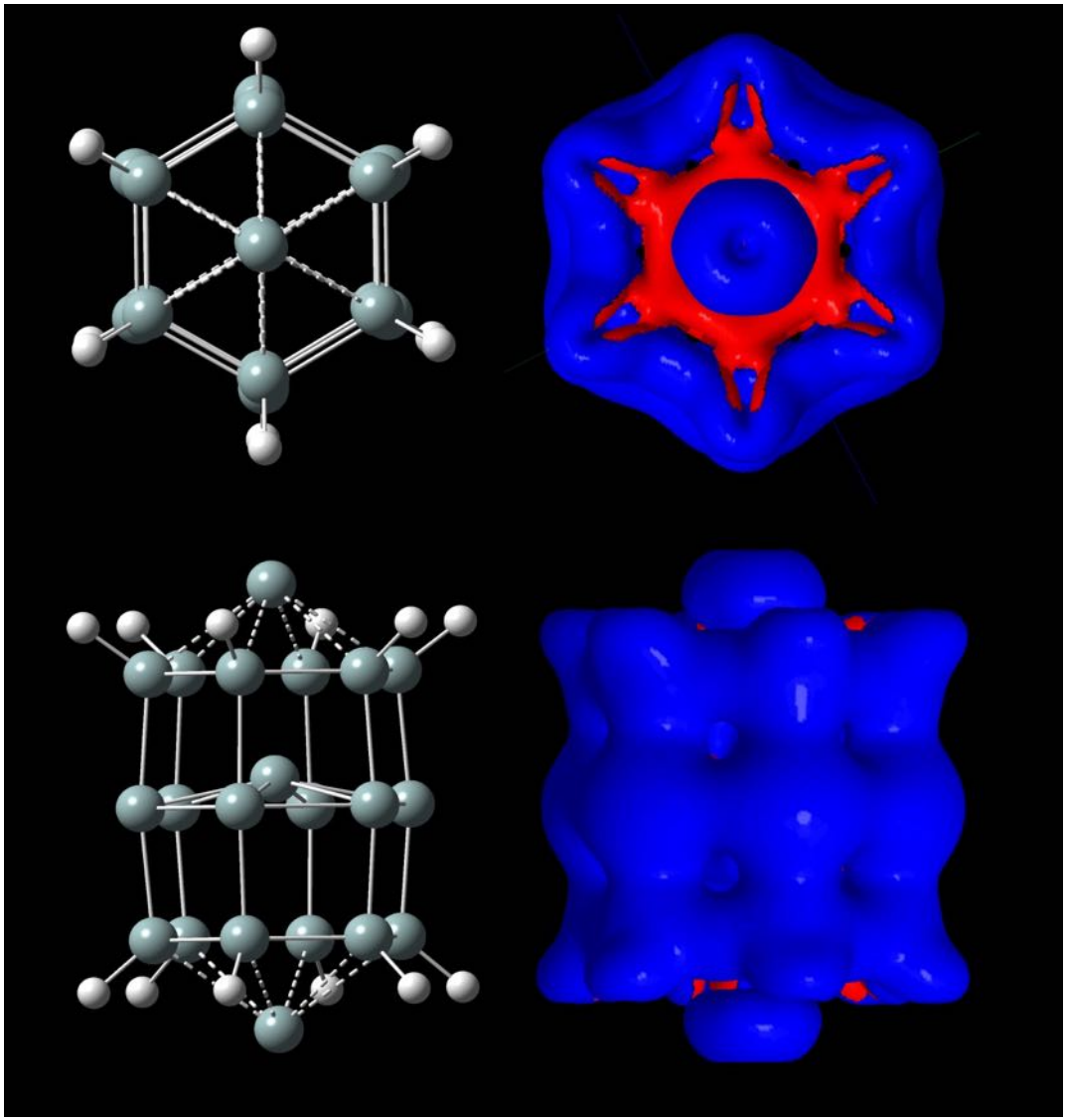

Red: paramagnetic contribution

Blue: diamagnetic contribution

How does over-coordination influence the degree of aromaticity?

=> We added two more hypervalent Si atoms to symmetric structure.

Symmetric $Si_{21}H_{12}$: Integration over all currents yields a net diamagnetic aromatic ring current of **+89.0nA/T**

=> 6 times higher than in benzene

Chemical Physics Letters **614**, 199-203 (2014)

Summary

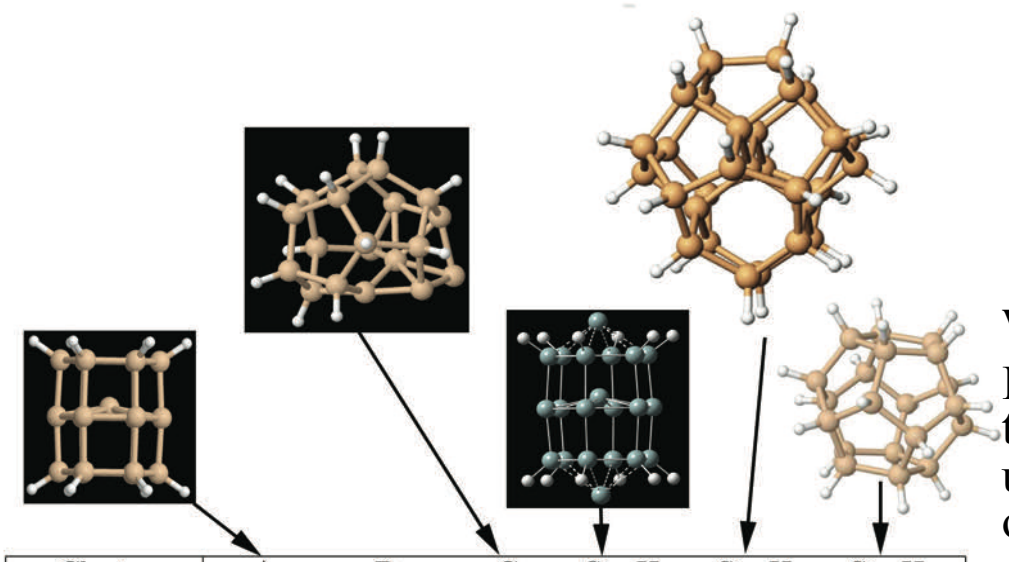

Cluster	A	B	C	$Si_{21}H_{12}$	$Si_{29}H_{24}$	$Si_{20}H_{20}$
Over-coordinated	YES	YES	YES	YES	NO	NO
$E_{coh,sk}$ $[eV/atom]$	2.9587	3.0282	3.1043	3.0742	3.0565	2.8481
Aromatic current $[nA/T]$	42.0	17.7	41.2	89.0	0.8	1.8
Optical gap $[eV]$	0.993	1.610	1.468	1.121	3.588	5.150
H-L_{B3LYP} $[eV]$	1.558	1.961	2.119	2.068	3.923	4.402
Dipole moment $[Debye]$	1.809	1.541	0.992	1.208	0.000	0.000

$$E_{coh,sk} = [BE(Si_nH_m) + m * \mu(H) - m * ZPE(H))]/n$$

We demonstrated theoretically that:

In standard SiH_4/H_2 plasmas, the precise control of the ratio of atomic and molecular hydrogen allows us to "program" the final structure and functionality of plasma-born nanoclusters.

We predict that specific H/H_2 ratios give birth to over-coordinated aromatic silicon nanocrystals that are ultra-stable and exhibit mechanical, optical properties that could so far only be obtained when adding toxic or expensive elements as PbS, PbSe, CdS, CdSe, or Au, Ag.

ELF analysis

The electron localization function
to a reference electron at a given
spatial localization of the electron
The ELF is defined in such a way
localization of the electron pair ar

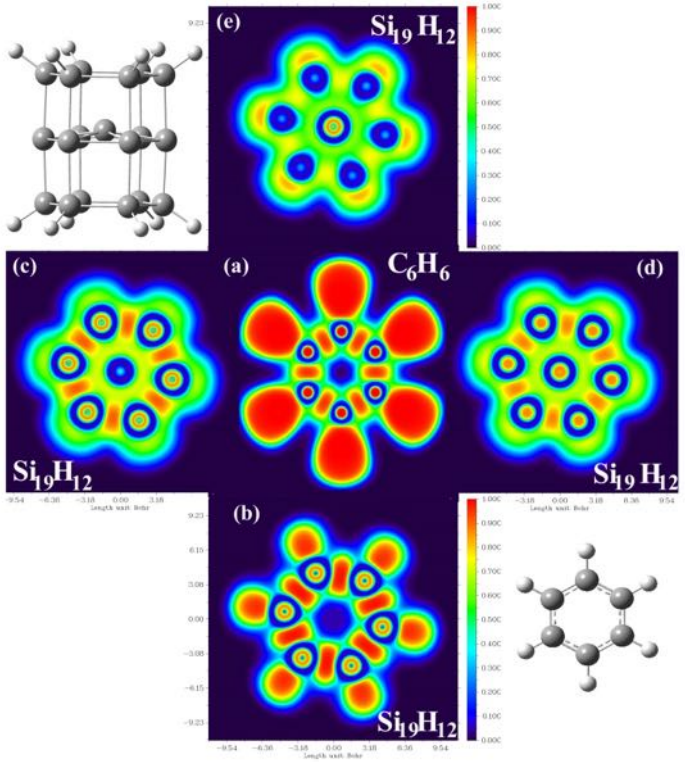

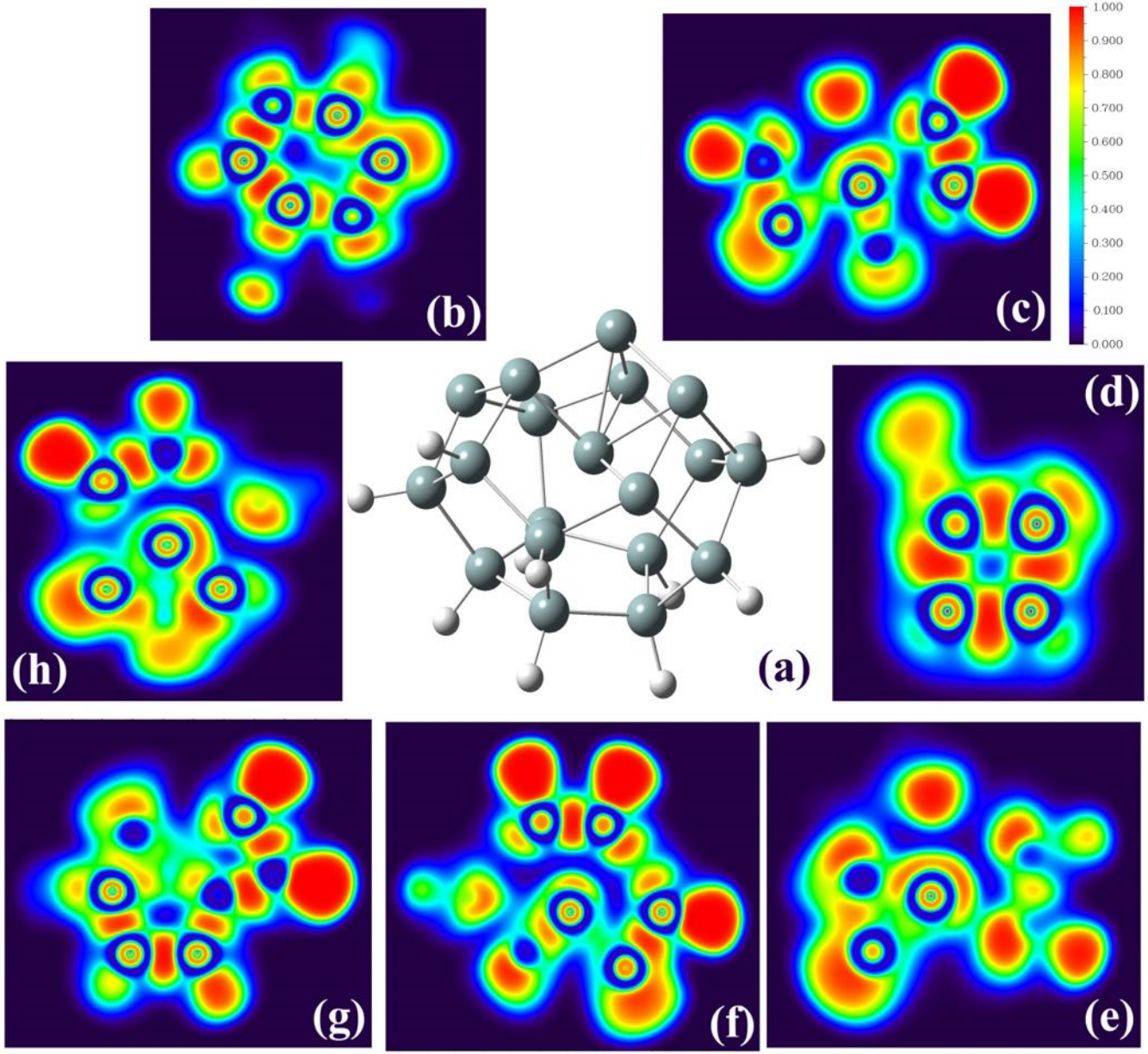

ELF analysis

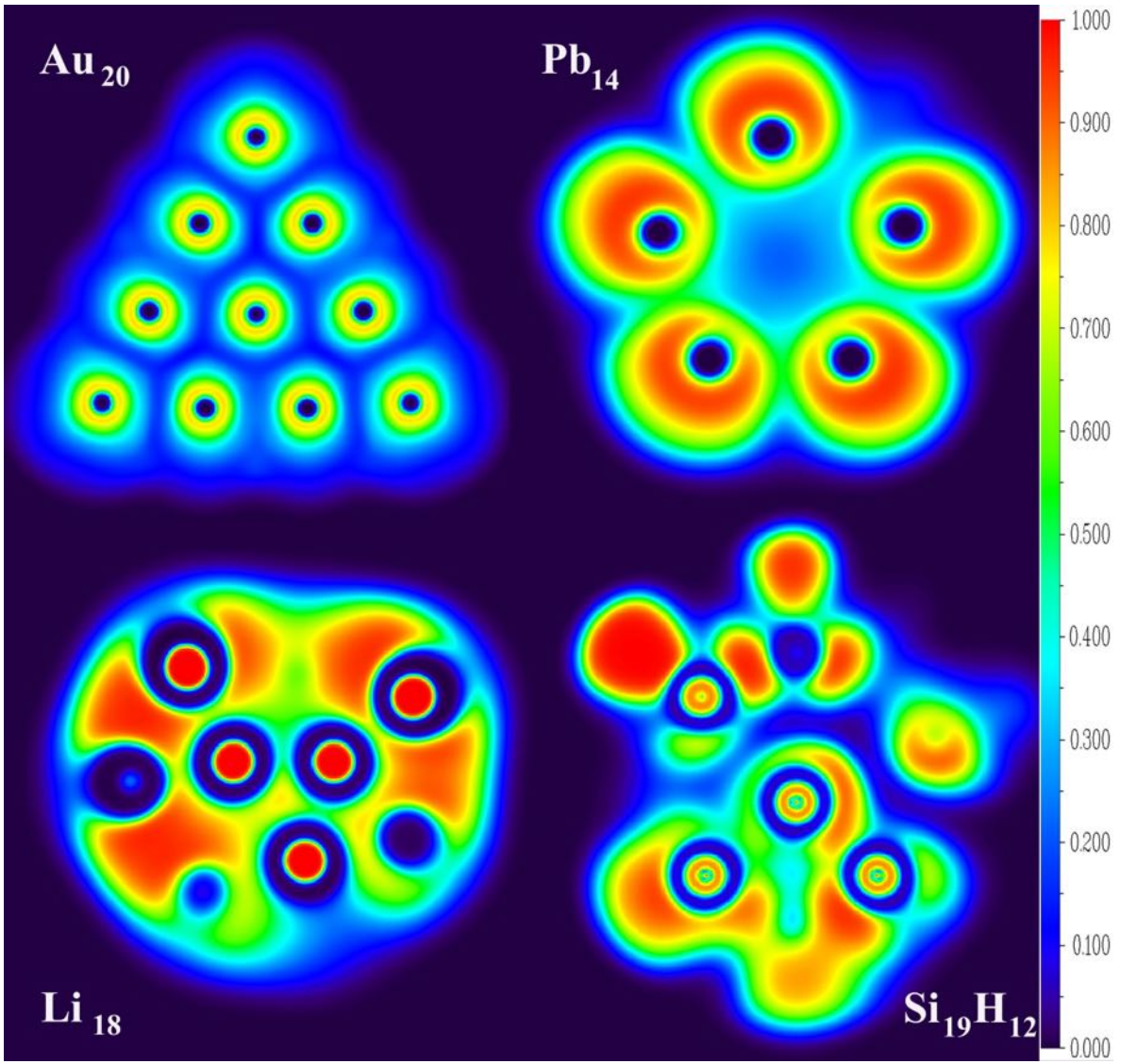

$Si_{19}H_{12}$ scaffold resulting from a Nudged Elastic Band (NEB) calculation

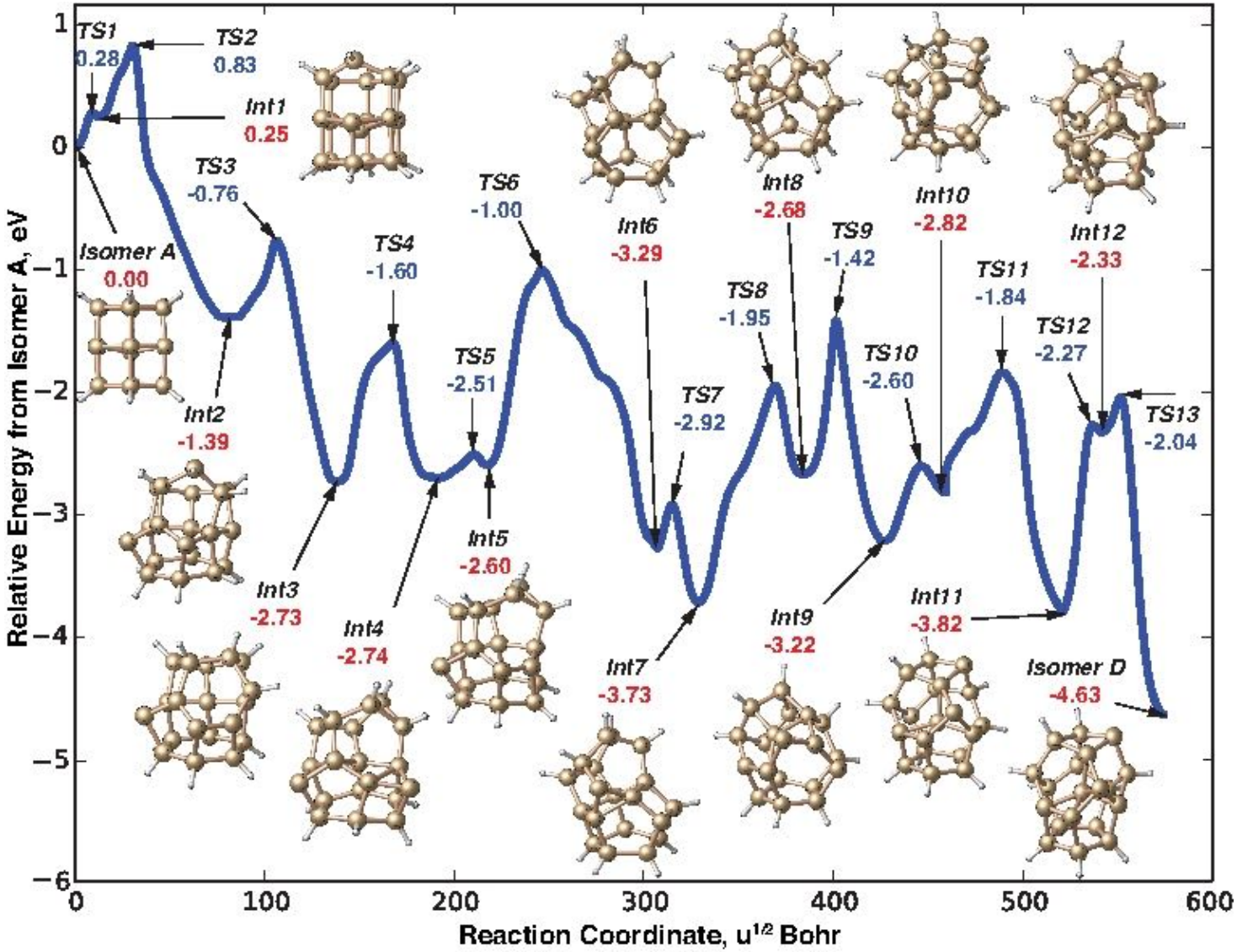

Doping effect: optical properties

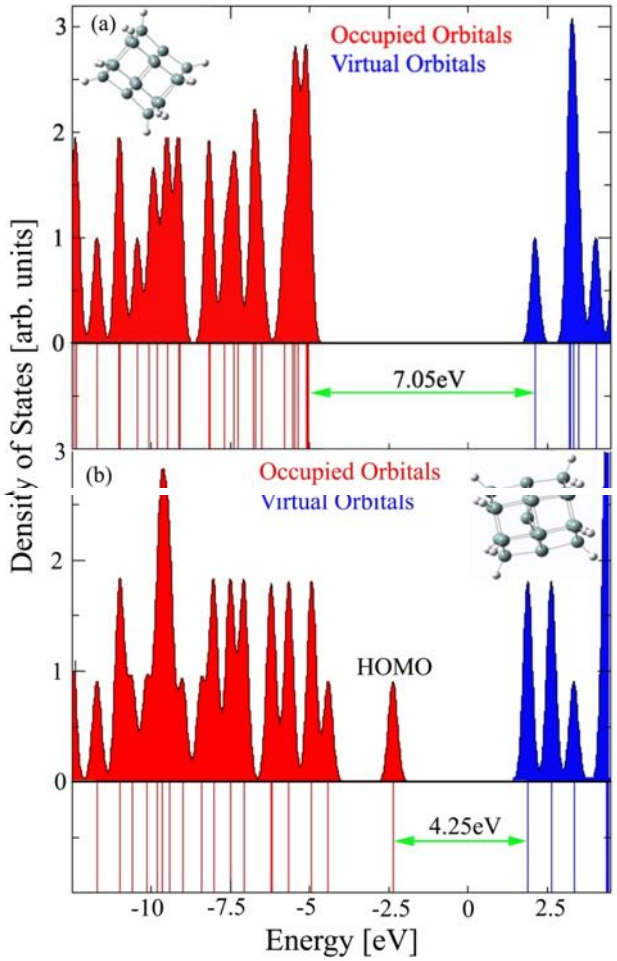

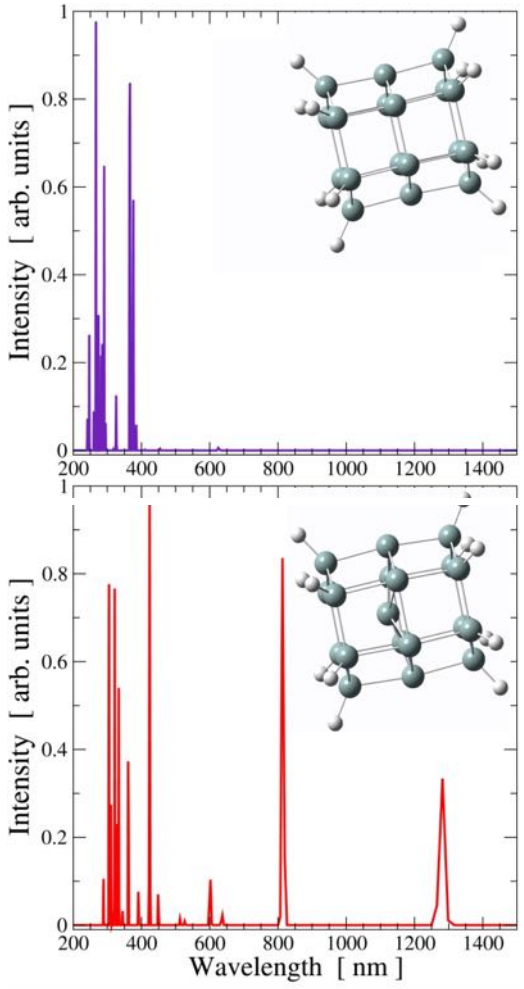

Holger Vach, *Nano Lett.* **11**, 54775481 (2011)

Application: Solar Cells

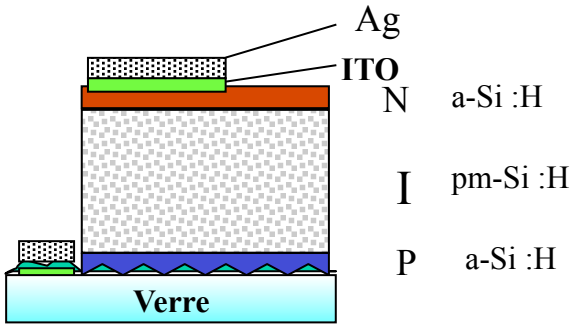

Diagram of a solar cell.

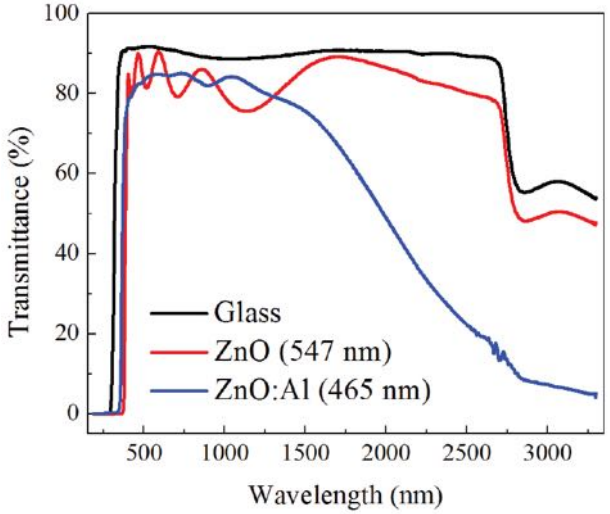

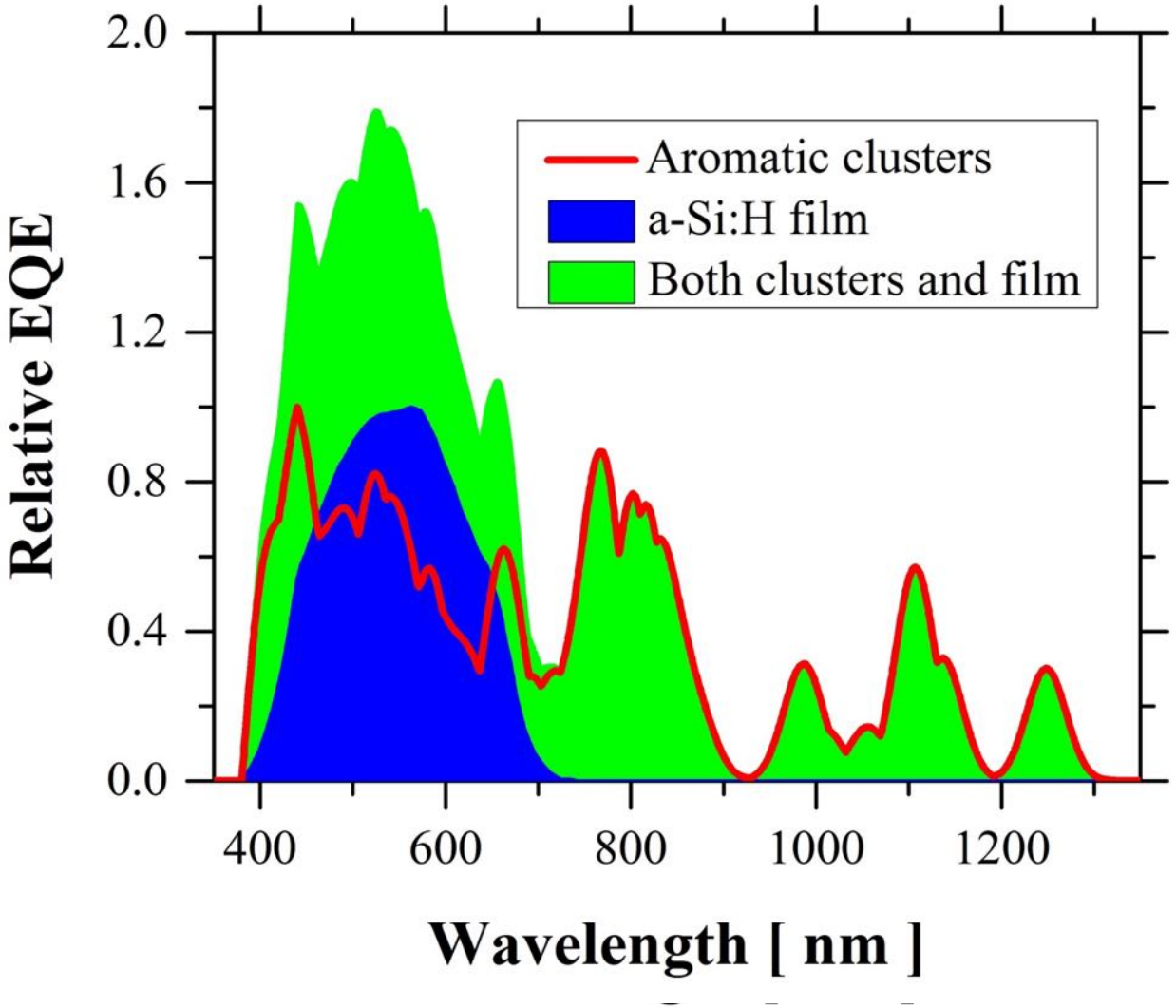

Holger Vach, Lena V. Ivanova, Qadir K. Tir
Fatme Jardali, Ha-Linh Thi Le

Nanoscale, 2016, Advance Article, **DOI:** 10.1039/C6NR04349F.

Back Cover image *Nanoscale* issue #42

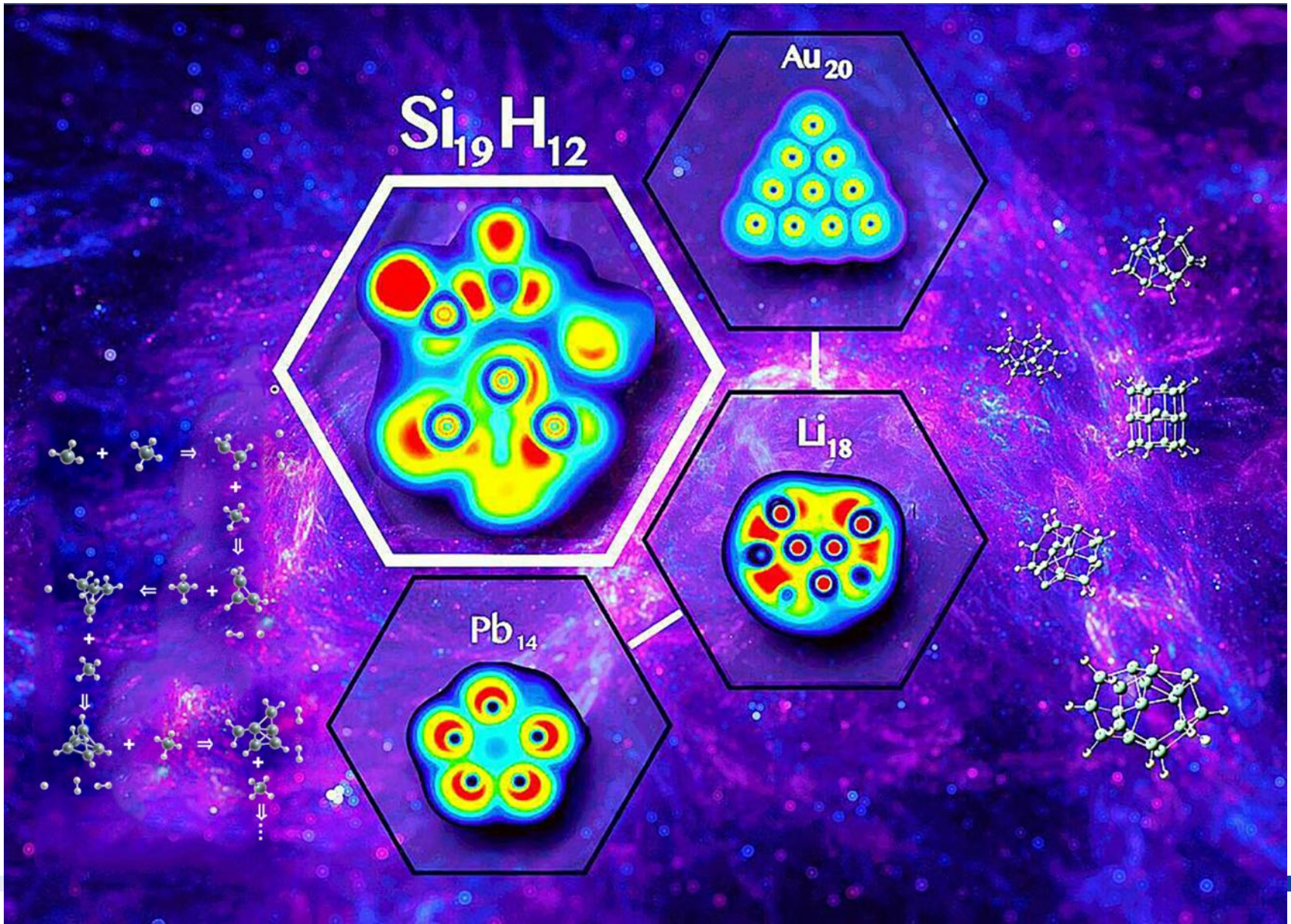

Acknowledgments

- Laïfa Boufendi
- David B. Graves
- Khaled Hassouni

- Pascal Le Floch
- Gilles Ohanessian
- Gilles Peslherbe
- Philippe Baranek

- Nihed Chaabane (Ingénieur Chercheur - Maître de Conférences, CEA)
- Ning Ning (postdoc Berkeley, Ingénieur de recherche LSPM)
- Ha Linh Thi Le (postdoc INSP)
- Hans-Christian Weissker (CR1, CNRS, CINaM)
- Nancy-Carolina Forero-Martinez (research assistant, MPI for Polymer Research)
- Qadir Timerghazin (Assistant Professor, Marquette University)

- Fatima Jardali (PhD student, LPICM)
- Christoph Lechner (PhD student, LPICM)
- Jean-Maxime Orlac'H (PhD student, LPICM)
- Elena V. Ivanova (PhD student, Marquette University)
- Bryan Patrick Keary (PhD student, Cork University)
- Marie Hénault (postdoc, GREMI)
- Olha Lisniak (intern student M2, LPICM)
- Jejune Park (intern student M1, LPICM)

HPC resources from GENCI-IDRIS